NAVAL POSTGRADUATE SCHOOL

MONTEREY, CALIFORNIA

THESIS

EXTENDING THE ENDURANCE OF SMALL UNMANNED AERIAL VEHICLES USING ADVANCED FLEXIBLE SOLAR CELLS

by

Christopher R. Gromadski

December 2012

Thesis Advisor:	Sherif Michael
Second Reader:	Rudolf Panholzer

Approved for public release; distribution is unlimited

THIS PAGE INTENTIONALLY LEFT BLANK

REPORT DOCUMENTATION PAGE			Form Approved OMB No. 0704–0188
Public reporting burden for this collection of information is estimated to average 1 hour per response, including the time for reviewing instruction, searching existing data sources, gathering and maintaining the data needed, and completing and reviewing the collection of information. Send comments regarding this burden estimate or any other aspect of this collection of information, including suggestions for reducing this burden, to Washington headquarters Services, Directorate for Information Operations and Reports, 1215 Jefferson Davis Highway, Suite 1204, Arlington, VA 22202–4302, and to the Office of Management and Budget, Paperwork Reduction Project (0704–0188) Washington DC 20503.			
1. AGENCY USE ONLY ***(Leave blank)***	**2. REPORT DATE** December 2012	**3. REPORT TYPE AND DATES COVERED** Master's Thesis	
4. TITLE AND SUBTITLE EXTENDING THE ENDURANCE OF SMALL UNMANNED AERIAL VEHICLES USING ADVANCED FLEXIBLE SOLAR CELLS		**5. FUNDING NUMBERS**	
6. AUTHOR(S) Christopher R. Gromadski			
7. PERFORMING ORGANIZATION NAME(S) AND ADDRESS(ES) Naval Postgraduate School Monterey, CA 93943–5000		**8. PERFORMING ORGANIZATION REPORT NUMBER**	
9. SPONSORING /MONITORING AGENCY NAME(S) AND ADDRESS(ES) N/A		**10. SPONSORING/MONITORING AGENCY REPORT NUMBER**	
11. SUPPLEMENTARY NOTES The views expressed in this thesis are those of the author and do not reflect the official policy or position of the Department of Defense or the U.S. Government. IRB Protocol number _____N/A_____.			
12a. DISTRIBUTION / AVAILABILITY STATEMENT Approved for public release; distribution is unlimited		**12b. DISTRIBUTION CODE** A	

13. ABSTRACT (maximum 200 words)

Most currently fielded small unmanned aerial vehicles (SUAV) have flight times limited to 90 minutes due to battery life and are often forced to work in teams of multiple craft to provide tactical level units with continuous observation of the battlefield. Continuous operations additionally place a strain on logistics trains by requiring either more batteries or fuel to support recharging. Prior theses have examined the ability of solar cells to extend the flight endurance and capabilities of SUAVs during peak sunlight conditions. This research demonstrated the viability of augmenting the onboard power supply with advanced thin-film photovoltaic (TFPV) cells made of copper-indium-gallium selenide (CIGS) over a longer period of time. The additional source of power will reduce, at times even eliminate, the demand on the lithium polymer batteries of a Raven SUAV as sunlight conditions change throughout the day. All components used in construction were commercially available, including foam wings that closely resembled the airfoil of a Raven SUAV with increased surface area. The laboratory tests used standard operating procedures from the operator's manual and input from the training community to accurately simulate flight conditions and field use. This research demonstrates that degraded components and non-ideal sunlight conditions still provide a significant improvement over the original system for a minimal cost in money and weight. The approach is relevant to the use of the system in austere combat zones which require results in conditions that are rarely ideal. The research additionally applied projections to the capabilities of the augmenting circuitry on unmodified Raven wings and Puma SUAVs.

14. SUBJECT TERMS Solar Power, Thin Solar Cells, CIGS, UAV, Raven, Expeditionary Energy			**15. NUMBER OF PAGES** 130
			16. PRICE CODE
17. SECURITY CLASSIFICATION OF REPORT Unclassified	**18. SECURITY CLASSIFICATION OF THIS PAGE** Unclassified	**19. SECURITY CLASSIFICATION OF ABSTRACT** Unclassified	**20. LIMITATION OF ABSTRACT** UU

NSN 7540–01–280–5500 Standard Form 298 (Rev. 2–89)
Prescribed by ANSI Std. 239–18

THIS PAGE INTENTIONALLY LEFT BLANK

Approved for public release; distribution is unlimited

EXTENDING THE ENDURANCE OF SMALL UNMANNED AERIAL VEHICLES USING ADVANCED FLEXIBLE SOLAR CELLS

Christopher R. Gromadski
Captain, United States Marine Corps
B.S., Virginia Military Institute, 2003

Submitted in partial fulfillment of the
requirements for the degree of

MASTER OF SCIENCE IN ELECTRICAL ENGINEERING

from the

NAVAL POSTGRADUATE SCHOOL
December 2012

Author: Christopher R. Gromadski

Approved by: Sherif Michael
Thesis Advisor

Rudolf Panholzer
Second Reader

Clark Robertson
Chair, Department of Electrical and Computer Engineering

THIS PAGE INTENTIONALLY LEFT BLANK

ABSTRACT

Most currently fielded small unmanned aerial vehicles (SUAV) have flight times limited to 90 minutes due to battery life and are often forced to work in teams of multiple craft to provide tactical level units with continuous observation of the battlefield. Continuous operations additionally place a strain on logistics trains by requiring either more batteries or fuel to support recharging. Prior theses have examined the ability of solar cells to extend the flight endurance and capabilities of SUAVs during peak sunlight conditions. This research demonstrated the viability of augmenting the onboard power supply with advanced thin-film photovoltaic (TFPV) cells made of copper-indium-gallium selenide (CIGS) over a longer period of time. The additional source of power will reduce, at times even eliminate, the demand on the lithium polymer batteries of a Raven SUAV as sunlight conditions change throughout the day. All components used in construction were commercially available, including foam wings that closely resembled the airfoil of a Raven SUAV with increased surface area. The laboratory tests used standard operating procedures from the operator's manual and input from the training community to accurately simulate flight conditions and field use. This research demonstrates that degraded components and non-ideal sunlight conditions still provide a significant improvement over the original system for a minimal cost in money and weight. The approach is relevant to the use of the system in austere combat zones which require results in conditions that are rarely ideal. The research additionally applied projections to the capabilities of the augmenting circuitry on unmodified Raven wings and Puma SUAVs.

THIS PAGE INTENTIONALLY LEFT BLANK

TABLE OF CONTENTS

THIS PAGE INTENTIONALLY LEFT BLANK

LIST OF FIGURES

LIST OF TABLES

THIS PAGE INTENTIONALLY LEFT BLANK

LIST OF ACRONYMS AND ABBREVIATIONS

AM	Air mass
CdTe	Cadmium Telluride
CIGS	Copper Indium Gallium Selenide
DC	Direct Current
DDL	Digital Data Link
eV	Electronvolt
GCS	Ground Control Station
IR	Infrared
I-V	Current-Voltage
Li-S	Lithium Sulfur
MPPT	Maximum Power Point Tracker
SSAG	Space Systems Academic Group
SUAV	Small Unmanned Aerial Vehicle
Te	Tellurium
TFPV	Thin-film Photovoltaic
UAS	Unmanned Aerial Vehicle
UAV	Unmanned Aerial System
ZnO	Zinc Oxide

THIS PAGE INTENTIONALLY LEFT BLANK

EXECUTIVE SUMMARY

Unmanned Aerial Vehicles (UAV) have been in use by the United States military since the Vietnam War [1]. However, their use in the Global War on Terror has expanded tremendously to include small UAVs (SUAV) as a regular asset to provide real-time intelligence, surveillance and reconnaissance to small front line units. Concurrent to that change has been an increased focus on Expeditionary Energy to decrease the logistic requirements of those same units [2]. Most currently fielded SUAVs have a flight endurance limited by battery life to 90 minutes. Continuous coverage requires SUAVs working in teams of multiple systems and either carrying more batteries or constantly recharging them using vehicles or other sources that require fuel resupply. Today's increasingly light and agile military requires a means to reduce the power demands of its systems or find available sources of energy to augment those it already has. Fortunately, the regions the military responds to most frequently [3] are also the areas with the greatest annual exposure to sunlight [4]. Previous theses have examined the ability of solar cells to extend the flight endurance and capabilities of SUAVS during peak sunlight conditions.

The objective of this thesis is to extend the endurance of a currently fielded SUAV with minimal modifications using commercially available components. The additional power will be collected utilizing the flexible and lightweight thin-film photovoltaic (TFPV) cells to conform to the airfoil of an SUAV without significantly increasing drag or weight on the system. The success in meeting these objectives is measured by the increase of endurance over that of the original system compared to the relative increase in weight and cost of components.

The SUAV for research was selected by comparing the currently fielded assets within the defined scope of size, compatibility with circuitry, starting endurance, and availability among other factors. The Raven was determined to be the best available asset. However, the Puma, though unavailable, was much more attractive due to a wingspan twice that of the Raven and with a longer endurance.

Following the selection of an SUAV, we explored the theory and performance of flexible solar cells. The competing technologies were compared, with efficiency and cost being the primary factors. After comparison, copper-indium-gallium selenide (CIGS) cells, used in previous theses, were determined to be the highest performing cells for a reasonable price.

Battery technologies were explored next, with a focus on energy density and handling procedures. The Raven's lithium polymer batteries were compared against emerging technologies and determined to be superior to lithium sulfur and lithium air batteries, which are not yet commercially available.

After selecting the solar cells and battery, the circuitry to interface those key components was selected. A combination maximum power point tracker (MPPT) and boost converter was selected due to the capability to tune the circuitry independently. A battery balancer was determined to be necessary for the ability to safely charge the battery using the solar array.

During assembly, the flexibility of the MPPT became important when the original array design was determined to be incompatible with the Raven battery. The redesigned array used a minimalist approach that limited handling of the cells, reduced temperature sensitivity, and allowed the boost converter to perform its intended function. That array was mounted on a modified wing that closely resembled the airfoil of a Raven wing.

The system was bench tested before and after modification to clearly demonstrate the effectiveness of the augmenting circuitry. During testing, the current demand of the Raven was recorded at each throttle position to provide a basis for future calculations. Endurance tests were designed to reflect current tactics, techniques, and procedures to not only prevent damage to the system but also provide an easily recognizable improvement in performance.

At the conclusion of testing, it was apparent that not only were the solar cells used significantly degraded, but the MPPT did not operate at the maximum power point of the solar cells. Despite these shortcomings, the augmented system still operated 2.7 times longer than shown by the average baseline bench test of the un-augmented system. An-

other critical piece of data collected for the first time was the parabolic curvature of the input current to the system caused by the sun moving across a stationary solar array during the course of testing.

Simulations were created to project the performance of the system with properly functioning components by multiplying the input current to the system by factors to maintain the shape of the curve. Those projections demonstrated that the Raven battery should have charged for two hours during mid-day by replacing only the degraded cells, while replacing the MPPT and cells could have achieved day-long charging of the battery, increasing performance by at least 269%, or 3.7 times, the original endurance.

Those simulations went further to predict the performance of properly functioning cells and MPPTs on an unmodified Raven wing and the larger battery and wingspan of a Puma. Utilizing only a single string of cells on a standard Raven wing would have provided 96.5% of the current input during the actual test, while a Puma could receive a significantly increased percentage of input current to the system, which reduces demand on the battery and increases flight endurance.

The difference between the endurance of bench tests and documented endurance from actual flight were also compared. A prediction of average current draw based on battery capacity was calculated to account for the average flight and translated into the measured current draw for throttle position. A 90 minute flight, according to operator manual procedures, would require an average current draw of 1.82 Amps. That current draw was found during bench tests to be between 65% and 70% throttle.

The most significant finding of this research was that flight during mid-day hours provides a significant increase in the endurance of a Raven. Those results were found to be affected by the system's flight profile, the movement of the sun throughout the day, and weather conditions. However, even during cloudy and other low light conditions, the augmenting circuitry was found to provide a significant input to the original system without harming a fully charged battery or draining the battery at night. Those benefits were provided at a cost of 3.8% increase in weight and 0.75% increase in materials cost over the original system. In short, for minimal changes to the cost and weight of the system, a

significant increase in endurance and capabilities were added using commercially available components that did no harm to the original system.

Future research should focus on:

- Observations of the current draw of the original system during actual flight to create an improved bench testing model that accounts for the behavior of operators in addition to sources of current draw that were not observed in these tests.
- An improved predictive model that accounts for the sun's movement and allows planners to calculate the best time to transition to and from day and night flight operations.
- Repetition of the testing process on a Puma UAV to observe the improvement in performance using a larger wing and battery.
- Eventual flight of a prototype.

This technology has the potential to provide a real and timely improvement to the performance and energy needs of warfighters. Future testing and development should continue to be done in realistic conditions. For warfighters, the greatest confidence comes from knowing the technology works, not only under ideal conditions, but when it is needed in the austere conditions of combat.

LIST OF REFERENCES

[1] Lexi Krock, "Time line of UAVs," NOVA. November 2002. [0nline]. Available: http://www.pbs.org/wgbh/nova/spiesfly/uavs.html. [Accessed July 2, 2012].

[2] Assistant Secretary of Defense for Operational Energy, Plans & Programs, "Energy for the warfighter: operational energy strategy," May 2011. [Online]. Available: http://energy.defense.gov/OES_report_to_congress.pdf. [Accessed July 3, 2012].

[3] Daniel J. P. Riveong, "In the midst of the swarm: reconceptualizing the (mislabeled) Global War on Terrorism." [Online]. Availabe: http://danielriveong.com/Reconceptualizing-the-Global-War-on-Terror-(GWOT).html. [Accessed July 19, 2012].

[4] Green Rhino Energy, “Yearly sum of global irradiance,” 2012. [Online] Available: http://www.greenrhinoenergy.com/solar/radiation/empiricalevidence.php#. [Accessed July 19, 2012].

THIS PAGE INTENTIONALLY LEFT BLANK

ACKNOWLEDGMENTS

I would like to take time to thank everyone who played a part in making my research and education a success. The below acknowledgments are not exhaustive, but represent a selection of those that deserve special recognition for their time and efforts.

I would be remiss not to recognize my lovely wife, Sam, and daughter, Shannon, as well as my nuclear and extended family and friends for their limitless patience and flexibility throughout my adult education, grounding my faith, and serving as the inspiration for my service.

I would like to thank Professors Sherif Michael and Rudolf Panholzer for guiding my research and providing input to make it a better product. Ron Phelps deserves special recognition for his generous donation of time and talent to repeatedly replace the microscopic tuning resistors which I had neither the equipment nor the experience to complete. Kevin Jones additionally provided early, critical, guidance on the design and selection of the wing along with important input for testing.

A special thanks goes to PMA-263, Naval Air System Command including Mr. Chris Sacco, Captain Steven Stepanic, and Jerome Adams for generously providing the Raven for testing and providing critical information to support testing. I could not have conducted this research without their support. Additional thanks goes to Jon Stiner, Jeffrey Bray, and Bill Nicoloff from AeroVironment who provided additional advice to conduct testing both professionally and safely.

I would like to thank the highly professional staff of the Electrical and Computer Engineering Department for their part in rounding my education. Special recognition goes to Jeff Knight for his steadfast dedication to supporting students with, not only equipment, but illumination for countless, complicated labs. I would also like to thank Professor Alexander Julian for his advice and support in troubleshooting during assembly. I cannot forget Chris Stephenson for his help in procuring and testing the maximum power point tracker, while constantly providing an important sounding board throughout research and testing.

I would like to thank the Virginia Military Institute, especially the Electrical and Computer Engineering Department, for challenging me on a daily basis. The high standards they set not only made future challenges more tolerable, but pushed me to produce better work and never accept mediocrity.

Finally, I wish to thank those that made life easier here. Thanks to Sean Ryburn for the distractions of fishing and golf. Gratitude to Maxwell for moral support and being the best running partner I could ever ask for, you will be missed. Also, thanks to Albert S. “G” Gispert and Pliny the Elder for their frequent outlets for stress.

I. INTRODUCTION

A. BACKGROUND

Unmanned planes, or Unmanned Aerial Vehicles (UAVs), are nearly as old as manned flight, pre-dating World War I and have been used in one form or another in nearly every American conflict since Vietnam [1]. However, the Global War on Terror brought a dramatic increase in the use and visibility of these platforms. Simultaneous with the expansion of UAV use has been a growing concern for the reduction of fuel usage and interest in renewable forms of energy as an alternative. This interest has been demonstrated in the establishment of the Marine Corp's Expeditionary Energy Office and the Defense Department's energy policy to increase the endurance and reduce the battery weight requirements on platforms of all types [2].

UAVs possess several key advantages to manned aircraft. Not only does the lack of an onboard pilot reduce weight and the likelihood of friendly casualties, but it also greatly simplifies the system by reducing the life support requirements for oxygen systems, G-forces, ejection seat, and more. The simplified system has the added benefits of decreased cost and a decrease in training requirements when compared to manned flight. UAVs, also known as Unmanned Aerial Systems (UAS), have been adapted to a wide range of missions from intelligence collection, through remote sensing and reconnaissance, to armed attacks on targets. With these advantages it is easy to conclude that UAVs will continue to be an important platform beyond the asymmetric conflict currently being fought.

UAVs defy simple classification. They can be defined by the mission they perform, power source, size, or other characteristics. While the individual services do not agree on a single classification system, the United States Marine Corps has adopted a system that assigns tiers to UAVs according to the size unit they are supporting. Tier I UAVs are assigned to support small units, Tier II UAVs support regiments or divisions, and Tier III UAVs support Marine Expeditionary Forces [3].

Most Tier II and III systems operate on combustion engines, have an endurance of multiple hours, and operate from larger units that have ready access to fuel. However, most Tier I systems, also known as Small UAVs (SUAVs), are battery powered, have endurances of 90 minutes or less and operate in units that frequently operate away from vehicles or the ability to recharge batteries. These systems have a pressing need for increased endurance and renewable sources of energy.

The issue of shorter endurance is compounded when considering that much of the battery life is expended in launching, traversing to and from the area to be observed, and recovery, leaving only a fraction of that time to perform its primary mission. Even when suites of three vehicles are used, the launch-recover-recharge cycle prevents continuous or sustainable observation for the small unit leader without a large supply of batteries and charging stations. When the battery load for the warfighter is estimated to already be 18 pounds each (to power radios and other devices) [2] and multiple aircraft are required to sustain operations, the ability of these UAVs to be man-portable is seriously tested during extended dismounted operations.

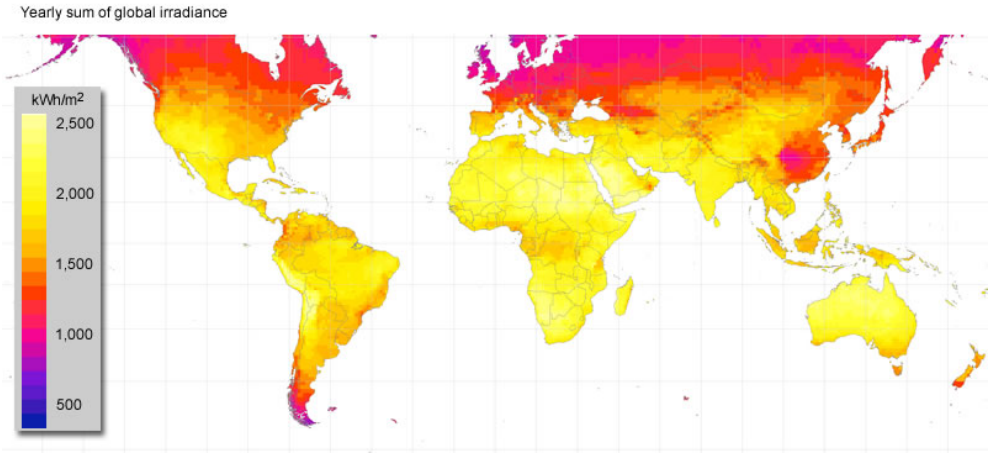

Figure 1. Annual regional solar irradiance (from [4]).

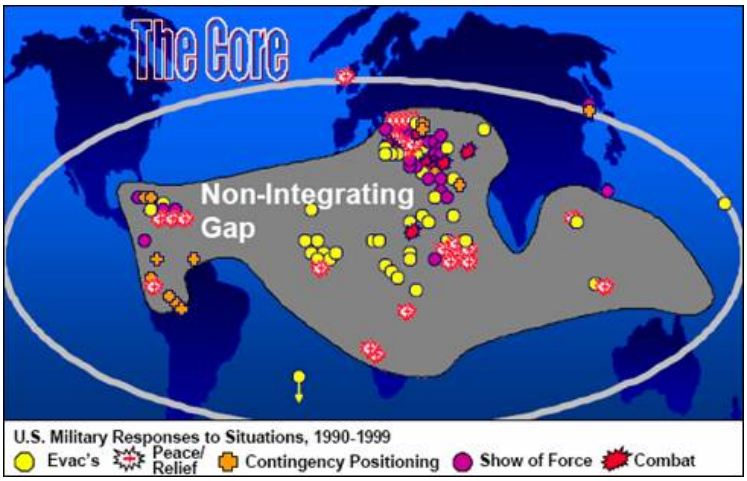

Figure 2. The Arc of Instability (from [5]).

The strong correlation between Figures 1 and 2 illustrates how many of the world's conflicts take place in regions where sunlight is intense. That correlation can be exploited as an opportunity to augment expeditionary energy needs with photovoltaic cells. Thin film photovoltaic (TFPV) cells have been developed that not only decrease the weight required to produce power but also add an element of flexibility and increased ruggedness. This technology has already been fielded in the form of solar blankets, seen in Figure 3, to recharge radio batteries and computers in Afghanistan [6]. Like many other forms of technology, with additional research and development, the efficiency of these cells has steadily increased over time to improve the power output on a similar available surface area.

Figure 3. Solar blankets in use in Afghanistan (from [6]).

B. OBJECTIVE

The objective of this thesis is to extend the endurance of a currently fielded SUAV with minimal modifications using commercially available components. The additional power will be collected utilizing the flexible and lightweight properties of TFPV cells to conform to the airfoil of an SUAV without significantly increasing drag or weight on the system.

The practicality of this research will be measured by the increased flight time compared to the weight and expense of modifications. As the efficiency of these cells improves, the contribution of power from the cells has the promise of transitioning from slowing the depletion of a battery to recharging a battery mid-flight. If a battery could recharge in flight, the endurance would be greatly increased. Systems in this configuration would additionally be able to self-charge batteries while grounded between flights, and possibly be able to charge other systems when not in use. The increased power contributed from solar cells would decrease the requirement for additional systems and batteries on the warfighter in addition to decreased reliance on vehicles and other sources of power.

While the focus of this thesis is timely support to small units in combat, the principles explored have a much wider range of applications. This technology could be expanded to operational and strategic UAVs, in addition to law enforcement and commercial applications.

C. RELATED WORK

While solar powered flight is not a new concept, dating back to 1974 [7], It has made great strides in recent days including the Solar Impulse manned craft, seen in Figure 4, that has set records with the first 24 hour manned solar flight [8] and, most recently, the first manned solar flight across the Strait of Gibraltar [9]. These flights were important because of the demonstration of being able to store energy and remain airborne after dark as well as an increasing confidence in the technology by including a human payload. However, most of these flights have relied on non-ruggedized, glider type, de-

signs. Those airframes often rely on high altitude flight to receive more intense, predictable, sunlight.

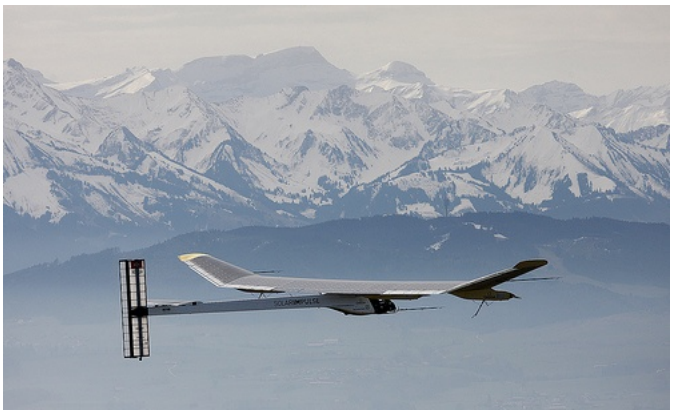

Figure 4. The Solar Impulse in flight (from [8]).

This thesis is a continuation of three prior Naval Postgraduate School theses on applying solar power to low altitude applications with SUAVs. In 2009 William R. Hurd experimented using a hobby plane to simulate a military craft, concluding from flight tests that flight endurance could be nearly doubled using solar cells [10]. In 2010 Javier V. Coba acquired a Raven UAV and, using a modified wing, estimated an improvement between 33–100% depending on the percentage of throttle used. The system did not fly because the wing did not have a proper airfoil [11]. Finally, in 2011, Chee Keen Chin took the results of Coba's thesis to create a computer model and apply it to his own solar array [12]. This research built on those lessons learned by both mounting the solar cells on an airfoil closely matching that of a Raven, testing according to user procedures, recording observations of behavior at every throttle position, and accounting for the movement of the sun during extended daytime testing.

D. APPROACH

The first step of this research was to reacquire an RQ-11B Raven in order to validate and test using an actual fielded system. The research was conducted using actual loads from the running motor and payload while streaming video and using procedures that reflected the operator manual and anecdotal input from the using community. This method most accurately simulated a system in operation. The Raven was tested for cur-

rent requirements and battery endurance both before and after modification to accurately document the relative system improvement and limit variables in the test.

Using an actual Raven wing, including the airfoil, as a template, we procured a modified wing to fit the intended solar array while simultaneously increasing the lift in order to overcome increases in drag and weight due to added circuitry.

Next, we acquired the most efficient thin flexible cells that were available. The cells were tested before and after encapsulation to validate their efficiency and confirm the successful mounting. Following mounting, the circuitry including the maximum power point tracker (MPPT) and direct current (DC)-to-DC power converter were connected and tested to ensure they perform as expected to improve the efficiency of the power delivered to the system.

Once integrated, the Raven was tested for current demand and battery endurance in a bench mounted environment, with and without input from the solar array. The percentage of current input to the system throughout the testing was plotted to show the observed variation in sunlight over the course of a day. Those results were modified to account for individual and combined changes in circuitry to assess the potential of the system.

E. ORGANIZATION

The types of SUAVs available along with their performance specifications and the pros and cons of each system are discussed in Chapter II.

The theory of solar cell operation, including factors affecting their performance, types, and construction of flexible solar cells will be covered in Chapter III. The pros and cons of each will additionally be discussed.

Power storage device types and operation, including factors affecting performance, are explored in Chapter IV.

The purpose and operation of the various power integration devices required for this research including MPPTs, DC-to-DC Converters, and battery balancers are analyzed in Chapter V.

The construction and assembly of the individual subsystems into the completed system including the initial testing of solar cells before mounting and circuitry integration are detailed in Chapter VI.

System testing procedures and results including bench testing are thoroughly discussed in Chapter VII.

The results from testing are analyzed to predict changes in performance using computer models in Chapter VIII.

The conclusions of this research are summarized while also recommending avenues for future research in Chapter IX.

THIS PAGE INTENTIONALLY LEFT BLANK

II. SMALL UNMANNED AERIAL VEHICLES

A. SELECTION CRITEREA

The Defense Department has spent over $444 million dollars in the last five years on the Raven UAV program alone [13 and 14]. With potential rewards this rich, the Small UAV market is unsurprisingly flooded with prototypes seeking a slice of the budget pie. Since this research is focused on augmenting the power of a fielded military SUAV, the selections will be limited to those systems that are currently in use by the U.S. Department of Defense. While a purpose-built solar powered SUAV would certainly provide improved performance in the long run, the reason for this limitation is to simplify the research and development to an improved system derived from one that has already met defense requirements for ruggedness, frequency management, and cryptographic security. The objective of this research was to extend the endurance of the airframe using solar cells, with the ultimate objective to recharge the batteries of the system mid-flight. To meet these objectives, the selection criteria to be considered are in order of precedence:

- An electric power source that can be recharged. If the power source is not rechargeable or easily compatible with a direct current input, the addition of solar cells will not meet the ultimate goal of this research by recharging mid-flight.
- An original endurance that makes the augmented endurance a significant improvement in capability. If the endurance of the power source is extremely limited, it will be less likely to overcome impediments such as passing clouds, and the improvement in flight endurance may still be less than the original endurance of a competing system.
- A system with a wing surface area to support a significant solar cell array. Larger surface area can have an impact on the total input power to the system, the expense of the cells required to provide the power, as well as the flexibility in the arrangement of the array for performance and survivability. Wing surface area will be correlated to wingspan in this comparison.
- A system that has payload capabilities that complement the increased endurance. If the system has cameras with poor resolution or limited capabilities, the increased system endurance will have a less significant improvement in capabilities to the warfighter.

- A system that is available. It must be both available for testing, as well as fielded in numbers that would make the investment of resources worthwhile.

The following systems meet the first criteria of being currently fielded military SUAVs. Their history and capabilities will be described along with an analysis of their pros and cons including the above selection criteria.

B. POINTER

The AV FQM-151A Pointer, shown in Figure 5 and made by AeroVironment, has been in use by the Army and Marine Corps since 1988. It saw service in DESERT STORM, Afghanistan, and OPERATION IRAQI FREEDOM. This early SUAV has a large, 9 ft, wingspan, and can operate on rechargeable batteries with a maximum reported battery life of 90 minutes. The system can be fitted with a choice of color streaming video or infrared (IR) cameras as well as other atmospheric sensors [15].

Figure 5. The AV FQM-151 Pointer (from [15]).

Some drawbacks of this system are the weight and availability. A single system requires two packs weighing a total 55 lbs for a UAV and ground control station (GCS). Additionally, the system lands in a deep stall causing a controlled crash. While this system had a long period of service, as of 2005, the Defense Department reported only 50 Pointers left in service. The Pointer has since been replaced by the Raven and Puma SUAVs [15].

C. DESERT HAWK

Developed by Lockheed Martin, the Desert Hawk, shown in Figure 6, was originally purchased by the Air Force in 2002 and saw immediate service for base security in Afghanistan. This UAV has a 4.5 ft wingspan. The system is designed to work in teams of six aircraft supported by a ground control station [16].

The latest version, the Desert Hawk III available since 2007, has five different payloads that provide optical, IR, and illuminated cameras with 360 degree rotation. The latest version additionally has an endurance of 90 minutes on rechargeable batteries. While the system is designed to break up into nine pieces, the recovery is designed to occur as a gliding belly landing [16].

Figure 6. A Desert Hawk being prepared for launch (from [16]).

While the individual vehicle is lightweight, 7 pounds, the combination of 6 vehicles plus support equipment weighs as much as 520 lbs. The launching procedure for this UAV is also complicated, requiring a bungee cord launcher or moving vehicle to attain enough speed. Availability is also an issue. As of 2007, the DoD planned to hold onto only 18 systems (108 aircraft). The Air Force has replaced the Desert Hawk with the Raven B [16].

D. RAVEN B

The RQ-11 Raven B, shown in Figure 7, was developed by AeroVironment as a lightweight improvement on the Pointer and was first placed in service in 2003. The system has a wingspan of 4.5 ft, and operates in teams of three aircraft supported by a ground control station [17]. In 2009, an upgrade featuring a digital data link (DDL) was

fielded to improve control and security. The Raven B has become the standard Small UAV across the Defense Department.

As the standard Small UAV, the Raven B has been fielded in large numbers and continues to be purchased. In fiscal year 2013, the U.S. Marine Corps plans to purchase 13 suites [18], while the Army plans to buy 234 suites [19]. The acquisition objective for the Army alone surpasses 6,000 individual vehicles. The rechargeable batteries on the Raven have a maximum endurance of 90 minutes and the 4 lb aircraft can be launched by hand as illustrated in Figure 7. Additionally, the ground control unit is also more compact than its competitors at 17 lbs, increasing the accuracy of the man-portable moniker [17].

Figure 7. Launching the Raven B (from [17]).

Some disadvantages of the Raven system are the limited capabilities of the dual optical and IR payloads when compared with the pivoting cameras on competing systems; however, the existing payloads are still very capable. Also, the deep stall landing procedure limits the life expectancy of the system to 100 flights [17].

E. AEROVIRONMENT WASP

Not to be confused with a similarly named UAV from Massachusetts Institute of Technology, the AeroVironment Micro UAV has a 2 ft, 4 in wingspan and is shown in Figure 8. It was developed from Air Force requirements for air strike targeting and battle damage assessment. The Wasp works in teams of two aircraft and was placed in service beginning in 2007 in Iraq [20].

Figure 8. The AeroVironment Wasp (from [20]).

The Wasp is extremely lightweight, at less than a pound each, making the weight of a suite the best in class. This micro UAV also has high resolution optical and IR cameras capable of zooming and rotating on two axes. The system is also designed for a belly landing, increasing the endurance of the aircraft.

Despite the advantages of weight and advanced cameras, the smaller wingspan and short endurance of 45 minutes hinder its applicability for solar power. The system is primarily used by the Air Force, with 1,200 individual UAVs fielding in 2010 [20]. However, the Marine Corps also purchased 40 systems in 2011 [18].

F. PUMA

The RQ-20 Puma, shown in Figure 9 and also developed by AeroVironment, is the most recent addition to be considered. It was developed for Special Operations Command in 2008. The 13 lb launch weight and wingspan of 9 feet, 2 inches makes the Puma one of the largest hand launched systems [21].

Despite its size, the Puma possesses an impressive endurance of two hours. With the recent development of the system, the Puma contains advanced cameras for optical, IR and illuminated IR in a belly mounted turret that rotates on two axis and features a digitally stabilized image. The Puma additionally uses the same Ground Control Station as the Raven and Wasp [21].

Figure 9. The Puma being prepared for launch (from [21]).

Some disadvantages of the system remain. The individual weight of the system is three times heavier than a Raven, limiting its portability. The system, like the Raven, is also designed for a deep stall landing [21], which could impact the endurance of the aircraft and the potential solar cells attached to the wing. The novelty of the system also impacts its availability for research. In addition to purchases by Special Operations Command, the Marine Corps purchased 40 systems in 2011 [18].

G. CONCLUSION

From the options presented in this chapter, it can be seen that the majority of systems have an endurance of about 90 minutes. Most have a wing span either 4.5 feet or 9 feet, and as time passes, the capabilities of the available payloads have advanced. On paper, the Puma is the most capable candidate for solar power augmentation with a combination of large wingspan, high initial endurance, and advanced payloads. However, this cutting-edge system simply was not available for research at this time. The Raven B is a strong alternative due to its solid 90 minute endurance and widespread fielding across the services. Since the Raven is the small UAV of choice for the foreseeable future, an improvement on this system could potentially have far-reaching benefits across the Defense Department. An analog version of the Raven, before DDL upgrade, was provided by Naval Air System Command for use in this research.

While limiting the scope of this research to fielded U.S. military systems simplifies the process, the long term solution would ideally be a purpose-built system. That de-

sign would need to maximize the ability to absorb available sunlight while maintaining the same ruggedness, frequency management, and security specifications the military requires. The importance of surface area available for solar cells in the selection criteria will become more apparent in the next chapter, as the theory and constraints of photovoltaics are detailed.

THIS PAGE INTENTIONALLY LEFT BLANK

III. SOLAR CELLS

A. INTRODUCTION

The solar cell performance is based on many factors. First, a solar cell must operate in plentiful sunlight. Then those cells must be constructed of materials that effectively capture and transform that energy into electric current. Finally, those cells must be protected from factors that will degrade their performance. These factors are discussed in this chapter in depth, and comparisons between current cell technologies to select the correct type to use for this research are made.

B. AVAILABLE SUNLIGHT

Before being able to utilize sunlight for energy, we must first consider the amount of sunlight available and the power it contains. From Figure 1, it is apparent that the equatorial regions have more available energy from sunlight than the polar regions. The reason for this stems from the width of atmosphere sunlight must pass through before reaching the Earth's surface. This factor is defined by Air Mass (AM). Air Mass Zero (AM 0) is defined as the power available outside the Earth's atmosphere, 1353 Watts/meter^2, and is normally used for satellites. AM 1 is the energy available at the Earth's Surface with the sun at its zenith and is not generally useful for calculations of energy available as the sun moves throughout the day. Once an angle is considered, the additional path of the atmosphere further attenuates the available power. These angles corresponding to Air Mass are displayed in Figure 10. At an angle of 48.2 degrees, AM 1.5, the available power is 930 Watts/meter^2, which is commonly used for terrestrial applications outside the tropics and often rounded to 1000 Watts/meter^2 [22].

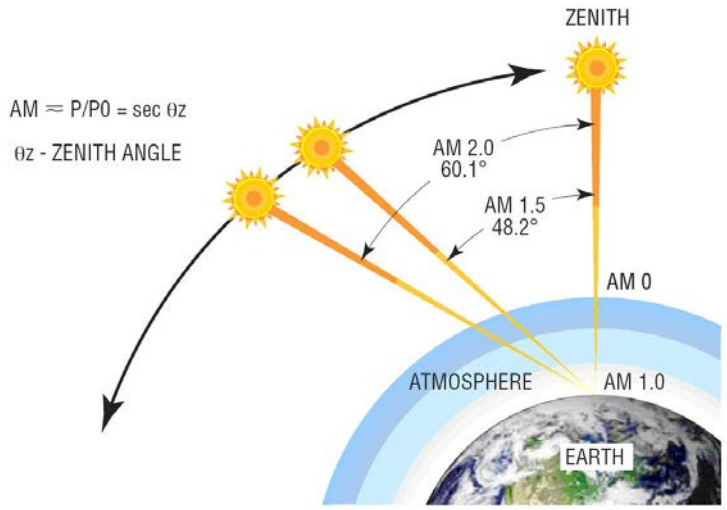

Figure 10. Air Mass indices with sun angles (from [23]).

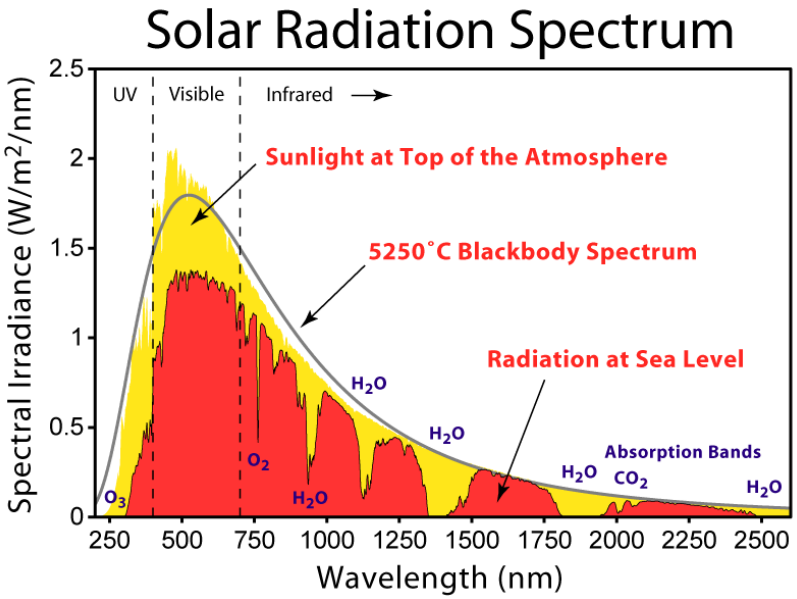

Figure 11. The solar radiation spectrum (from [22]).

The sunlight available at the Earth's Surface is composed of wavelengths beyond the visible spectrum. Figure 11 is a display of how those wavelengths form a generally round curve at AM 0. However, when solar radiation passes through the atmosphere, several distinct notches are created due, primarily, to water vapor and oxygen and, to a lesser extent, carbon dioxide and ozone [22]. This attenuation has an impact on the choice of

materials to utilize the available sunlight. The wavelength can additionally be related to the material's bandgap by the Planck relationship

$$E = \frac{hc}{\lambda} = \frac{1239.84187}{\lambda} \tag{3–1}$$

where the wavelength is expressed in nanometers and the solution E is the material's bandgap expressed in electron-volts [24].

C. PHOTOVOLTAIC THEORY

1. Introduction

Converting available sunlight to electric current is achieved by a chemical reaction caused by the collision of photons within a semiconductor and directed by the presence of a p-n junction. Photovoltaics all take advantage of this basic design, but the details are most easily explained using crystalline silicon or germanium as examples.

2. Semiconductors

Semiconductors are easily distinguishable from conductors and insulators by the energy required for an electron to pass from the outermost , valence, electron band of the atom to a free state in the conduction band. These energy levels are graphically represented on the band diagrams shown in Figure 12. Insulators have a band gap exceeding five electron-volts (eV), while conductors have no band gap, and semiconductors, logically, fall in between [25].

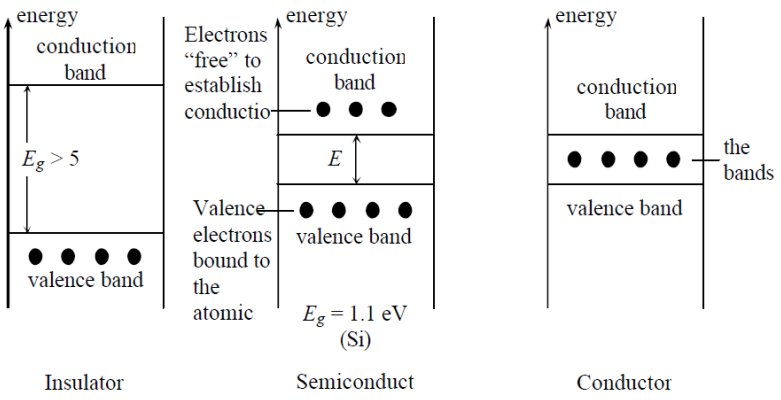

Figure 12. The energy bands of insulators, semiconductors, and conductors (from [25]).

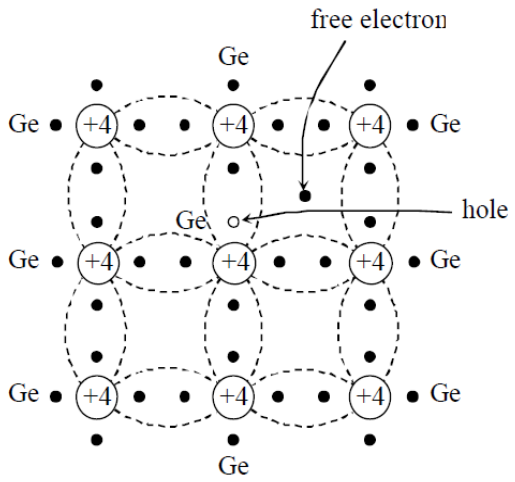

Figure 13. Intrinsic germanium crystalline structure (from [25]).

Semiconductors use covalent bonds to form stable, crystalline structures as shown in Figure 13. Each atom requires four valence electrons to complete the lattice. The lack of an electron is referred to as a “hole” and represents a positive charge to the electrons negative charge. Intrinsic semiconductors have an equal number of electrons and holes. When an element with a different number of valence electrons is added to the crystal lattice, an excess of either electrons or holes are created in the material. That excess of electrons or holes is represented in the band diagram as the material’s Fermi level. An element with more than four valence electrons is called an electron “donor.” Those excess electrons raise the Fermi level above the center of the band gap, and the material is called an “n-type” semiconductor. That Fermi level is shown as the dotted line in Figure 14. Likewise, an element with fewer than four valence electrons is called an electron “acceptor”, and the resulting material has more holes than electrons. An excess of holes lowers the Fermi level below the center, and the material is called a “p-type” semiconductor [25].

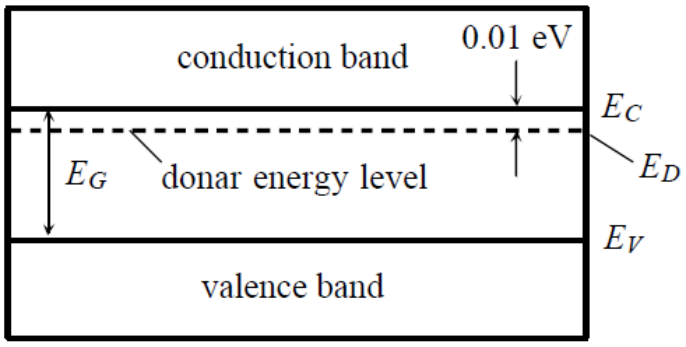

Figure 14. N-type semiconductor energy band diagram (from [25]).

3. P-N Junctions

When a p-type and n-type semiconductor are connected, the difference in the excess charges in each material causes a diffusion of the excess holes or electrons across the junction into the neighboring material. The diffusion across the boundary will end up in the recombination of electrons into holes on both sides of the junction. The diffusion of those charges builds to the point where the diffused charges form a local excess in the otherwise oppositely charged material. This area on both sides of the junction is called the depletion region. Similarly, the difference in charge on either end results in a "built-in-potential" or voltage difference in the junction. This is displayed in Figure 15 [25].

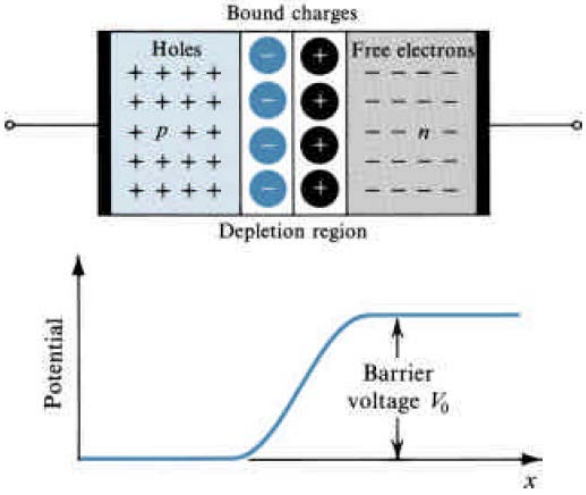

Figure 15. The depletion region and built-in potential (from [25]).

4. Solar Cells

When a photon with energy greater than the band gap of the material strikes an atom, it can free an electron from the valence band and creates an electron-hole pair in the semiconductor that did not previously exist, as shown in Figure 16. The electron has enough energy to reach the conduction band. Once in the conduction band, the presence of the p-n junction permits the electron to be swept downhill to the n-type side of the solar cell. The corresponding hole is swept uphill to the p-type side, indicating the direction of current in the solar cell [25].

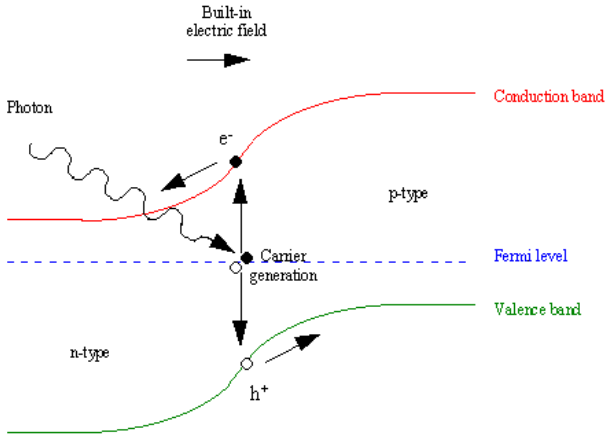

Figure 16. A photovoltaic band diagram (from [11]).

The current of an illuminated solar cell flows in the opposite direction of a forward biased p-n junction due to the internal generation of the electron hole pairs. Therefore, the characteristic current –voltage (I-V) curve of a solar cell is located in a different quadrant than a normal diode. This relationship is clearly shown in Figure 17.

The open circuit voltage is roughly similar to the junction's built-in potential, while the short circuit current is the maximum current available from the given sunlight conditions. The maximum power point occurs at the "knee" of the graph and is the point where the product of the cells operating voltage and current are greatest [26]. The current is shown as negative in Figure 17; however, future figures will use the more common I-V characteristics convention for solar cells with a positive current.

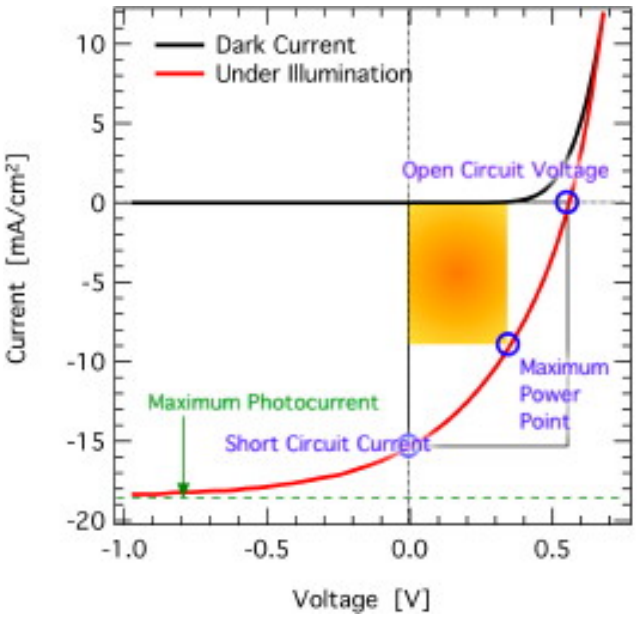

Figure 17. Light and dark diode characteristic curves (from [26]).

5. Solar Cell Construction

The order of the p-n junction for terrestrial applications is irrelevant to performance, though for consistency with the radiation resistance requirements of space, the vast majority of available cells have the n-type layer on top of the p-type material, also known as n/p (said “n-on-p”) [27]. The standard construction of a solar cell can be seen in Figure 18 and from bottom to top consists of a rear contact, a p-type semiconductor base, an n-type semiconductor emitter that is usually much thinner than the base, antireflection coating and front contact. When an electron-hole pair is created, in either the base or emitter, the electron is collected by the front contact and the hole is collected by the rear contact. Therefore, the conventional direction of current originates from the rear contact.

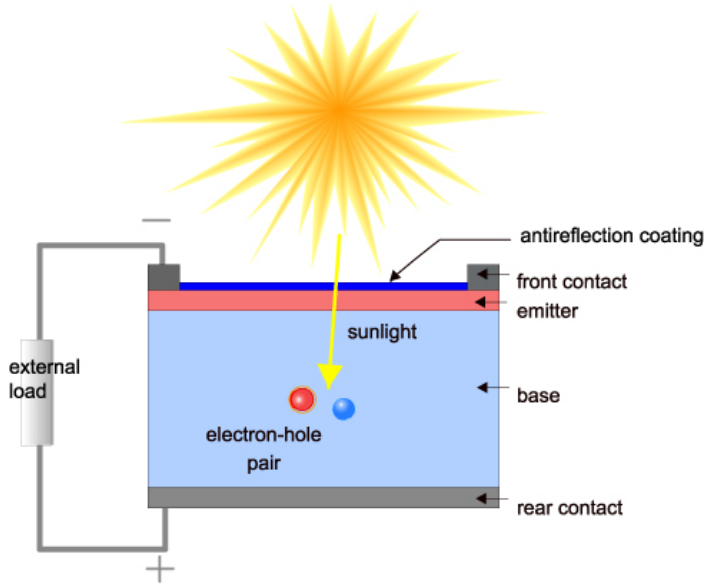

Figure 18. A diagram of typical solar cell construction (from [28]).

6. Solar Cell Calculations

The two most important calculations when considering solar cell performance are the Fill Factor, and Efficiency, each a measurement of the utilization of power with available resources.

The Fill Factor *FF* is defined by,

$$FF = \frac{I_{mp}V_{mp}}{I_{sc}V_{oc}} = \frac{P_{\max}}{I_{sc}V_{oc}} \tag{3–2}$$

and provides a means to compare the maximum power to the open circuit voltage V_{oc}, in volts, multiplied by the short circuit current I_{sc}, in amps. The calculation is essentially a measure of the sharpness of the knee described earlier in the I-V characteristic curve [25]. The difference between the theoretical maximum P_T displayed in Figure 19 as well as in the denominator of (3–2), and the maximum power point $P_{\max}$ of the I-V curve are graphically represented in Figure 19.

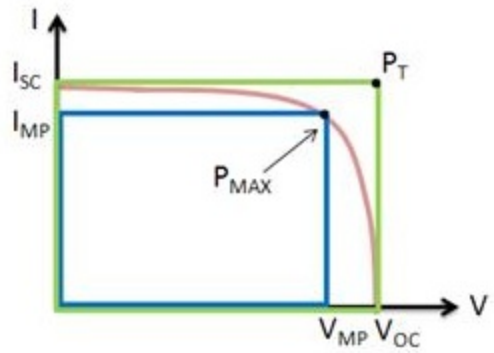

Figure 19. I-V curve with fill factor (from [29]).

The cell efficiency η_{cell} is given by

$$\eta_{cell} = \frac{I_{mp} V_{mp}}{P_{sun} A_{cell}} = \frac{P_{max}}{P_{in}} \tag{3–3}$$

and is a comparison of the maximum power point to the power from the available sunlight. The power from the incident sunlight P_{sun}, measured in Watts (W) per meter (m), multiplied by the surface area of the cell under investigation A_{cell}, measured in square meters [25]. Unless directly measured, we use a P_{sun} of 1000 W/m^2, or 100 mW/cm^2 (paired with a cell area calculated in square centimeters).

The output power of a cell is the most frequently used measurement of performance in the commercial market. However, care must be taken before using these measurements at face value. While the efficiency of a cell changes little between sunlight conditions, the greater concentration of sunlight available at AM 0, as seen in Figure 11, creates a higher current in the cell. Many companies use an unrealistic Air Mass measurement or do not reveal the Air Mass used. An accurate output power should reflect a relevant operating environment.

The previous examples used single cells. However, once multiple cells are placed in a circuit, additional calculations must be made. Cells placed in series add their individual voltages but are limited in current by the lowest current producer in series. Cells placed in parallel add their individual currents but are limited by the lowest voltage of an individual branch [25]. Therefore, the maximum power and efficiency calculations for a

solar array are best completed with the limiting factors of the array design taken into consideration and not simply adding the individual cells.

D. FACTORS AFFECTING PERFOMANCE

The ideal performance of a solar cell can be undermined by many factors. The source of those losses may be materials, design, or poor implementation. Those causes manifest themselves as a loss of available light, heat, corrosion, recombination, and resistance within the cell. The result of all these factors is a drop in the maximum output power of the cell.

1. Loss of Available Light

The antireflective coating mentioned in Figure 18 is critical since any light that reflects off of the cell's surface is not able to create an electron-hole pair. A greater degree of absorption is achieved by creating a textured, angular, surface that remains transparent. The angled surface, shown in detail in Figure 20, directs reflected light to another part of the surface of the cell to have a second chance to penetrate into the body of the cell. Texturing alone is shown to increase the efficiency of a cell approximately 8% [27].

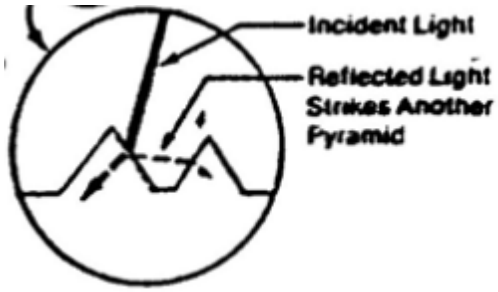

Figure 20. Detail of textured surface (from [25]).

The front contacts noted in Figure 18, when made of metal, create an opaque area that prevents light from entering the cell and creates "self-shading." For this reason the contacts are made as thin as possible. Another option is a transparent conductive layer that is discussed further when cell types are compared.

The direction of sunlight also affects the incident power on the cell. The maximum sunlight is incident when the sun is at an angle normal to the surface of a cell. Any

deviation from that normal incidence reduces the incident power to a cosine of the angle from normal. For this reason, the solar cells are limited to the horizontal surfaces of the aircraft.

Any reduction on the light entering the cell reduces the output current and decrease the output power. Therefore, cells are designed and installed to reduce external reflections, self-shading, and offset angles.

2. Heat

Heating of a cell is commonly caused by incident photons that have an energy different than the band gap of the material. Photons with less energy than the band gap cannot create an electron-hole pair that can be utilized for electricity and instead have the energy transferred to heat. Photons with a larger band gap than the cell material create a electron hole pair that can be used, but the excess energy also creates heat within the cell. The result of cell heating is a decrease in the voltage of 2 millivolts per Celsius rise in each solar cell. The movement of the open circuit voltage moves the maximum power point of the I-V curve and decreases cell efficiency [25]. The effects of heat can be mitigated by selecting materials that operate in a bandwidth that closely matches the available light in Figure 11 and selecting array designs that minimize the numbers of cells in series. Another method is to cool the cell. Fortunately, for this application, the movement of air over the wing during flight should significantly contribute to heat dissipation.

3. Corrosion

The presence of humidity on metal contacts has been shown to cause corrosion. The long term effect of this corrosion results in mechanical failure of the connection between the contacts and the emitter. For this reason solar cells in terrestrial applications are encapsulated with a clear cover to protect them from humidity [30].

4. Recombination

Once an electron-hole pair is created in the cell, it must travel across the depletion region before finding a contact. Defects in the semiconductor crystal lattice can create opportunities for electrons to re-enter the valence band, or recombine, before entering the

front contact. Those defects can be caused by impurities during production and damage during handling. Additionally, some inexpensive cells are made of multi crystalline silicone that is much cheaper to grow than mono crystalline cells. However, the numerous grain boundaries found in the cells present many material defects and opportunities for recombination [31]. The effect of recombination is a loss in efficiency in the cell since a electron-hole was made but could not be utilized. Recombination can be reduced by creating both thin n-type top layers, known as shallow junctions or blue cells, and by heavily doping the rear of the cell, known as a back surface field. Both of these procedures cause the electron-hole pair to move more quickly to their respective contacts before recombination can occur [25].

5. Resistance

Internal to the cell are series and shunt parasitic resistances. Ideally, the series resistance should be zero, while the shunt resistance should be infinite. However, when those resistances deviate from the ideal, the slope of the I-V curve is affected. Figure 21 is an illustration of the effects of a small increase in series resistance, which dramatically degrades the slope from the open circuit voltage, while a decrease in shunt resistance degrades the short circuit current side of the I-V curve, respectively [30]. It is apparent, from Figure 21, that the changes in resistance affect the fill factor of the cell and significantly reduce the maximum output power available.

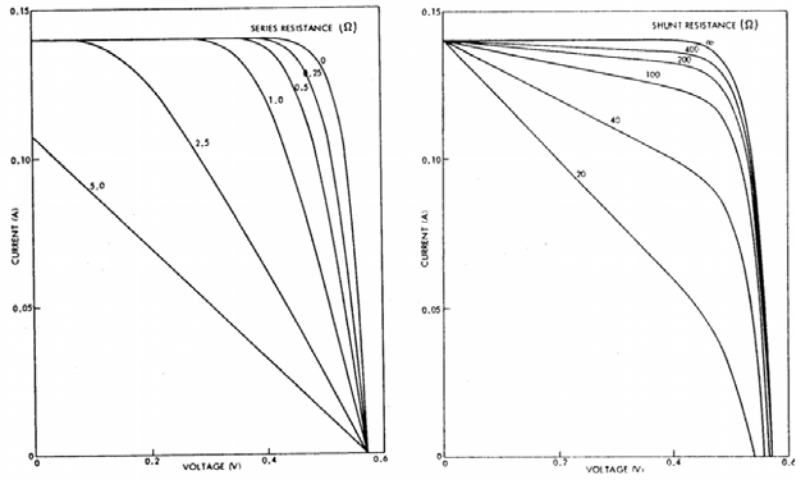

Figure 21. Series and shunt resistance effects on I-V curve (from [25]).

One of the sources of series resistance are the contacts. Therefore, a balance must be made between thicker front contacts with lower resistance and the self-shading that thick contacts would create.

E. FLEXIBLE CELL TECHNOLOGY

While the operating principles and basic design remain similar to the examples previously discussed, an increasing number of solar cells are being designed with materials and in thicknesses that decrease weight and allow the cell to flex without breaking or damaging the cell. Some of these cells are used in solar "blankets" discussed in Chapter I. However, the flexibility also allows much larger cells to conform to the airfoil of a SUAV. Larger cells will provide a larger current per cell, as well as decrease the wiring required which can contribute to extra weight, series resistance and losses in the array. Some options in the flexible cell market are explored in this section. The options include amorphous silicon, cadmium telluride, copper indium gallium selenide (CIGS), and epitaxial lift-off cells. In Figure 22 we can see how these technologies all show steady improvement in efficiencies over the last three decades. However, these numbers are single examples made in a lab environment and are not likely to be immediately available in large production or without great expense.

One of the reasons for the disparity of efficiencies between the technologies is the spectrum that the respective materials operate in. Recalling the sunlight spectrum in Figure 11, we see illustrated in Figure 23 the efficiency for each competing technology relative to the available sunlight. The output power of the cell is represented by the area under the cell's curve that falls within the available sunlight. Hence, crystalline silicon cells have a higher efficiency than amorphous silicon because more area of the light spectrum is found under its curve.

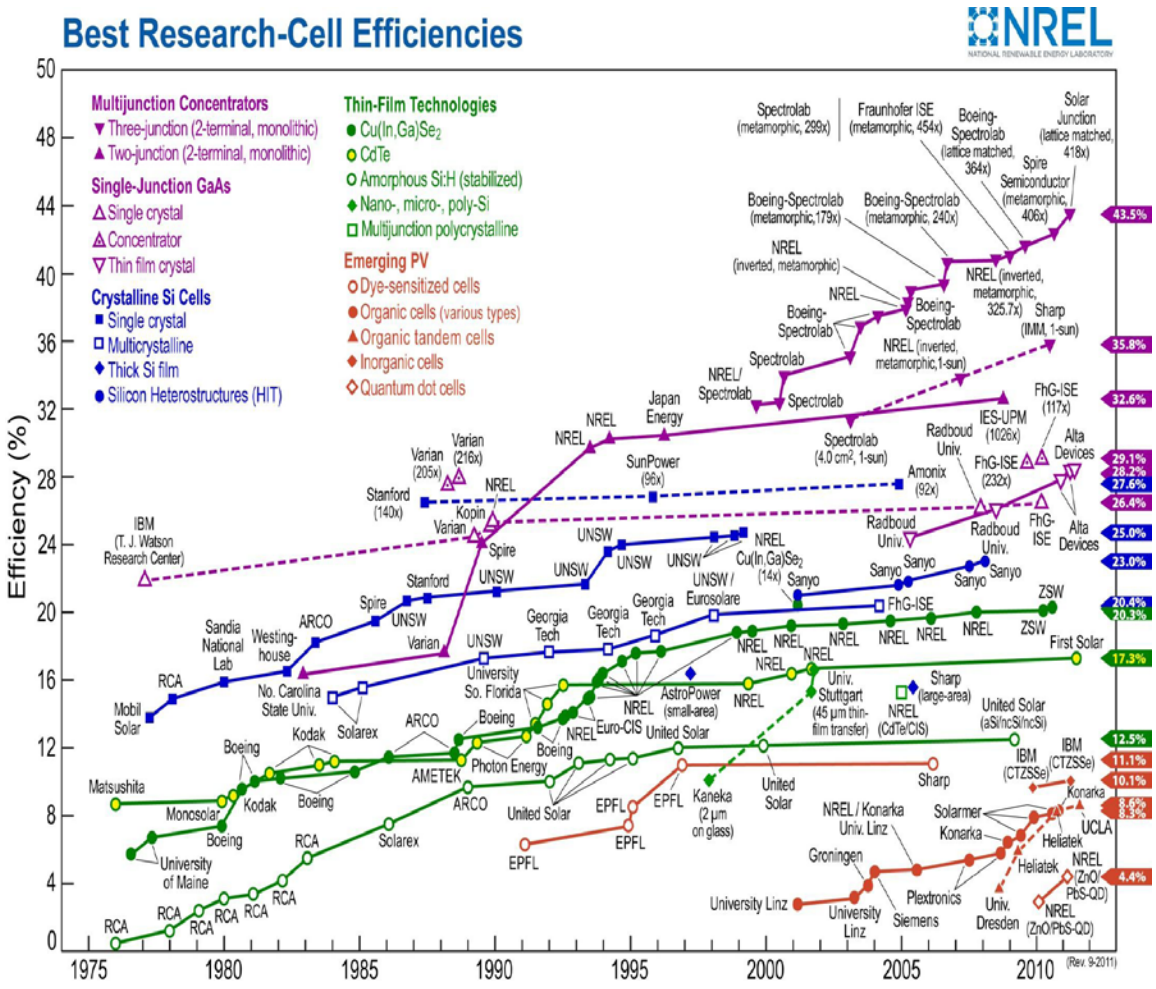

Figure 22. Best research-cell efficiencies through 2011 (from [32]).

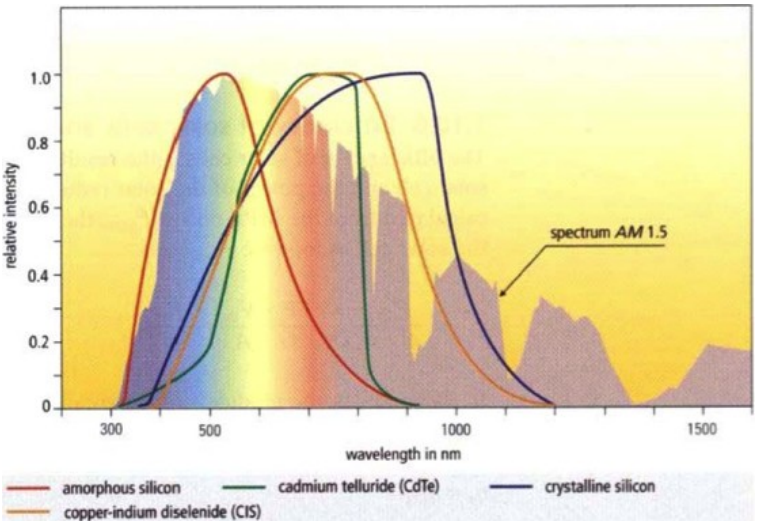

Figure 23. Frequency response of thin-film cells and crystalline silicon (from [33]).

1. Amorphous Silicon

Amorphous silicon differs from crystalline silicon, because the gas deposited material does not form a normal crystal lattice. Instead, due to the current processes, hydrogen atoms fill many of the bonds. Thus, the cells are often called hydrogenated amorphous silicon, or Si:H [34].

Amorphous silicon has several advantages over crystalline silicon. At a comparable cell thickness (0.3–0.7 microns), amorphous silicon has 2.5 times higher efficiency than crystalline silicon. Additional advantages include a decrease in raw materials required to fabricate cells, as well as lower temperatures required to produce them (less than 300 C compared to over 1000 C for crystalline Si) [34]. These properties decrease the overall cost of production.

Despite those advantages, the efficiency of amorphous silicon still lags behind its competition. The highest recorded efficiency was 12.5% in 2011 (from Figure 22). An additional disadvantage to the presence of hydrogen in the crystalline structure is a behavior known as the Stebler Wronski effect. It is believed that exposure to light frees some of the hydrogen atoms and leaves "dangling bonds." The effect lowers efficiencies of the cells before stabilizing after 1,000 hours of illumination. One potential fix for this problem is replacing hydrogen with fluorine, which is more stable, during deposition [34].

2. Cadmium Telluride

Cadmium telluride (CdTe) cells are named for the base layer of the junction with Cadmium Sulfide making the emitter layer, as shown in Figure 24. CdTe cells are probably best known for the First Solar, rigid panel, designs that are nearing the sale price of $1 per Watt [35]. Those cells, which are encased in glass panels, have achieved 17.3% efficiency shown in Figure 22. The two main flexible designs incorporate either a metallic substrate forming the back contact or a polymer substrate that forms a transparent window for the front of the cell, and the last layer added in production is the metallic back contact, essentially making the cell manufactured upside-down.

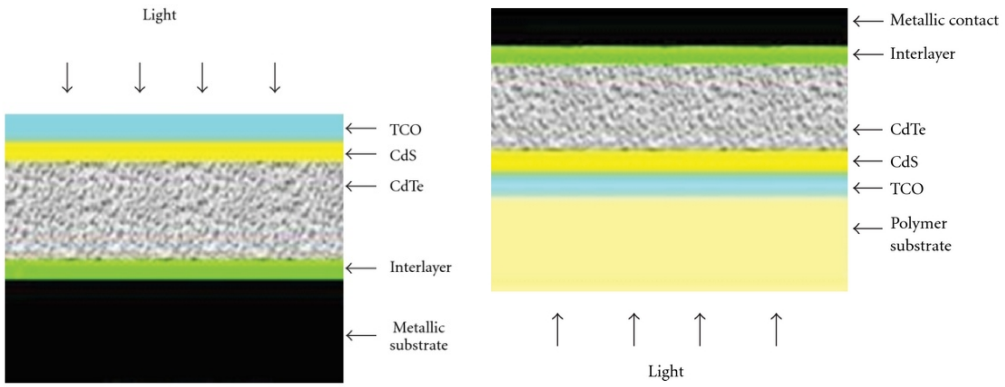

Figure 24. CdTe flexible cell designs: substrate (left), superstrate (right) (from [36]).

The highest recorded efficiency for flexible CdTe cells was 13.8% with a superstrate design. Substrate designs lag behind in efficiency with only 7.8% using metallic foils. The limit in efficiency for both designs is due to poor connections with the back contacts. One additional advantage of the lower efficiency, metallic substrate, designs is the availability of a low cost process using roll-to-roll manufacturing [36].

Despite the increased efficiency over amorphous silicon, CdTe cells have some disadvantages. The thickness of the emitter layer is inversely proportional to the efficiency of the cells. However, the processes must be improved to produce consistently thin layers without pitting [36]. Also, the cadmium used in both the base and emitter of the cell is known to be toxic, requiring care in the manufacturing, handling, and disposal of cells [35]. Finally, the tellurium (Te) in the base material is also a rare earth metal that can be subject to shortages and price swings without development of better collection techniques [32].

3. CIGS

Like CdTe, CIGS cells are named for the base material of the cells. Shown in Figure 25, the substrate can be formed by many thin flexible materials, while the back contact is normally composed of molybdenum. The zinc oxide (ZnO) layer serves as both the emitter and a transparent front contact through aluminum doping. Between the emitter are a CdS layer to form a buffer along with a thin layer of intrinsic ZnO [37].

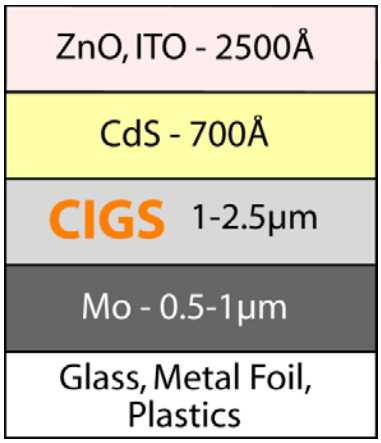

Figure 25. Typical CIGS cell construction (from [32]).

CIGS cells have a clear advantage in efficiency over their thin-film competition. From Figure 22, their maximum measured efficiency in 2011 was 20.3%. The cells, like CdTe, can also be quickly produced using roll-to-roll processes at speeds of 100 feet per minute, shown in Figure 26 [32].

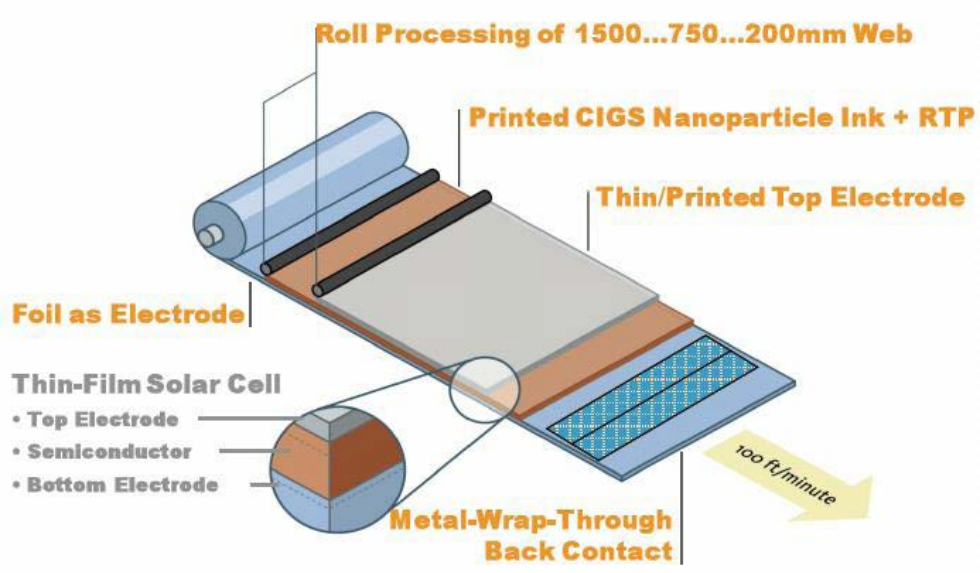

Figure 26. Roll-to-roll CIGS cell production (from [32]).

CIGS cells still have some disadvantages. Like CdTe, CIGS have some cadmium in the buffer layer, however far less than CdTe. Additionally, the extra layers and elements involved in manufacturing increase the production complexity. That increased

complexity is not enough to prevent some companies such as MiaSole from producing 13.5% efficient cells at 80 cents per watt like the one shown in Figure 27 [32].

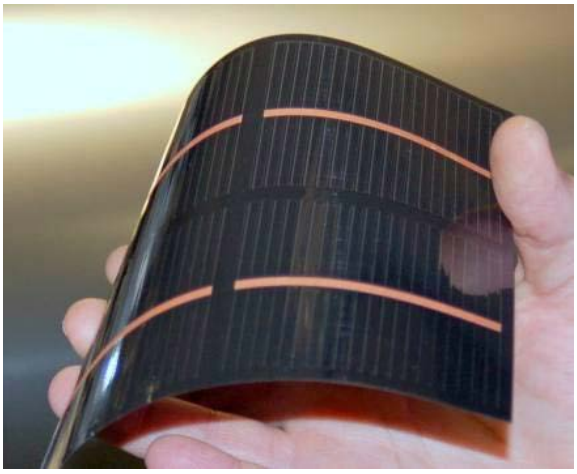

Figure 27. CIGS cell produced by MiaSole (from [32]).

4. Epitaxial Lift-Off

Epitaxial lift-off is a method to produce thin, flexible, cells on a thicker wafer and then release the cell from the wafer before completion. Companies such as MicroLink Devices have used this method to create crystalline solar cells with extremely high efficiencies. Their method deposits the material by chemical vapor deposition on a reusable gallium arsenide wafer. A release layer is the first layer placed on the wafer, followed by the cell itself built up in reverse order, with the back contact structure placed last. The release layer is removed to free the cell, before the cell is flipped and the front contacts are added. This process is illustrated in Figure 28 [38]. This method has been used to produce flexible cells that boast efficiency as high as 31%.

The design that achieves such high efficiencies is known as a multi-junction cell. Multi-junction cells vertically stack varying p-n junctions with increasing band-gap in the higher layers. With this method, the lower band-gap photons, which normally only create heat in the top cells, have the opportunity to pass to another material and make a usable electron-hole pair. The cumulative effect of the cell is an addition of the open circuit voltage, while the cell is limited in current to the lowest producing cell, similar to those same cells in series without the increased surface area [25]. The materials used by Mi-

croLink Devices and their respective spectral responses are shown in Figure 29 to illustrate the band-gap methodology.

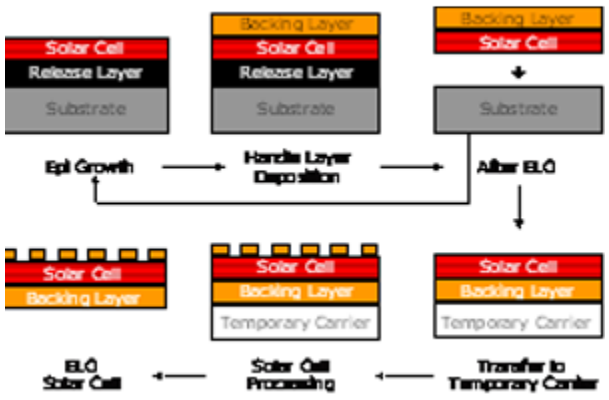

Figure 28. MicroLink Devices epitaxial lift-off process (from [38]).

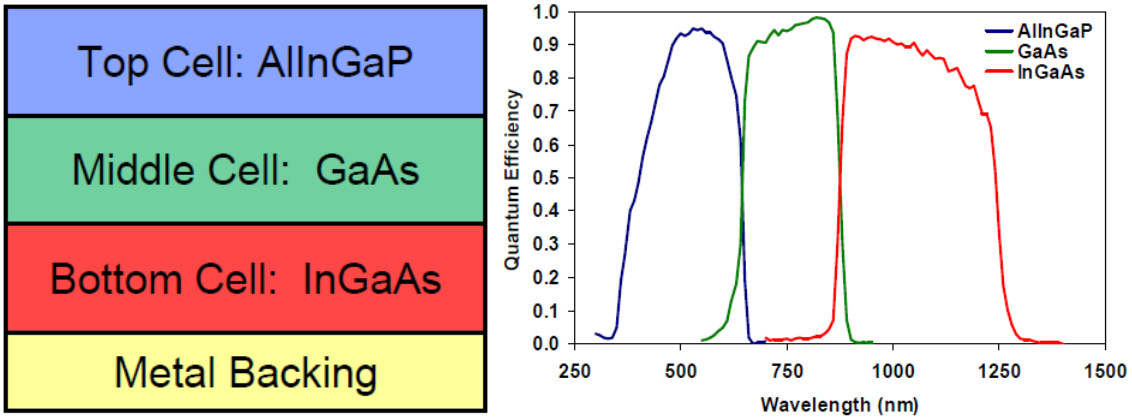

Figure 29. MicroLink triple-junction cell design and spectrum response (from [39]).

While the increased efficiency over thin-film cells is attractive, that performance comes at a price. The thickness of these multi-junction cells is listed as less than 40 microns [39]. That thickness is nearly ten times thicker than comparable CIGS cells, with only a 50% increase in maximum efficiency. That thickness increases the weight to the system. Additionally, the increased volume of materials and number of process steps required for production has an associated increase in cost.

F. CONCLUSION

Effective use of photovoltaics requires a combination of independent but critical factors. First, the sunlight available should be abundant. The cells should be deployed to capture that incident light at an angle that is as near to normal as possible. The cells should be designed to operate in the same spectrum as the incident light, and the cells should be configured to take advantage of their voltage and current properties to meet power requirements. Of the available solar cells, CIGS cells provide the greatest efficiency for their cost and weight. From Figure 22, we can see that this determination is a snapshot in a constantly changing field. Future advances in technology may increase the efficiency of solar cells or reduce cost to a point that would make them a more attractive option to collect power. Once that power is collected, it must either be directly utilized or stored for future use. In the next chapter, another degree of complexity is added in the system by illustrating the importance of battery technology in determining the power requirements and design of a solar array.

IV. BATTERIES

A. INTRODUCTION

The energy storage component of the UAV was established as a critical element in the overall performance of the system in Chapter II. The importance of energy storage applies to the original design and is even more important to the design of a modified system. The scope of the research was further narrowed in Chapter II to rechargeable batteries. The Lithium Polymer batteries currently used in the Raven B, including handling instructions, as well as competing technologies under development and their pros and cons are examined in this chapter.

B. LITHIUM POLYMER BATTERIES

1. Description

Lithium polymer batteries are an improvement of standard lithium ion batteries. Lithium ion batteries used a metal can to contain the liquid electrolyte. However, the solid polymer electrolytes used by lithium polymer batteries allows a much lighter and durable packaging within a smaller volume. The construction of a lithium polymer cell is shown in Figure 30 [40].

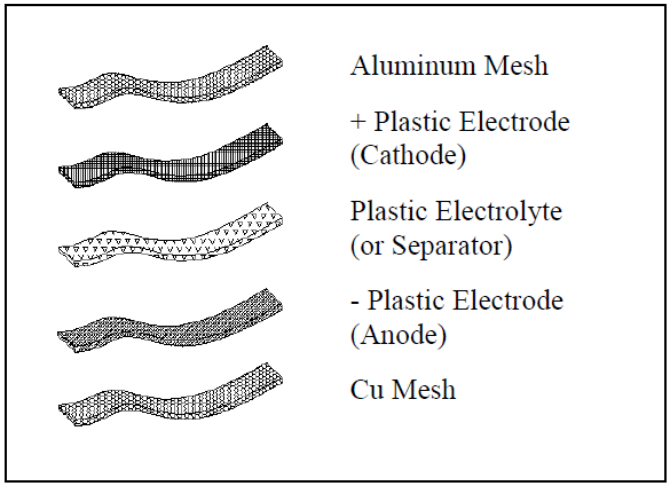

Figure 30. Lithium polymer cell construction (from [40]).

2. Handling Instructions

Lithium polymer cells operate from a low voltage of 3 Volts (V) to a maximum charge of 4.2 V per cell. However, the cells are generally characterized by a voltage of 3.7 V per cell. Therefore, battery packs of composed of several cells in series are characterized in multiples of 3.7 V, with the low and high voltage parameters following suite [40].

An advantage of Lithium Polymer batteries over other batteries is that they do not suffer from the memory problems from charging and discharging [10]. However, due to the low and high voltage characteristics, the cells cannot be deep cycled or trickle charged above the threshold voltage. For these reasons, lithium polymer batteries should never be charged using nickel metal hydride or nickel cadmium battery chargers [41]. Low voltages can permanently damage a cell, while high voltages can cause an explosion or fire. When charging a lithium polymer battery, the initial current can be near 1 Ampere (A), however, once the voltage gets near 4.2 V, the current should drop near 3% to complete charging [40].

Lithium polymer cells used in series do not discharge at the same rate. For this reason it is critical to use a balancer when charging. A balancer will check the voltage on each cell to ensure that the maximum charge of 4.2 V is not exceeded as each individual cell is charged. Otherwise, unbalanced cells could be overcharged to bring the pack up to its maximum voltage, with possibly disastrous results [41].

Temperatures also play a role in the charging and discharging of lithium polymer batteries. The capacity of batteries during discharge drops below 90% at 0 C and 70% at −10 C. Fortunately, in solar cell applications, most temperatures will likely be above freezing. Additionally, charging should be conducted between 0-45 C [40]. While some likely operating environments will reach the limits on the ground, the airflow over the plane during flight will provide some cooling effects.

3. Raven B Battery

The Raven B Operator's Manual and packaging list the Lithium Polymer batteries powering the air vehicle list the maximum voltage at 25.2 V. By simple division, the pack

should contain six individual cells. The ground control station alerts the user to low voltage in the battery at 21.9 V, allowing 10–15 minutes to land the craft [42]. The listed low voltage on the battery is 21 V. Dividing the low voltage by six provides the low voltage of each cell at 3.5 V, giving a healthy buffer from damage due to low voltage. The battery case additionally lists the battery capacity at 4 A-hours, which will factor into later calculations. Another benefit of the lithium polymer battery for the air vehicle is that it can use the same charger as the ubiquitous BB-2590, which powers the ground control station as well as many tactical radios. That interoperability reduces the weight requirements of the suite and provides the ability to interchange chargers and batteries with other common tactical equipment.

C. DEVELOPING TECHNOLOGIES

1. Lithium Sulfur

Lithium sulfur (Li-S) batteries have demonstrated, in a lab environment, a significantly higher energy density than lithium polymer technology as shown in Figure 31. Additional benefits due to research by companies like Scion Power have developed designs that short or stop current flow to prevent overcharging and discharging, respectively, without the use of circuitry [43].

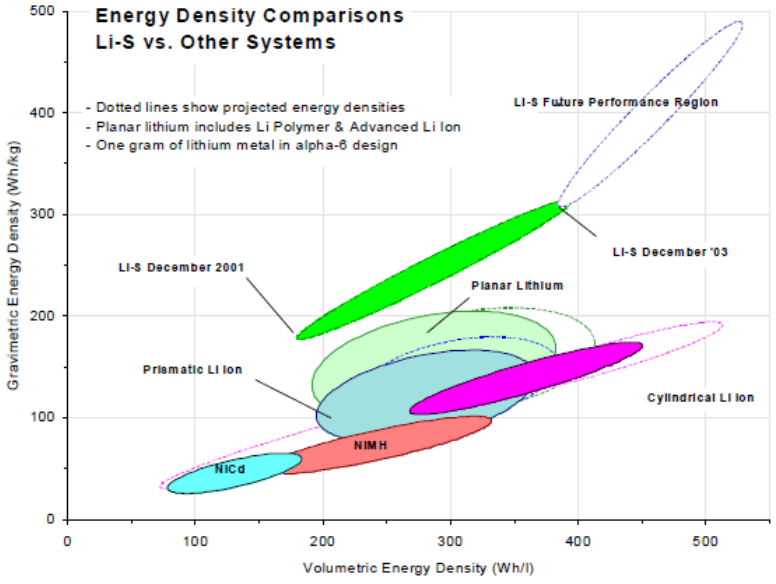

Figure 31. Energy density comparison including Li-S (from [43]).

While the sulfur itself is inexpensive, without advanced designs, these batteries suffer from degradation over many charging cycles. However, recent studies by Stanford University have shown that introducing graphene into the cathode improves the performance by limiting degradation to 10% after 100 cycles. The remaining energy density represents a performance significantly greater than current lithium polymer technology [44]. The ability to reliably produce these results outside the lab will likely lead to greater commercial availability in the future.

2. Lithium Air

Lithium air is another battery technology that, in a lab environment, has demonstrated energy densities several times greater than lithium polymer batteries. The battery operates by separating oxygen from the outside air to create lithium peroxide [45]. The challenge with this design is preventing water from reaching the highly reactive metallic lithium [46] as well as producing pure lithium peroxide in order to prevent degradation. Using a porous gold cathode, University of Waterloo researchers have developed a lithium air battery with only 5% degradation after 100 cycles [45]. Predictions for the energy density of this technology range from 800–1300 W-hours/kilogram (4–6.5 times current lithium polymer batteries). However, a commercial product is not expected any time soon [46].

D. CONCLUSION

Lithium polymer batteries are the most mature battery technology available on the market. They are also the batteries currently used in the Raven B as well as the most common rechargeable battery technology currently used by the military. These batteries are both light weight and lack memory from charge/discharge cycles. However, they require care to not overly charge or discharge the battery, including a requirement to balance the cells when charging. These requirements frame the decisions for circuitry design in the next chapter that form the interface between the solar array and battery.

V. INTERFACE CIRCUITRY

A. INTRODUCTION

The circuitry that interfaces the solar panel and battery are critical to ensuring that the maximum power is safely delivered according to the specifications of each. The characteristic curve of the solar array, as well as the operating voltage range of the battery and its individual cells are the primary drivers of these decisions. The operations of maximum power point trackers, boost converters, and battery balancers as they relate to this research are discussed in this chapter.

B. MAXIMUM POWER POINT TRACKER

The characteristic curve discussed in Chapter III is only a snapshot in time of the operation of a solar array. As variables change such as solar intensity, incidence angle, temperature, and internal resistances, the knee of the characteristic curve changes. Changes in the knee occur both continuously throughout the day, and larger, permanent changes in performance over time. An MPPT uses software or other means to seek the knee and constantly deliver power from that point.

Figure 32. GENASUN MPPT used in previous theses (from [47]).

Previous theses used MPPTs from GENASUN, shown in Figure 32. The GENASUN MPPTS came tuned from the factory when ordered and performed with satisfactory results [11]. Another MMPT discussed in [12], but not used, was the SPV1020 from ST. Both MPPTs find the knee by sampling the power over a range of voltages several times per second; however, the GENASUN samples 15 times per second [47], while the ST unit samples 390 times per second [48]. During sampling the circuit is broken momentarily to sample the current and determine the input power which creates minute losses across the MPPT. Both panels utilize a built-in boost converter, of which the input and output voltages are the parts requiring tuning. The SPV1020, however, comes mounted on an AN3392 evaluation board that can be tuned by the user. The SPEV1020 was selected mainly because the solar array designs had changed significantly since the previous testing. However, the board was also attractive because of its higher sampling rate and as another element to evaluate in this research. The ST AN3392 unit used in this research is shown in Figure 33. The ST evaluation board also features blocking diodes to ensure current cannot reverse direction across the board. The makers advertise the error from the maximum power point to be within 0.2% and the overall efficiency of the board at up to 98%, depending on tuning [48].

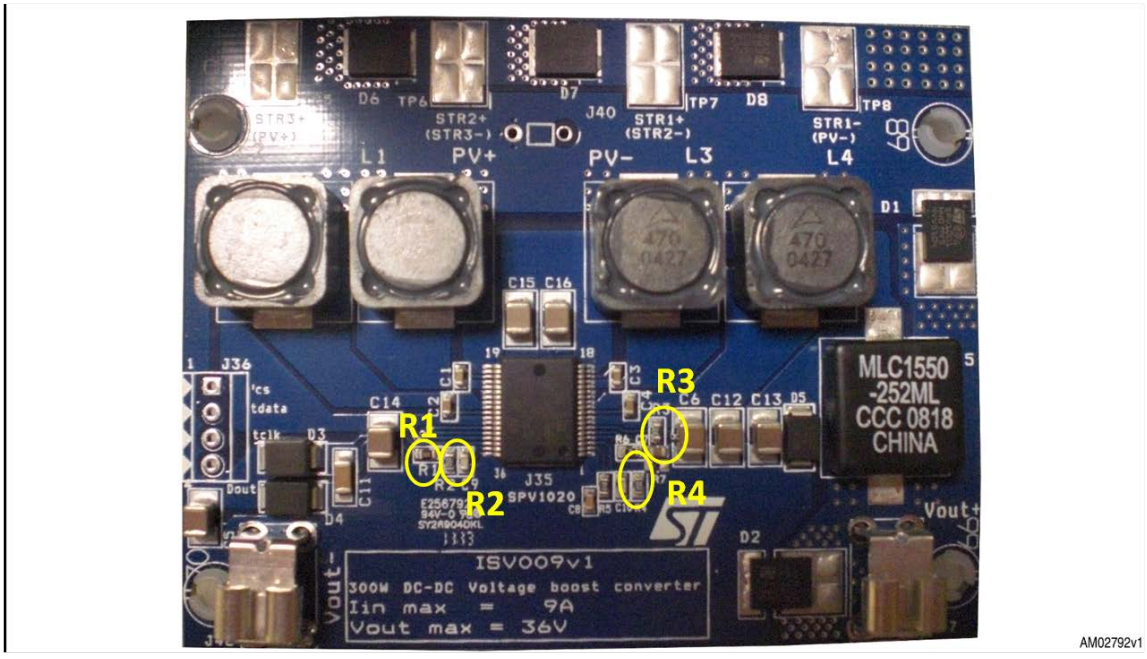

Figure 33. The ST AN3392 evaluation board used during research (from [48]).

C. BOOST CONVERTER

A boost converter produces a constant voltage on the output that is higher than the input voltage. A boost converter operates using a switch with inductors and capacitors to multiply the input voltage while proportionately dividing the current to maintain power across the circuit with only minor losses. The constant output voltage is maintained by varying the duty cycle of the switch to operate at the correct multiple of input voltage [49]. In this board, the duty cycle is controlled automatically. However, the input and output voltages are tuned by replacing resistors on the board highlighted in Figure 33. The general boost converter circuit design for the ST evaluation board is displayed in Figure 34 with the input voltage on the left and increased output voltage on the right.

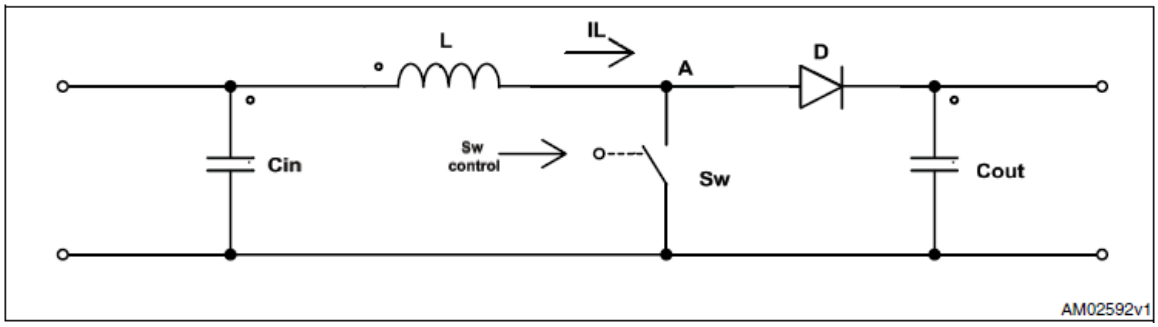

Figure 34. ST evaluation board boost converter circuit design (from [48]).

The tuning resistors *R1*, *R2*, circled in Figure 33, are related to the input, open circuit voltage V_{oc} by

$$\frac{R1}{R2} = \frac{V_{oc}}{1.25} - 1 . \qquad (5\text{–}1)$$

The resistors *R3* and *R4*, also circled in Figure 33, are related to the maximum output voltage $V_{out\_\max}$ by

$$\frac{R3}{R4} = V_{out\_\max} - 1 . \qquad (5\text{–}2)$$

The bill of materials provided with the evaluation board listed the board as initially tuned for an open circuit voltage of 30 V and an output voltage of 36 V with the resistor values listed in Table 1.

Table 1. Resistor values from ST evaluation board bill of materials (from [48]).

Resistor	Value (Ohms)
R1	3.3 M
R2	110 k
R3	3.9 M
R4	110 k

The boost converter and evaluation board are additionally limited to an output voltage of 40 Volts, input voltage of 5 V to charge, and 9 A maximum input current.

D. BATTERY BALANCER

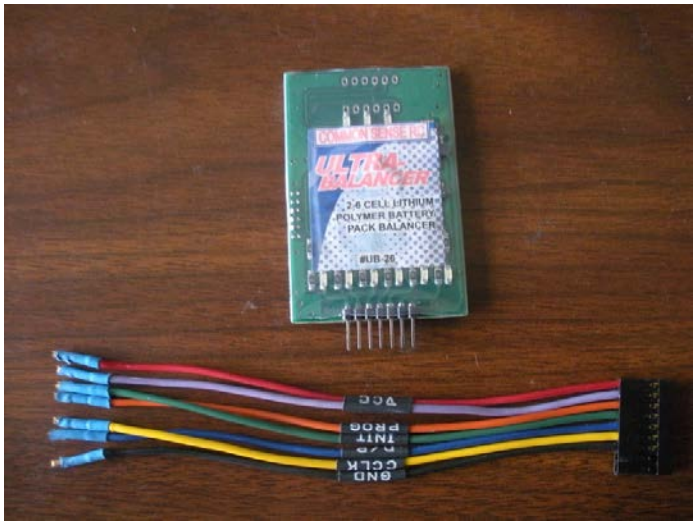

Figure 35. Ultra-Balancer and associated cables used in testing.

The final additional piece of circuitry required to operate with multiple cell lithium batteries is a battery balancer. Battery balancers plug into the charging ports of the lithium battery and repeatedly measure the voltage across each individual cell. The circuitry then compares the voltages, and if one cell is above the lowest voltage cell, it discharges the excess charge at a rate of 150 mA until the cells have equal voltage[50]. The circuitry is important in this application to ensure that, if the panel is expected to charge the battery at low throttle positions, it needs to be done in a balanced manner. If one cell reaches 4.2 V before the others, it prevents further charging of the battery. The same Ultra-Balancer from Common Sense RC used in previous theses was selected for this research due to its light weight and proven track record. The display on the Ultra-Balancer

lights a light emitting diode when a cell is being discharged. The display additionally indicates the voltage ranges of individual cells, with demarcations at 4.15 V, 3.7 V, and 3.2 V, to indicate the recommended speed of charging. The Ultra-Balancer used in testing, with its associated cables, are shown in Figure 35.

E. CONCLUSION

The components that interface the solar cells with the battery and load need to be carefully chosen to meet the requirements of each end of the equipment string while ensuring the maximum power is delivered to the load. The same battery balancer used in previous theses is used here. However, the combination MPPT and boost converter use the previously untested ST AN3392. The reason for the change was a desire for flexibility and as an additional variable from previous testing. The additional design decisions that went into tuning the ST board to interface the final solar array and equipment string are discussed in the next chapter.

THIS PAGE INTENTIONALLY LEFT BLANK

VI. ASSEMBLY

A. INTRODUCTION

Once the major pieces were selected for testing, they needed to be assembled and tuned for connection into the final equipment string. In this process, the flexibility offered by the ST evaluation board MPPT was very useful when changes were made to the initial design of the solar array. The process began with construction of the wing before mounting the final solar array on it. The MPPT was then tuned to operate with that solar array, and the battery balancer was connected to the battery. Finally, the separate subcomponents were connected into the complete equipment string for testing.

B. WING

Of the previous theses addressed in the first chapter, none utilized an actual Raven airfoil when mounting their arrays for testing. The closest to mimicking the wing was Reference [11]. However, the flat, angular design of the homemade airfoil not only poorly mimicked the curvature of an actual Raven but also prevented proper flight in testing.

Figure 36. Cross-sections of Raven wing above purchased wing.

For this thesis, it was decided to purchase a foam wing online that possessed an airfoil similar to that of a Raven. The cross section of the purchased wing can be seen next to a Raven wing in Figure 36. The wing design was, however, modified to mount an array the same size as the one tested in Reference [12]. The original Raven wing, shown in Figure 37, has a wingspan of 129.8 cm and width of 20.5 cm. The cord length of the center, alone, will not hold the 21 cm wide cells. Additionally, the wingspan will not hold 16 cells that were 10 cm each with 0.3 cm spacing between. To allow 0.3 cm connections on each end, a minimum wingspan of 165.1 cm is necessary. Therefore, wings were purchased that had a cord length of 22.5 cm and wingspan of 180 cm which could be trimmed as necessary during assembly.

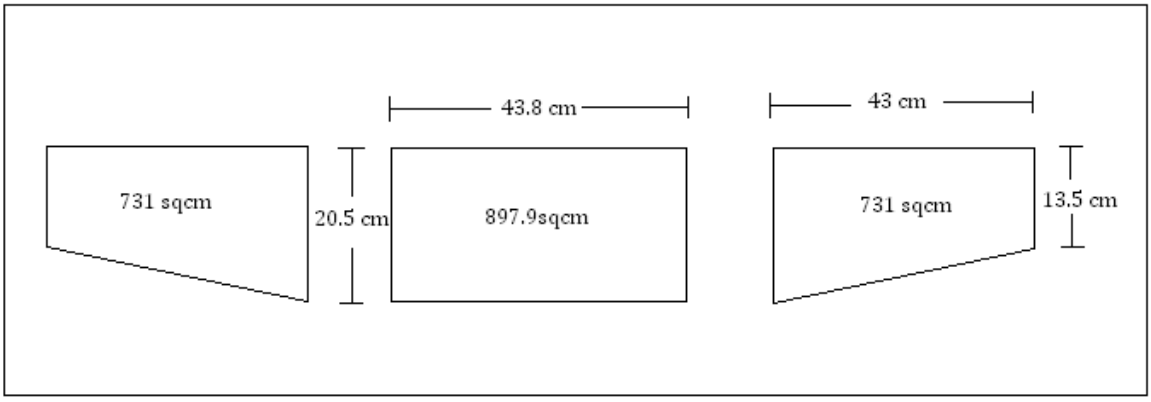

Figure 37. Raven wing original dimensions (from [11]).

C. SOLAR ARRAY

The initial design of the solar array was planned to follow the model of reference [12] by slicing the 21 cm wide cells into thirds and stringing the 48 smaller cells in series. However, during initial testing with the MPPT, the boost converter will multiply the array's open circuit voltage of 28 V to an output voltage above the battery's 25.2 V maximum. The behavior occurred even though the normal knee was near 22 V. Therefore, it was decided to not cut the cells. Instead, the boost converter will multiply the smaller voltage of the large cells to the battery's operating range. There are several distinct advantages to this method. First, removing the need for cutting removed the potential of cutting off-center and limiting the array to the current produced from the smallest cell.

Second, by putting fewer cells in series, the array's temperature sensitivity was cut to one third the previous design. Third, by not cutting, the mounting process was simplified while also limiting the handling of the cells which could damage them and limit their performance. Finally, by leaving the cells whole, the need to space them was negated, making possible a wing with a smaller cord length.

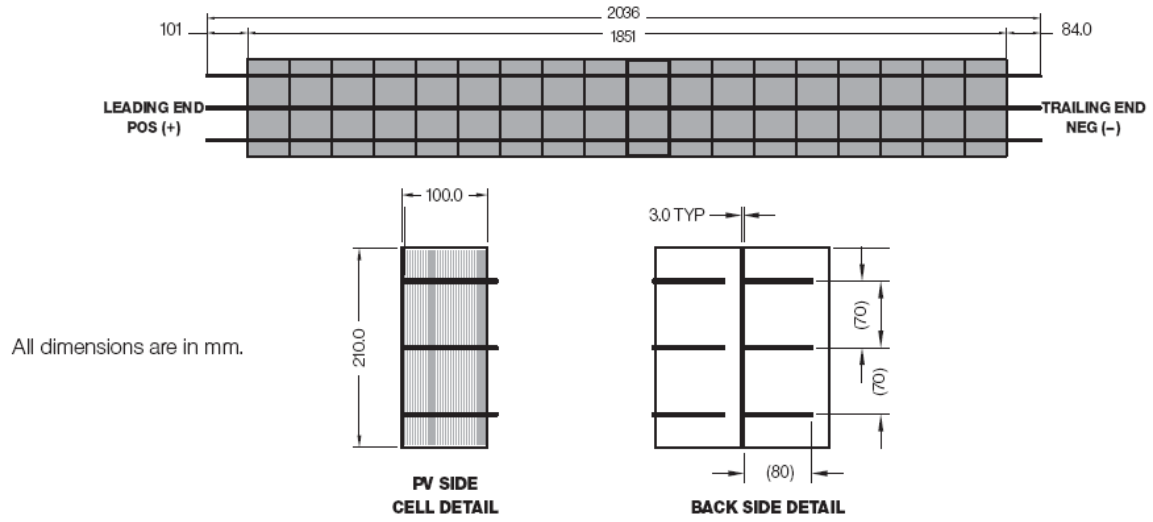

Figure 38. CIGS cell dimensions from Global Solar (from [11]).

The solar cells available for this thesis came from Global Solar. The cell and total string dimensions are outlined in Figure 38. That same order of cells had previously been tested at the end of research by Reference [12]. The string used in testing was set aside in the container as the highest performance string in factory testing. The container indicated that the string had been tested with an output of 46–48 W under AM 1.5 illumination. The original string consisted of 18 cells. Therefore, by multiplying that data by 16/18 cells, a 16 cell array was expected to produce between 40.89 and 42.67 Watts. The entire string was tested outside using a solar analyzer to attain the I-V curve in a process that will be discussed further in the next chapter. Next, the top two cells were carefully peeled away from their back contacts to leave the 16 cell array with the maximum amount of contact wires for mounting. A length of copper tape was soldered between the end contacts on both the positive and negative sides to provide a better connection between the three wires in the manner shown in Figure 39. The copper tape used was that same used

in Reference [11]. The new 16 cell array was tested again with the solar analyzer to confirm that it was operating before encapsulation. All handling of bare cells was done with surgical gloves to prevent oils on the skin from degrading the surface of the cells.

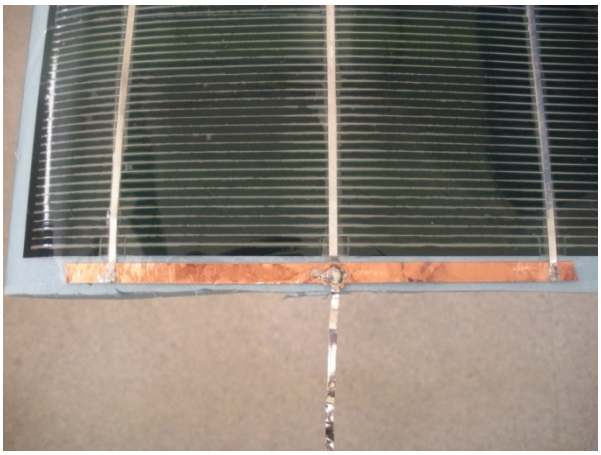

Figure 39. The copper tape used for end connections.

While practicing for mounting the cells, it was noted that the tape used for encapsulation would not adhere to the bare foam. Therefore, a spray adhesive was applied to the front and back of the wing before mounting and encapsulation. The spray adhesive used was tacky enough to hold the tape during encapsulation, but it was not so tacky that it prevented easy handling of the wing.

Figure 40. Encapsulating cells on the foam wing.

Following testing of the bare cells and spraying the wing, the final array was laid atop the wing and securely pulled taught on either end with the same clear packing tape used in Reference [12]. Then, from one end to the other, additional strips of packing tape were laid from front to back with a slight overlap in the manner shown in Figure 40 to prevent further exposure of the surface to air. Any air bubbles that formed during this process were carefully pushed to the edges of the cells with gloved hands and dry paper towels. The encapsulation tape was then secured to the underside of the airfoil by additional strips of tape running the length of the wingspan.

When the wing was finally encapsulated, excess wingspan was trimmed away with a blade. The completed wing was brought outside and tested again to confirm that the cells were still operating and had not been damaged. In Figure 41 the original Raven wing is compared to the wing constructed for testing.

Figure 41. Completed array above the original Raven wing.

D. MPPT

The new array design required replacing resistors on the ST board. Using equations 5–1 and 5–2, we chose the ideal resistances for an output voltage of 25 V and open circuit voltage of 9.5 V (measured using the solar analyzer). The calculated resistances

were done by maintaining R2 and R4 at 110 kΩ to minimize the number of changes on the board. The results of those calculations are displayed in Table 2.

Table 2. Calculated resistances for ideal board performance.

Specification	Formula	Calculated Value (Ω)	Purchased Value (Ω)
V_{oc} = 9.5 V	5–1	R1 = 726 k	R1 = 732 k
V_{out} = 25 V	5–2	R3 = 2.75 M	R3 = 2.74 M

The resistors on the board were extremely small, size 603 thick film chips. Soldering them to the board required special equipment that was only available with help from the Space Systems Academic Group (SSAG).

The performance of the board was initially tested with a direct current source and high power resistors to confirm the output. It was noted that under lower load conditions (resistances over 30 Ω), the output voltage was greater than 25.2 V. Therefore, a second resistor was selected, replacing R3 with a 2.55 MΩ resistor that was calculated to produce an output voltage of 24.18 V.

E. BATTERY

In order to insert the battery balancer and test equipment between the battery and the Raven body, the battery needed to be separated from its normal position during testing. To achieve a solid connection for cables, tabs were created using the same copper tape used in the array. The copper tape was taped tightly to the battery's contacts using packing tape. The copper tape's plastic backing remained attached to provide greater durability with the alligator clips attached. The connections are shown in Figure 42. It should be noted that the outside contacts are the negative terminal, while the inside contact is the single positive contact.

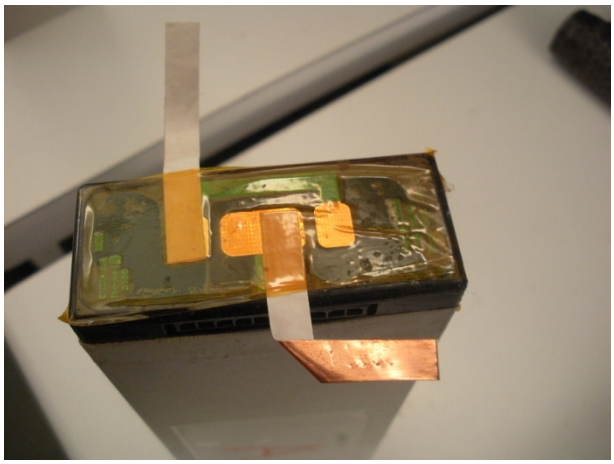

Figure 42. Battery contacts prepared for testing.

Once the contacts were prepared, the battery balancer needed to be inserted. The balancer uses the charging port on the battery's side. The pin-out for the battery charging port is displayed in Figure 43. The cables to connect the balancer needed to be inserted first before attaching the balancer itself for proper initiation of the balancer.

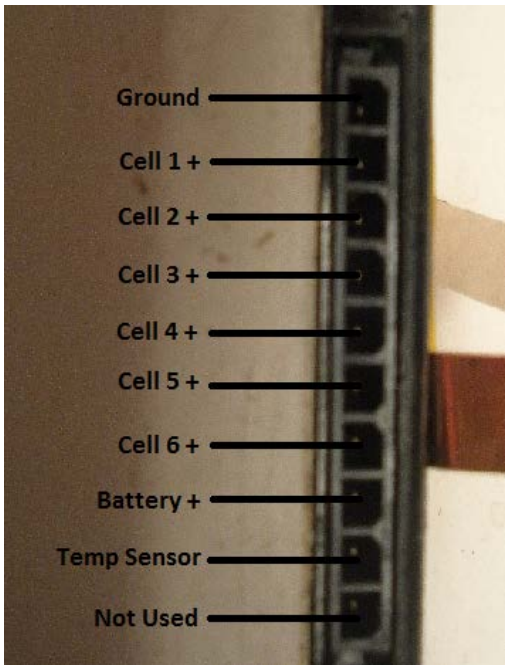

Figure 43. Battery pin-out used for balancer, with copper contacts on top (right of figure).

F. SUBSYSTEM ASSEMBLY

Once each of the subsystems were assembled, the final equipment string needed to be brought together. Care was taken to ensure that the voltage conventions were correct with each connection. Reversing the solar panel would have negated the blocking diode located in the board. Additionally, reversing the MPPT and battery connections would cause a 20 A fuse in the battery to blow. The battery was connected to the Raven with insulated alligator clips, as shown in the Full Equipment string Schematic of Figure 44, using two negative connections on the outside to maintain consistency with the battery contacts.

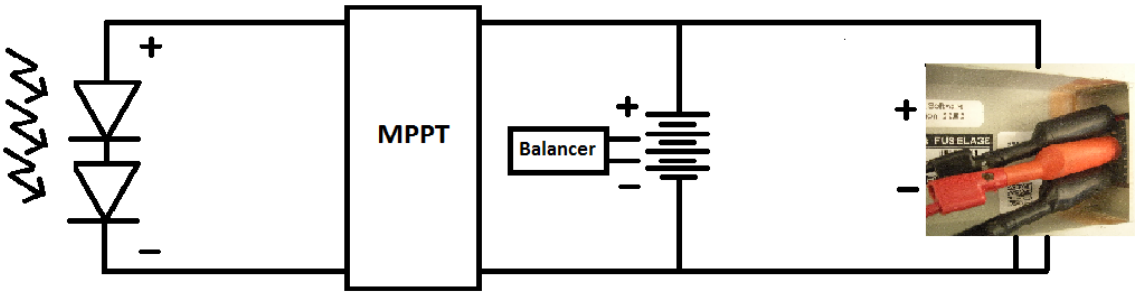

Figure 44. Full Equipment String.

G. CONCLUSION

The assembly of subcomponents and the full equipment string required great care and consideration for the components they would attach to. During assembly, minor testing was done on the subcomponents to ensure their functionality before integration into the final string. Some of the lessons learned from this process, including the behavior of the MPPT under DC bench testing, shaped the initial testing procedures as well as spurring minor design changes before proceeding with testing. The procedures and results of testing with the established equipment string are outlined in the next chapter.

VII. TESTING

A. INTRODUCTION

The testing of the system was the culmination of all of the labor placed into research and assembly to this point. The purpose of that research was to create an accurate model and effective equipment string that could accomplish testing goals in the limited time frame available. Testing discussed in this chapter was completed in three major phases, I-V curve tracing, baseline testing, and solar augmented testing. The goals of testing are creating a working system that significantly increases endurance during daylight hours and, in the tradition of physicians, does no harm to the original system during nighttime and operations where the solar array does not make a significant contribution. Additional data was collected to make informed predictions of performance under different conditions.

B. I-V CURVE TRACING

As discussed in the previous chapter, the solar array was tested before and after encapsulation to ensure that the array was functioning properly. Additional curve tracing was done during the solar augmented test to estimate efficiency across the equipment string, including estimated cell efficiency.

1. Solar Analyzer

The I-V curve tracing completed in this research was done using an Amprobe 600 Solar Analyzer shown in Figure 45. The Amprobe 600 can automatically measure a solar panel up to 60 V and 12 A within 1% error [51]. In addition to the I-V curve, the display also shows the associated power curve. Critical data points that the analyzer lists seperately for each curve include the maximum power point location and magnitude, open circuit voltage, short circuit current, and fill factor. The analyzer can be controlled remotely from a laptop computer, and the results can be recorded and downloaded as an Excel spreadsheet.

Figure 45. The Amprobe 600 solar analyzer (from [51]).

2. Solar Array Mounting Tests

As discussed in the previous chapter, the string of cells used for the array was quickly tested before encapsulation. The cells were suspended on a board for support and angled to capture the afternoon sun. The produced I-V curve is displayed in Figure 46. From the maximum power point of 26.58 W, it was immediately apparent that the anticipated output over 40 W could not be achieved and that the cells had likely degraded over time due to exposure to moisture and oxygen. However, the output was still significant and, with the limited time to work with unprotected cells, it was assumed that the string being measured was the one set aside during packaging for its superior performance. Based on these assumptions, the decision was made to press forward with encapsulation.

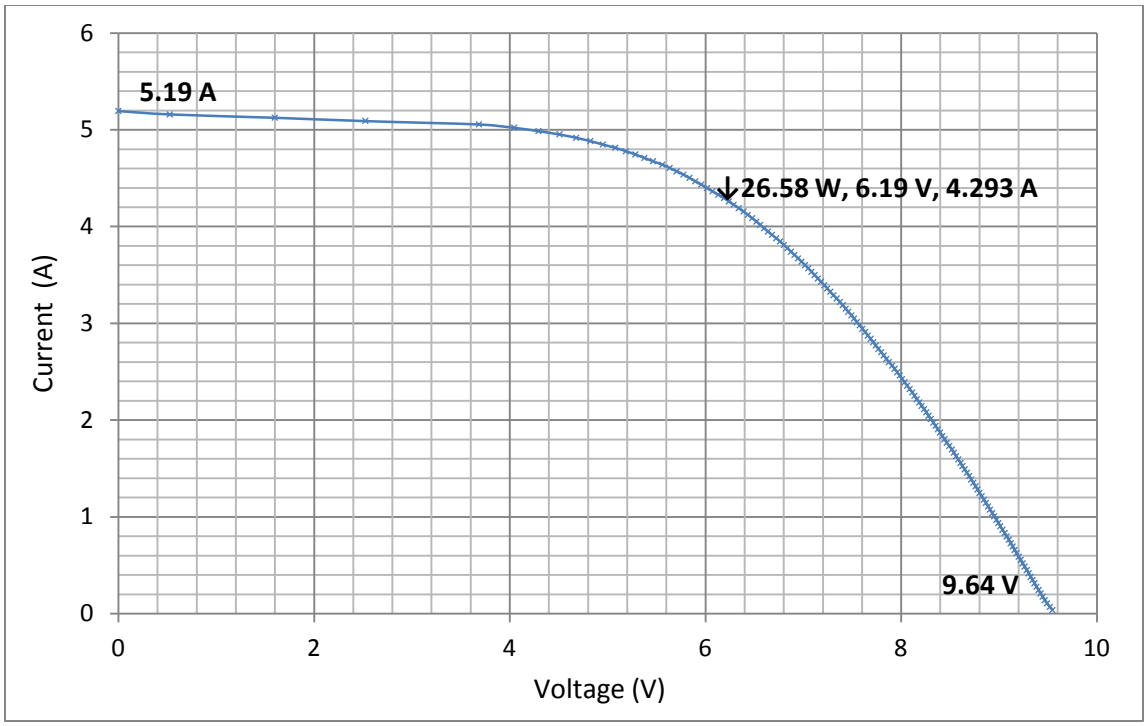

Figure 46. The solar array I-V curve measured prior to encapsulation.

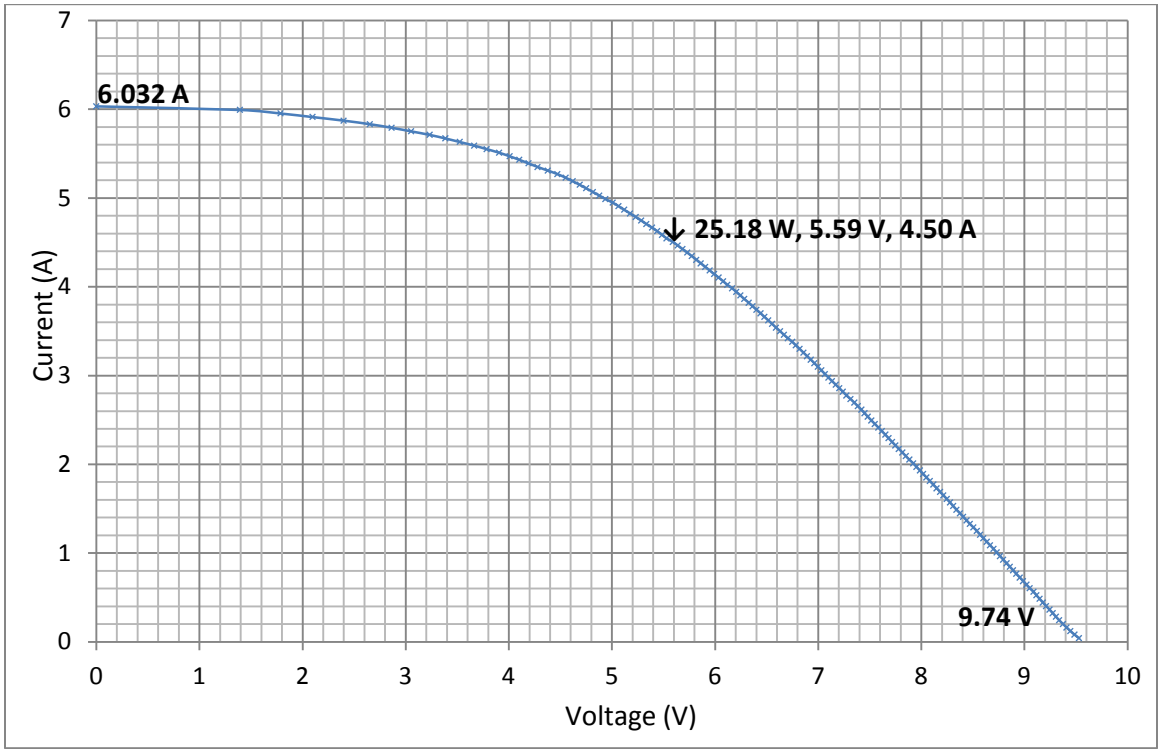

Figure 47. The solar array I-V curve measured following encapsulation on wing.

Following encapsulation, the I-V curve was measured again. The results of the test are presented in Figure 47. The gain in short circuit current due to encapsulation was expected from the theory covered in Chapter III. What was not expected, however, was the increase in series resistance apparent in the decreased slope rising from the open circuit voltage. That slope resulted in a decreased voltage at the maximum power point which slightly decreased the maximum output power. This decrease in power output ran counter to the previous theses. Regardless, the decrease in power was only 5.3%. Additionally, when compared to the already degraded performance of the cell, the loss was not enough to demand repeating the entire process with a new wing.

C. BASELINE TESTING

1. Purpose and Setup

Before connecting the circuitry to augment the the system, the performance of the original system was documented to form a basis for comparison. The testing was done in two parts. First, the current draw of the system was recorded at each throttle position. Then, tests were conducted to measure the endurance of the batteries under a standard mission profile.

For both tests, the system was connected in the manner shown in Figure 48. The system was controlled by the Raven's ground control station. Digital multimeters were inserted into the equipment string to measure the voltage across the battery as well as the current flowing into the Raven. The ground control station additionally displayed battery voltage and was the primary source of voltage data for testing. Box fans were placed in front of the Raven to cool the transmitter and prevent it from going to a failsafe, low power state during testing [42].

3. Current Tests

The current draw of the original system was recorded at each throttle position from 25% to 100% in the five percent increments set on the ground control station. The measurements were done by slowly increasing the throttle and pausing for recordings at each position and then repeating the recordings as the throttle was decreased to observe if the current draw had changed.

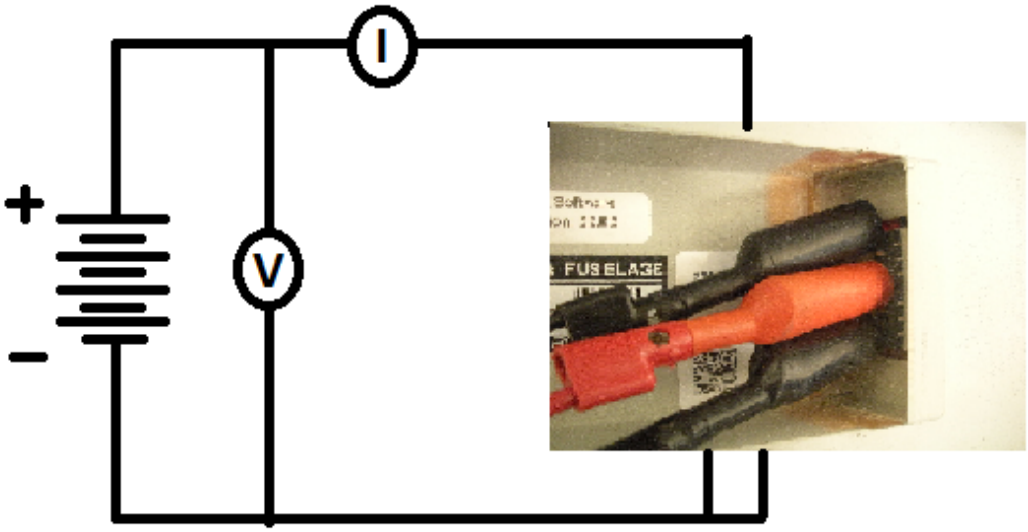

Figure 48. The equipment string for baseline tests.

Table 3. Current demand of Raven for rising and falling throttle positions.

Throttle %	Rising Throttle Current Demand (A)	Falling Throttle Current Demand (A)
25	0.35	0.35
30	0.48	0.44
35	0.61	0.57
40	0.74	0.71
45	0.9	0.9
50	1.06	1.03
55	1.22	1.21
60	1.38	1.35
65	1.56	1.56
70	1.8	1.83
75	2.14	2.11
80	2.52	2.55
85	3	2.97
90	3.33	3.39
95	3.96	3.9
100	6.14	6.14

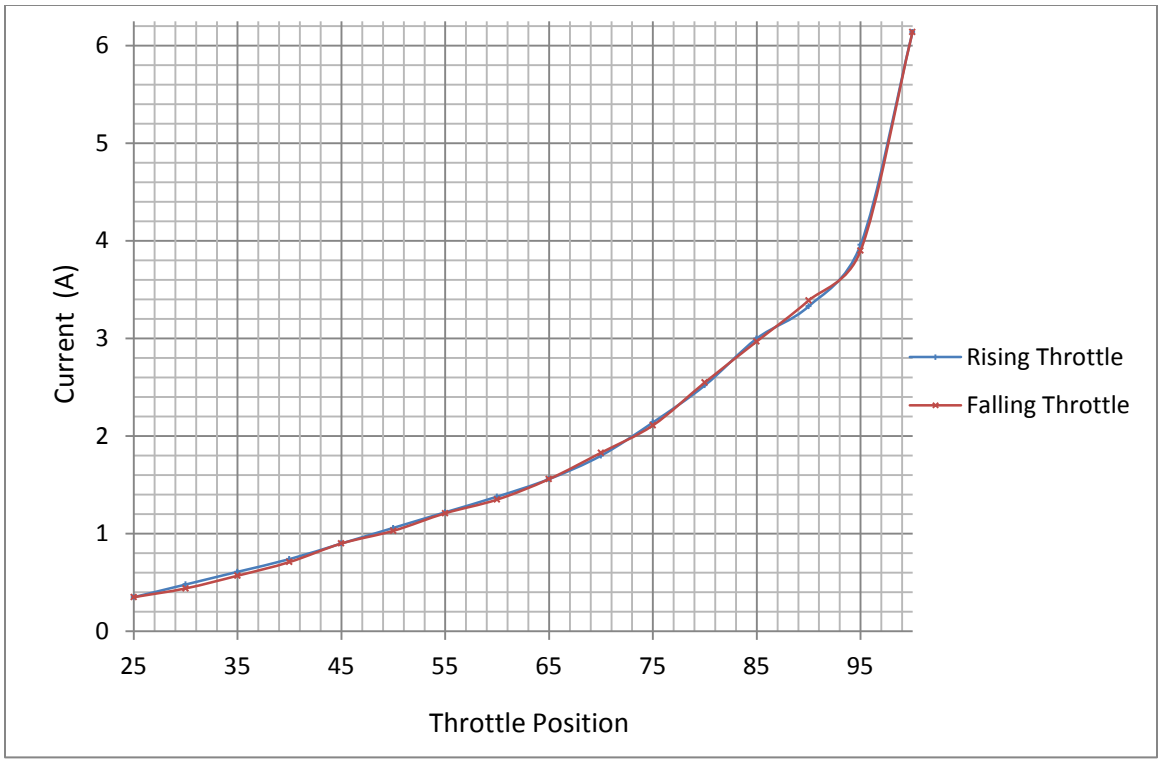

Figure 49. The current demand of a Raven for each throttle position.

The results of that test are documented in Table 3 and plotted in Figure 49. While the current did not vary greatly between rising and falling throttle positions, the trend did show a slight drop in current demand when lowering throttle positions. The change in current demand between 95% and 100% showed a significant increase for full power demand. Additionally, when the battery was connected but the propeller was not yet turning, the current was observed to be 0.2 and 0.15 A for before and after the test, respectively.

D. BATTERY ENDURANCE TEST

1. Procedures

The equipment string used in the battery endurance test was the same as used in the previous current tests. The procedures for the test involved starting with a throttle position of 100% for 20 s before reducing the throttle to 55% and remaining there until the ground control station indicated a battery voltage of 21.9 V. This procedure was derived, and independently confirmed, from the advice of training personnel from both Aerovi-

ronment [52] and the SUAV office of Naval Air System Command [53]. Both sources defined the normal operating altitude to between 300 feet and 500 feet, the normal operating throttle to be 55% on autopilot, and the time at 100% throttle while launching was less than 20 s. Additionally, each regarded the low voltage indicator as a 10–15 minute warning to return to base. The operator's manual confirms these procedures. Also, the documented climb rate of 800 feet/minute at 100% throttle would easily place the Raven at the normal operating altitude within 20 s [42]. While conducting the test, the voltage and current were recorded before starting, during the 20 s of 100% throttle, and at five minute increments from the starting time until the low voltage was reached. The test was conducted with two different identified batteries labeled A and B, twice each, to identify both the consistency of individual batteries as well as the uniformity of performance between batteries.

2. Results

The results of the initial endurance tests are presented as voltage over time in Figures 50 and current draw over time in Figure 51, as well as the raw data in Appendix A. While the shape of the individual curves closely resembled each other, the time at completion showed increased variation with one battery. Battery A completed its first and second tests in 125 and 126 minutes, respectively, while battery B varied from a low time in test 1 of 120 minutes to a high time in test 2 of 134 minutes. The average ending time of the four tests to account for the average battery in later calculations was 126.3 minutes. At first glance this is over 30 minutes longer than the published 90 minute flight time, which could reflect on problems with the mission profile. However, the data will be used as an even comparison to the augmented endurance testing yet to be conducted.

The current plots in Figure 51 display two behaviors of interest in the research. First, the variation of the current over time approached the observed levels in Table 3 for both the throttle position below and above the 55% used during the test. Second, the average of the currents recorded over the tests showed a marked downward trend, from 1.28 A at the start to 1.17 A at 125 minutes.

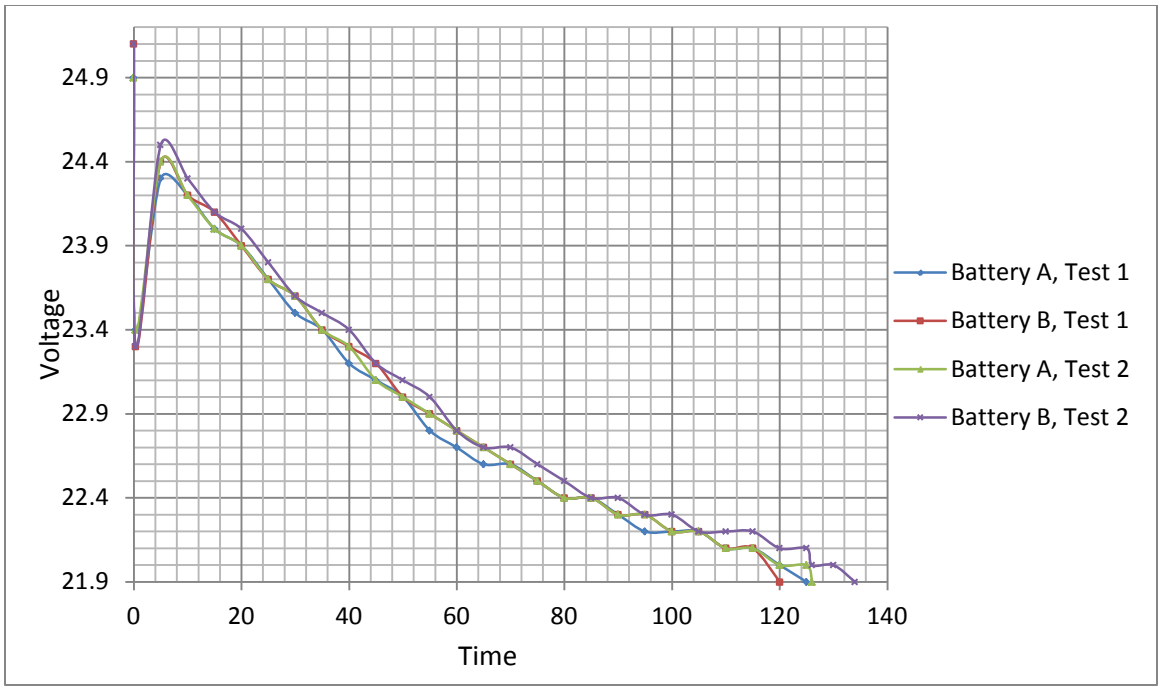

Figure 50. Voltage of initial Raven battery endurance tests.

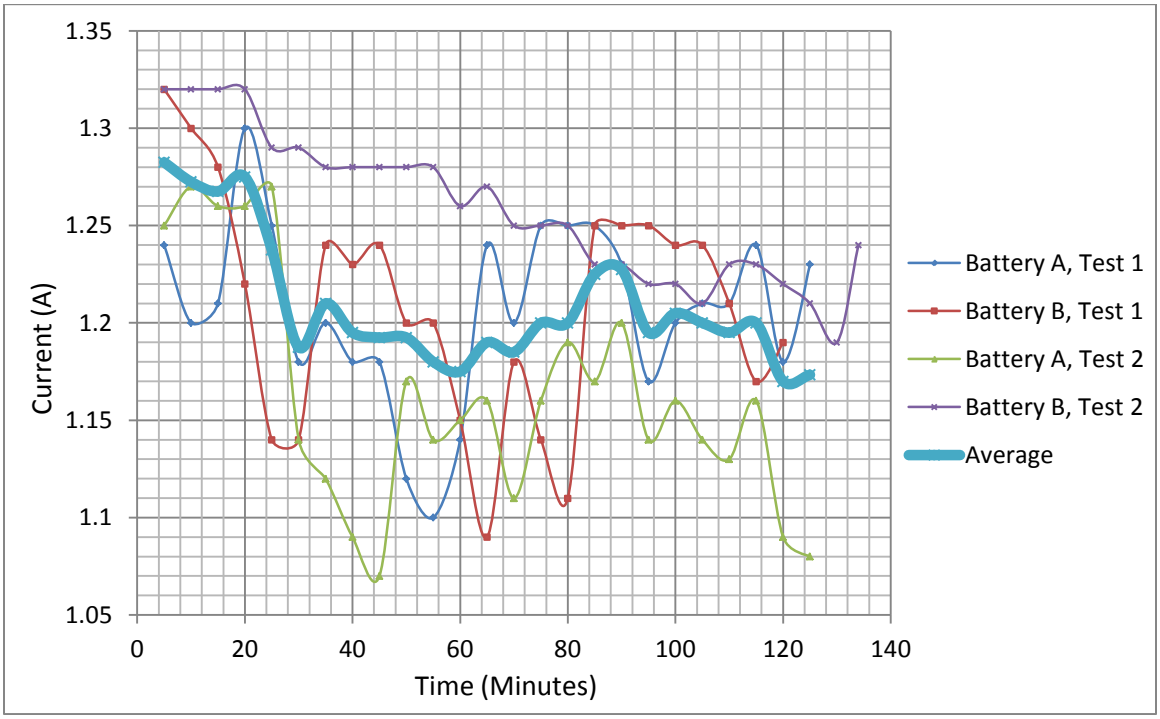

Figure 51. Detail of current for initial Raven battery endurance tests.

E. SOLAR AUGMENTED TESTING

1. Design

The final testing was conducted with the full equipment string described in the previous chapter. For testing, digital multimeters were added to record the voltages on the array side and battery side of the MPPT, while current was measured flowing into and from the MPPT as well as into the Raven. The current flowing from the battery was calculated using Kirchhoff's current law as the difference between the demand of the Raven and the current supplied by the MPPT. The equipment string with the location of meters is shown in Figure 52. Like the baseline testing, a box fan was used to cool the Raven and the array. The breeze produced by the box fans was likely less than what would be encountered during flight, but still helped prevent unnecessary loss in voltage and overheating the transmitter. The system was set up on the roof of Spanagel Hall, as pictured in Figure 53, with the array angled approximately 45 degrees from ground and facing south. This positioning was done to account for the low angle of the Sun in Monterey in late October. The array remained stationary throughout the test to remove excess variables from calculations.

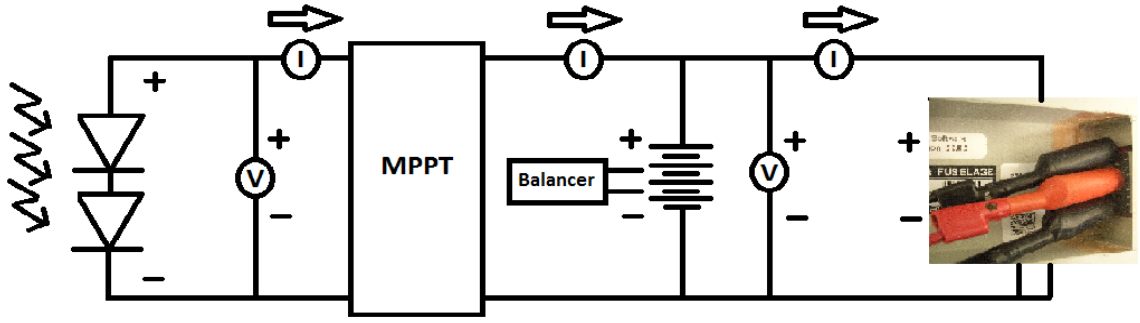

Figure 52. Solar augmented test equipment string.

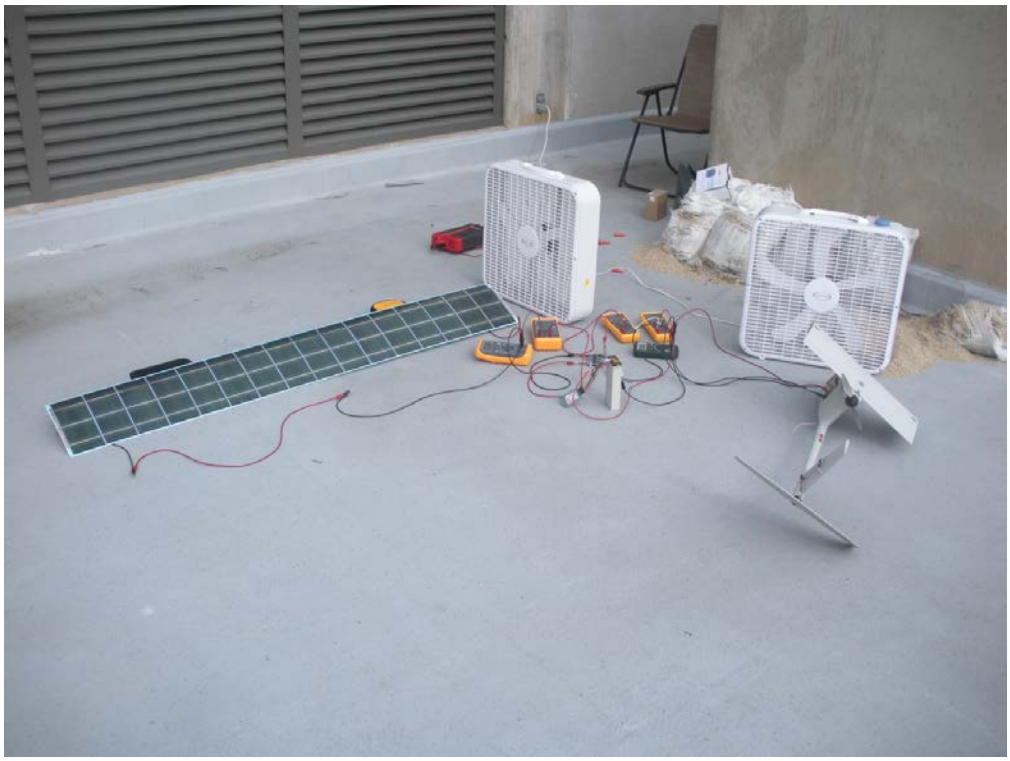

Figure 53. Equipment positioned for augmented tests.

The procedures for the solar augmented tests were the same as those for the baseline tests, validating the current demand for different throttle positions before conducting endurance testing. Additional measurements of I-V curves were taken during endurance testing to calculate the efficiency of the MPPT.

2. Current Tests

The current tests from the baseline system were repeated to confirm the additional equipment would not significantly affect the performance of the base system. Only a single set of data was collected when the rising and falling throttle changes did not significantly affect the results. The testing results can be found in Figure 54. Additionally, the current demand of the Raven in idle was measured at 0.30 A. While the current demand was consistently higher than previously measured, it was not outside the range observed during the baseline endurance tests and remained the same after disconnecting the MPPT. Additionally, the current provided from the MPPT ranging between 0.88 A and 1.10 A significantly lowered the demand on the Raven battery. Another observation during this

testing was that the current input of the MPPT was not dependent upon the throttle position of the Raven. The MPPT's input was only dependent upon the input of the solar array.

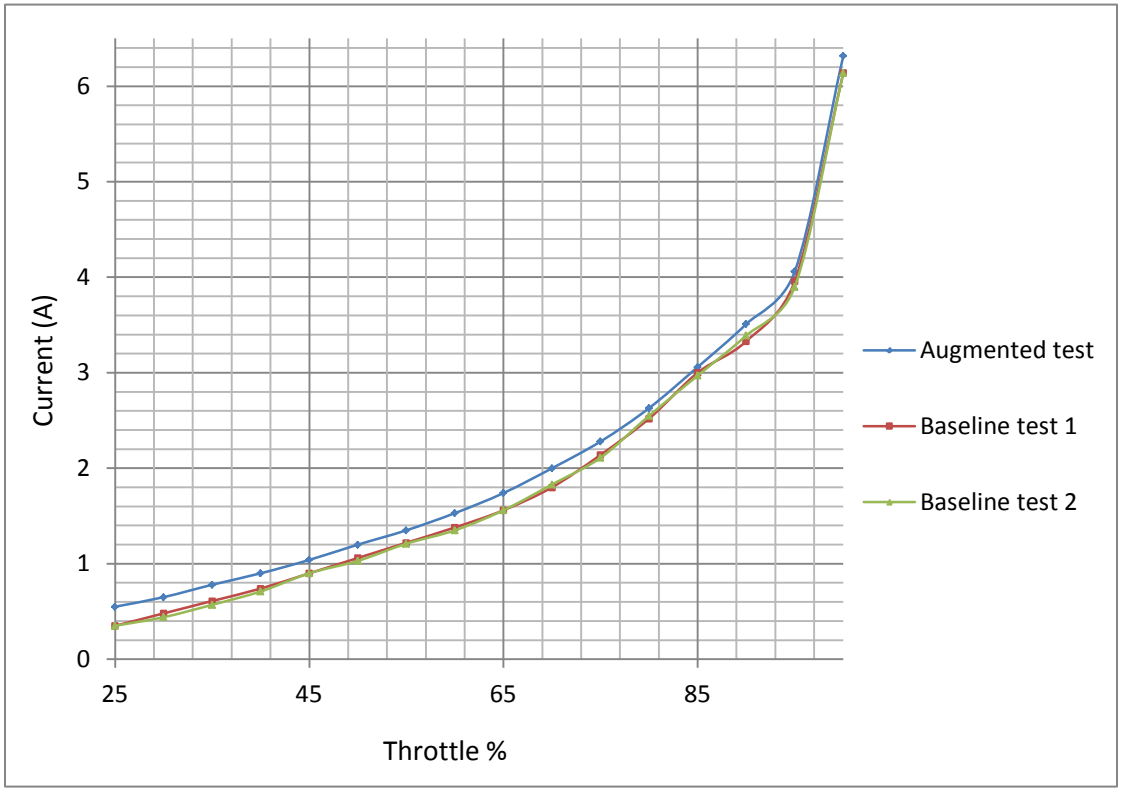

Figure 54. Augmented system current demand compared to baseline demand.

3. Augmented Endurance Tests

The mission profile used for the augmented endurance test was unchanged from the baseline endurance testing. However, to support calculations of power efficiency an I-V curve of the solar array was taken immediately before the test began. That I-V curve is displayed in Figure 55.

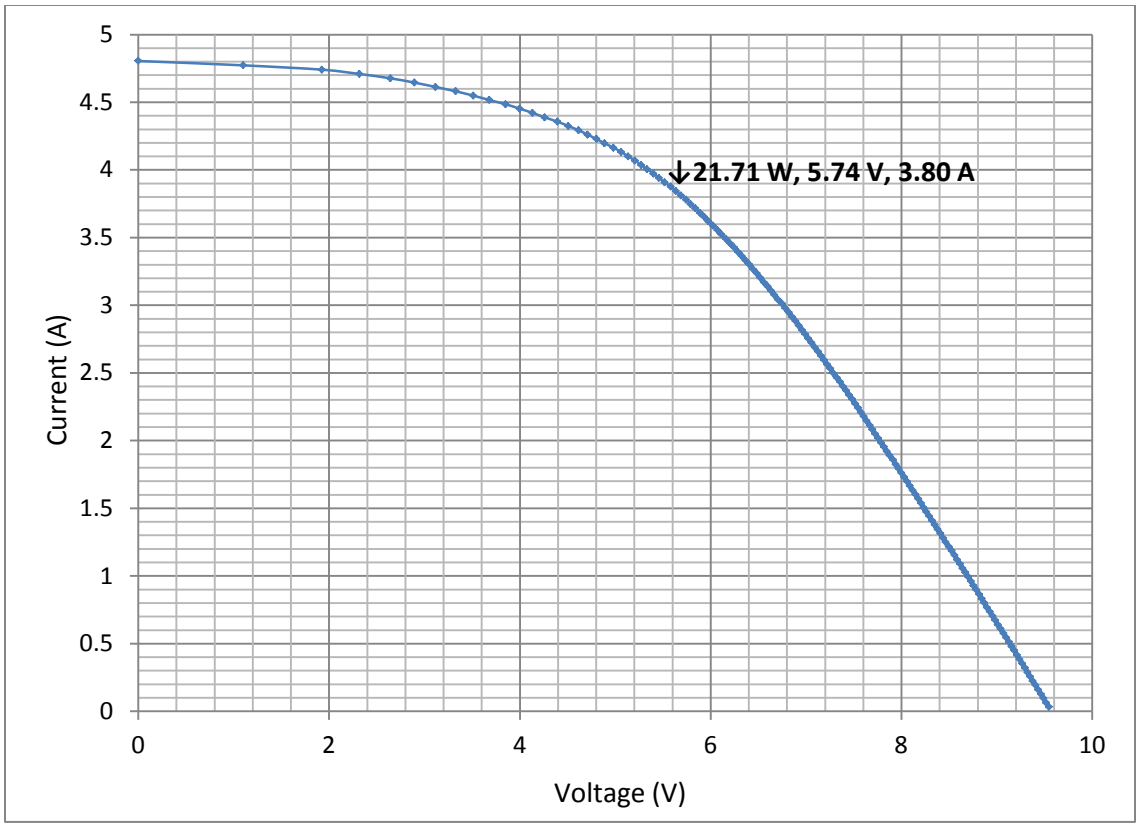

Figure 55. I-V curve taken prior to augmented endurance test.

The endurance test began at 9:15 AM, and one issue that was noted immediately was that the voltage across the solar array remained locked at 6.9 V. That voltage was greater than the point in Figure 55, indicating that the MPPT was not properly functioning. However, data collection continued to observe the final results. During testing only a diffuse jet contrail at 45 minutes and a single high cloud at the end disturbed an otherwise clear day. The test ended 340 minutes later at 2:55 PM when the voltage on the ground control station reached 21.9 V. The voltages recorded over time are displayed in Figure 56 compared to the baseline voltage tests. The current produced by the MPPT during the test, in Figure 57, also generally rose and fell with the arc of the sun across the solar array. The peak MPPT output of 0.846 A occurred at 170 minutes, which corresponded to 12:05 PM.

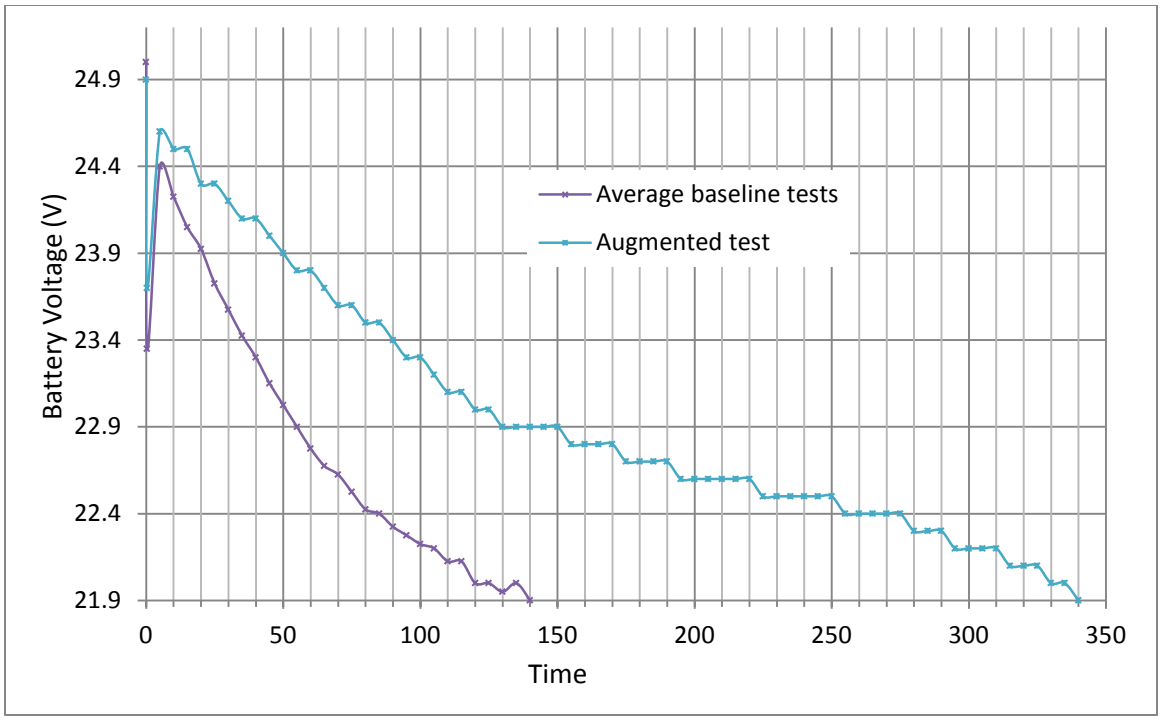

Figure 56. Augmented endurance test voltage compared to average of baseline tests.

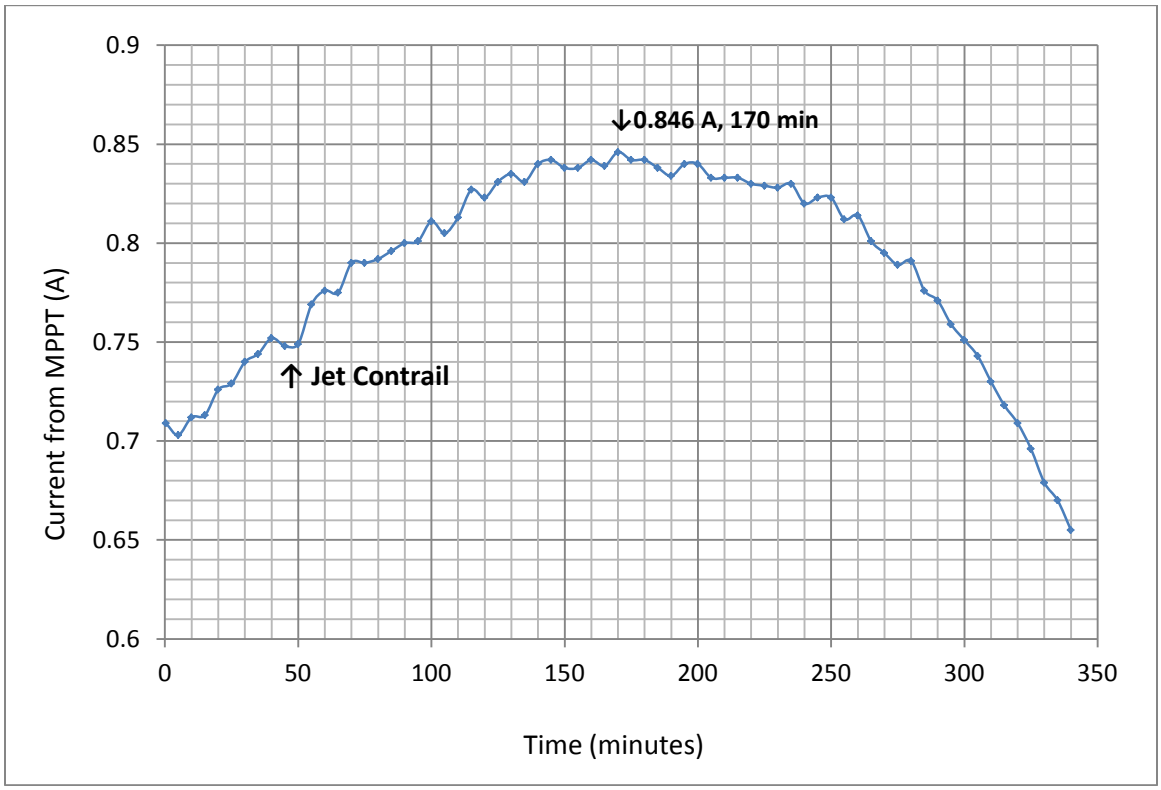

Figure 57. Current supplied from MPPT during augmented endurance test.

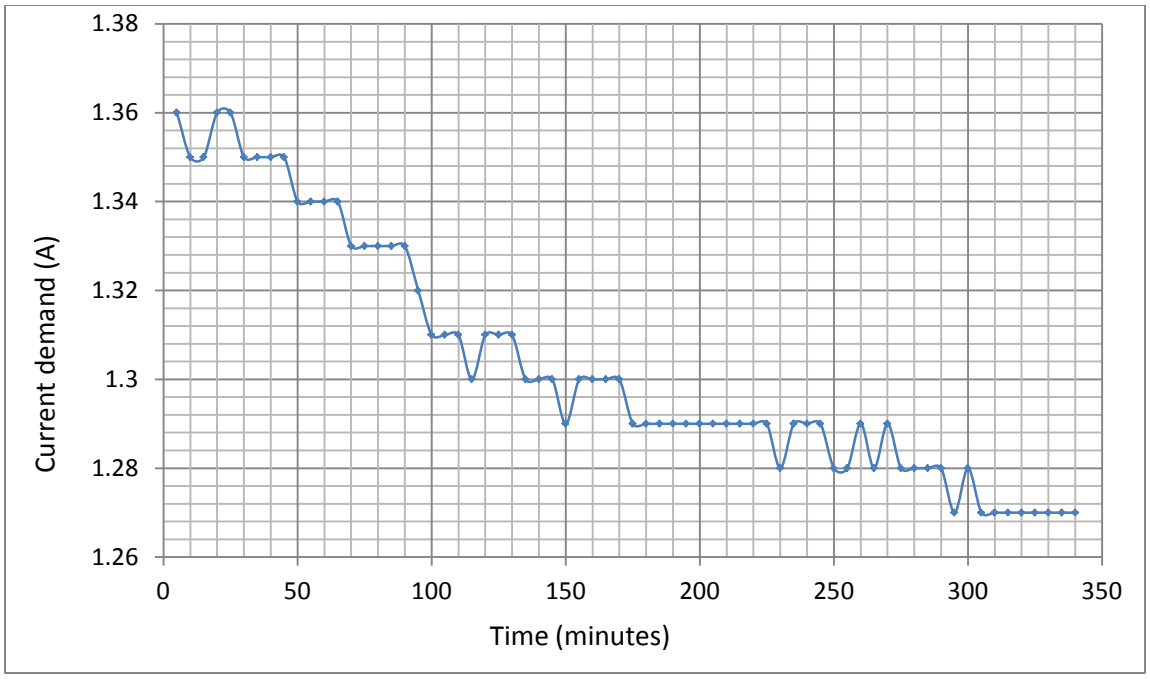

Figure 58. Current demand over time during augmented endurance test.

As a comparison to the baseline tests, the augmented system's current demand, plotted in Figure 58, remained much more stable. However, in addition to the increased stability, the steady decline in current as time progressed remained, dropping from 1.36 A to 1.27 A at the end of testing.

Since a measurement of the solar array performance could not be taken during the endurance testing without breaking the circuit, an I-V curve was recorded two days later. The follow-up measurement was done at the same time as the peak measurement under conditions identical to the endurance test to provide a reliable source of data for calculations. That I-V curve is displayed in Figure 59. The maximum power point should have been located at 5.31 V and produced 25.06 W. However, the MPPT being locked at 6.9 V only allowed a measured input power from Appendix A of 22.01 W.

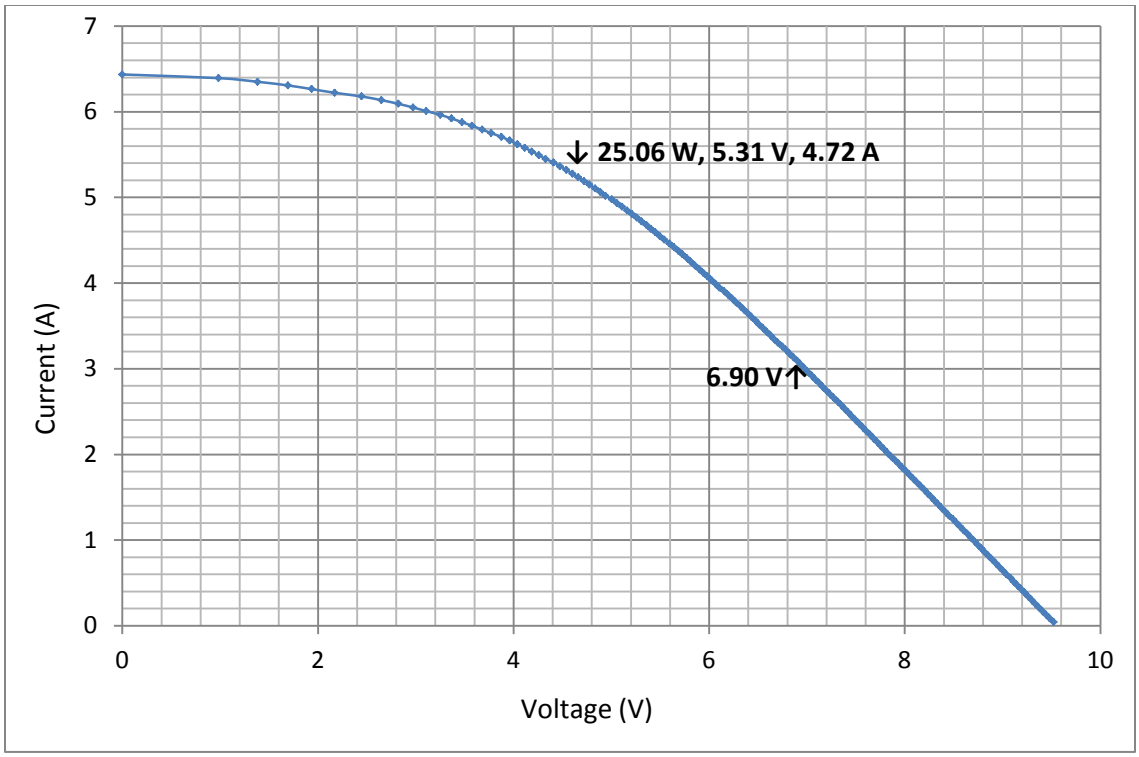

Figure 59. I-V curve correlating peak array input for augmented endurance test.

F. FURTHER OBSERVATIONS

In addition to the current and endurance tests, several other smaller experiments were conducted to observe the behavior of the system.

1. Charging a Full Battery

From the tests during assembly it was believed that the high output voltage under no load conditions could be dangerous to the battery. The solution to that issue was developing a procedure to connect the Raven to the battery before connecting the MPPT. However, in augmented testing, this procedure was determined to not be necessary. A fully charged battery choked off the MPPT, which operated near the open circuit voltage of the solar array. As a result the MPPT input very little current to the battery. Once the Raven was connected, the MPPT supplied only enough current to match the demand of the Raven, but provided no surplus current to the already full battery. Once the Raven's current demand increased, the MPPT returned to full operation with the minimum voltage

of 6.9 V from the array. Additionally, under lower throttle positions in high sunlight, the input of the MPPT could exceed the demand of the Raven so long as the battery was not fully charged. From these observations it was concluded that it was not only possible but safe to connect the battery to a fully assembled system. Furthermore, the battery could also be charged while disconnected from the Raven system and connected only to the augmenting circuitry.

2. Limited Light Operations

Additional testing under less than optimal conditions demonstrated the value of the augmenting circuitry. Under cloudy conditions, the MPPT still input 0.44 A into the system, which is not an insignificant contribution to the current demand at 55% throttle. Also, when the panel was laid flat or angled away from the sun, the array still provided power to the system. Finally, when the solar array was disconnected from the MPPT, no measurable current was drawn from the battery across the MPPT. From these observations, it can be concluded that with the exception of flight characteristics that could not be evaluated, the additional circuitry does no harm to the original system but instead augments the battery under every observed sunlight condition.

G. CONCLUSION

The system was tested under its original configuration before testing under augmented conditions to measure the benefit of the augmenting circuitry. The current draw of each throttle position was recorded in both configurations to observe the performance of the system under various conditions. Finally, the endurance of the batteries were tested using a mission profile derived from the operator's manual and training personnel.

From the testing, a significant increase in endurance was observed, while under various testing conditions, no drawbacks to the augmenting circuitry could be found. The increase in endurance was accomplished with a solar array that was significantly degraded from its original specifications and an MPPT that did not operate at the array's true maximum power point. The data that was collected is used in the next chapter to make informed projections of what the performance could be with improvements to the tested system.

VIII. CALCULATIONS

A. INTRODUCTION

While testing showed a marked improvement in the system's endurance, the conditions of testing left several unanswered questions. How well could the system have performed with better cells or MPPT? Why did the original system last longer than 90 minutes? How would the system perform on an unmodified wing or a Puma? The data collected to project performance under different conditions is used to answer those questions in this chapter.

B. MEASURED BENEFIT

The measured flight endurance of the augmented system compared to the original was (340 minutes)/(126.3 minutes), 2.7 times longer than the original system. The measure of success in Chapter I was defined as the increase in flight endurance compared to the increase in cost and weight of the original system. These comparisons are documented below.

1. Weight of Augmenting Circuitry

Table 4. Changes in weight to augmented system.

Component	Original Weight (oz)	Augmented Weight (oz)	Change (oz)
Wing	10.4	10.7	+0.3
MPPT	0	1.7	+1.7
Battery Balancer	0	0.7	+0.7
Total System	10.4	13.1	+2.7

The listed weight of the original Raven system is 4.4 lbs [42] or 70.4 ounces. The increased weight of the augmenting circuitry is documented in Table 4 and is only 2.7 ounces including the wires for the battery balancer, which would likely be much shorter.

However, the foam wing did not have a wrap included that would have increased both the rigidity and weight of the final wing. With those factors considered, the 169% increase in flight endurance was achieved at a cost of (2.7 oz)/(70.4 oz), a 3.8% increase in weight

2. Cost of Augmenting Circuitry

Table 5. Cost of augmenting system components.

Component	Cost Each ($)	Quantity	Total Cost per SUAV ($)
Wing	65.18	1	65.18
Solar Cells	5.00 [56]	16	80.00
MPPT	87.50	1	87.50
Battery Balancer	29.95 [11]	1	29.95
Total Augmentation	--	--	262.63

The cost of a single aircraft was documented in [11] as $35,000. This figure is used again here for the sake of simplicity. The cost of augmenting circuitry used in testing is documented in Table 5. The cost of the copper tape and packing tape used for encapsulation are not included but would either be extremely small or would not translate well to industrial applications. With those factors considered, the 169% increase in flight endurance came at an increased cost of $262.63, or 0.75%, of the original system.

C. BASIS OF PROJECTIONS

Of all the variables measured during testing, the ratio of current provided by the MPPT I_{mppt} to the current demand of the Raven I_{raven} provides the clearest perspective of both the demand on the battery and when charging of the battery occurs. For this reason, I_{mppt} will be the basis of comparison. The current provided by the MPPT can be derived from [25]

$$I_{mppt} = \frac{A_{cell} N_{cell} P_{sun} \eta_{cell} \eta_{mppt}}{V_{battery}} = \frac{P_{mppt}}{V_{battery}} \tag{8–1}$$

where the area of each cell A_{cell} is measured in square centimeters, N_{cell} is the number of cells in the array, the power input from the sun P_{sun} in Watts per square centimeter, the efficiency of the cells is η_{cell}, and efficiency of the MPPT is η_{mppt}.

D. EQUIPMENT REPLACEMENT.

1. Curve Fitting

While a voltage drop is shown in Figure 56 with augmentation similar to the base-line system, from Figure 57 we see that the current provided by the MPPT varies over time with a peak when the sun is at its maximum. Since the curve of that current was not a perfect parabola and defied easy definition with an equation, the peak current of 0.846 A and the corresponding voltage of 22.8 V are used at the basis for all calculations, with each data point multiplied by the given ratio to maintain the shape of the curve.

2. Cell Efficiency

Unfortunately, without access to a test cell of known efficiency, two variables in Equation (8–1) are unknown. However, the angle of the sun at 12:05 PM on October 26 in Monterey was found in [54] to be 40.5 degrees from the horizon. Referring back to Chapter III, we see that the angle is within 1.2 degrees of the definition of AM 1.5. Given a clear day, the use of AM 1.5's definition of 0.093 W per square centimeter is reasonable for P_{sun}. Therefore, substituting P_{sun}, a cell area of 210 square centimeters, 16 cells and the maximum power measured in the correlation I-V curve in Figure 59 as 25.06 W into Equation (3–3), we get an efficiency η_{cell} of 0.08.

Even if the previous calculation of efficiency based on sun angle is flawed, the following results are accurate since Equation (8–1) multiplies irradiance by efficiency, which in Equation (3–3) has irradiance as the denominator, canceling irradiance from the equation and basing the calculation of efficiency on an assumed AM 1.5 irradiance. Therefore, under actual AM 1.5 the irradiance, the projection would be the unchanged.

3. MPPT Efficiency

The efficiency of the MPPT accounts for both the losses across the boost converter as well as the power lost by the MPPT not operating at the true knee of the solar array. The efficiency is determined by dividing the power input to the system, $I_{mppt}V_{battery}$ = (0.846 A)(22.8 V)= 19.29 W, by the maximum power point of the array, yielding (19.29 W)/(25.06 W)= 0.77. The efficiency of the MPPT at the peak current was very similar to the efficiency at the beginning of the endurance test, (0.703 A 24.6 V)/(21.71 W) = 0.80, where the higher voltage of the full battery increases the overall efficiency of the circuitry.

4. Simulated Load

The recorded Raven current demand from the augmented endurance test was very stable, however, it was likely not applicable to every test, as seen in the baseline tests. Therefore, to simplify the projected data, a straightline approximation of the load was made. The linear equation $y = ax+b$ was used with the slope being determined by the endpoints over the time at 55% throttle, (1.27 A−1.36 A)/(335 minutes), multiplied by 60 minutes, to yield −0.0162 A per hour. To solve for *b*, the time *x* was converted to decimals where 12:05 PM = 12+(5/60) = 12.083. The current demand I_{raven} at that time was 1.30 A. Substituting those values into the linear equation, (1.30 A)= (−0.0162 A/hour)(12.083 hours)+*b*, and solving for *b* yields *b* = 1.50 A. Therefore, the 55% throttle load used in the Matlab code documented in Appendix B was written as *load* = (−0.01612 *time*) + 1.5. The simulated load compared to the recorded I_{mppt} are displayed in Figure 60. At the peak, the MPPT provides 64.8% of the current demand.

5. Replacing the MPPT

For the first projection, I_{mppt} is adjusted to account for replacing the calculated 77% efficient MPPT with one that was 95% efficient as many are marketed to be. By keeping every other variable in Equation (8–1) the same, the curve is adjusted from the peak by multiplying every data point by (0.95/0.77). The results of this projection com-

pared to the measured data and simulated load are displayed in Figure 61. At the peak the improved system provides 1.04 A, or 80% of the 1.30 A current demand.

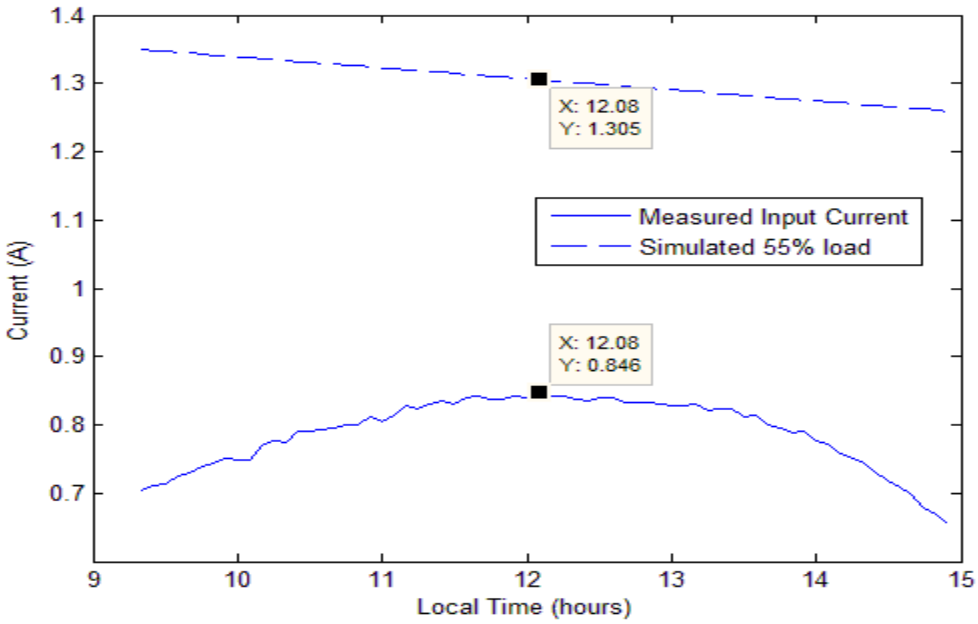

Figure 60. Simulated load with measured MPPT current input.

6. Replacing Solar Cells

Similar to the equation for MMPT replacement, the second projection replaces the measured 8% efficient cells with 13% efficient cells that are commonly found on the market today, as well as the original efficiency of these cells before they degraded. Again, each data point is multiplied by the ratio (0.13)/(0.08). The resulting projection is displayed in Figure 62. Most notable in this projection is that the battery would be charging for two hours of operation. At the very least, the battery would have the same battery voltage at 2 PM that it had at 11 AM.

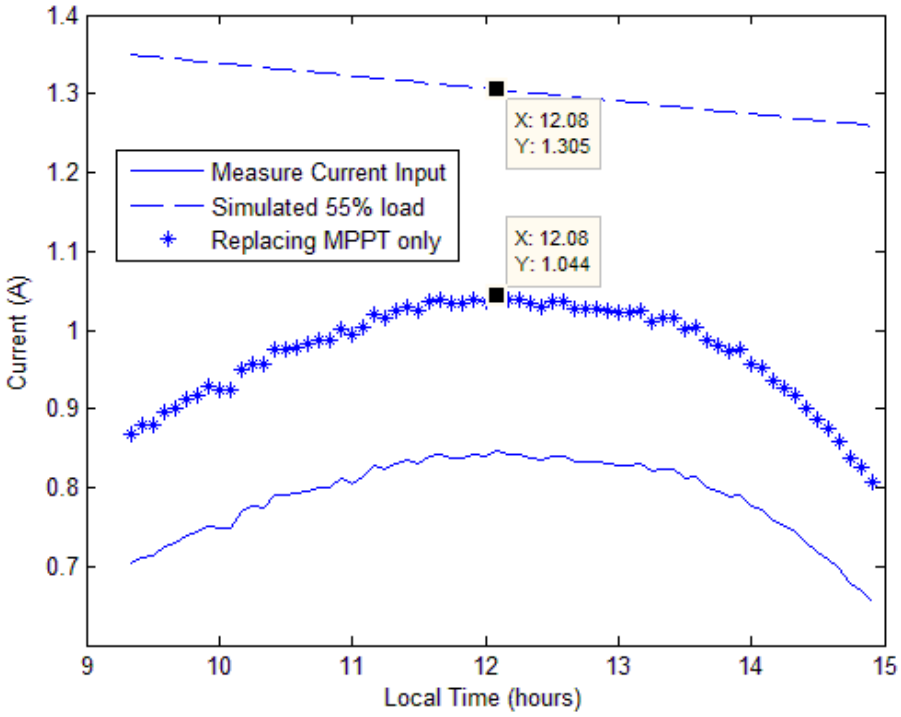

Figure 61. Projection of replacing MMPT only on current input.

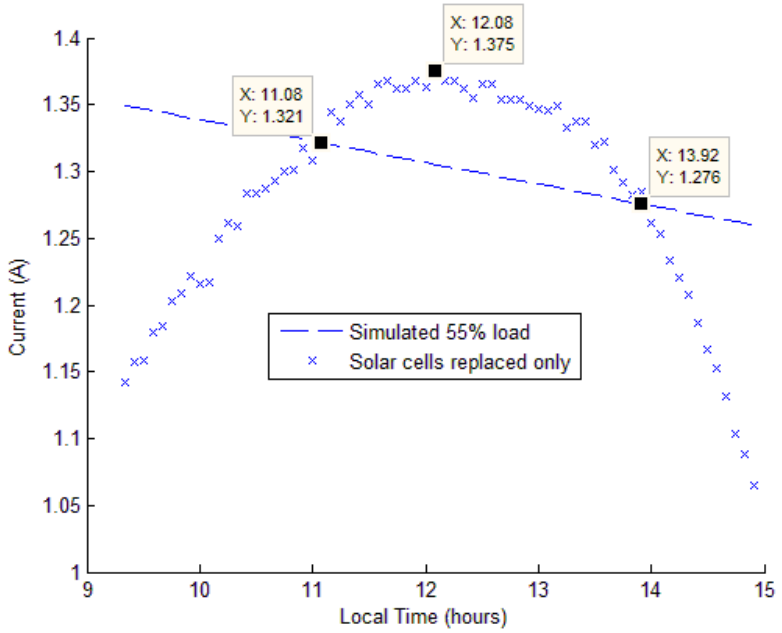

Figure 62. Projection of replacing solar cells on current input.

7. Optimized System

If both the MPPT and solar cells were replaced, the system would have the capabilities originally expected from the advertised components. Each data point is multiplied by both of the previous ratios (0.95/0.77)(0.13/0.08). The projected performance of the system is displayed in Figure 63. Of note, the optimized system is charging the battery for the duration of flight. In this scenario, the Raven would be able to fly for at least two hours after 3 PM using the results of the baseline system endurance tests, an overall improvement of at least, 169% + 100% = 269%.

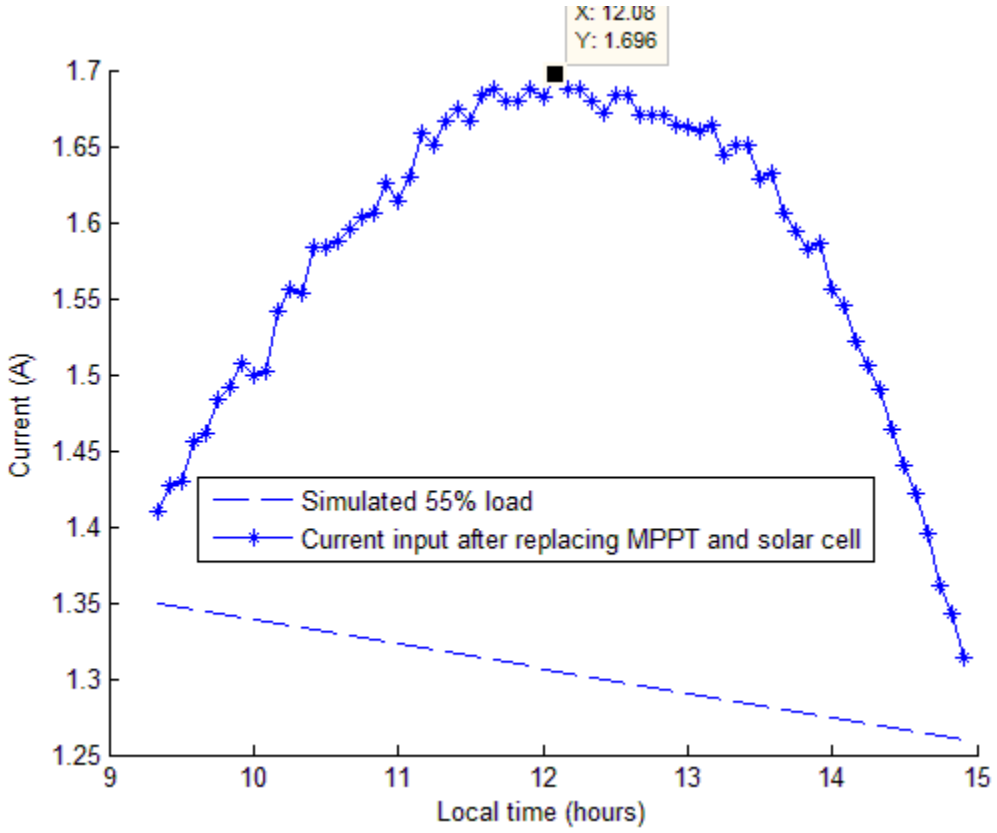

Figure 63. Projection of current input of an optimized system.

E. CHANGES TO THE MISSION PROFILE

Since the baseline testing lasted for over two hours instead of the expected 90 minutes, there are likely flaws in the model used. One of those flaws could be due to the system being so close to the ground control station that it requires only a fraction of the

transmit power to maintain a link. Additionally, there could be other drains on power not tested, including a tendency for operators to sprint to the target area, natural variance in throttle by the autopilot to maintain altitude, crosswinds, and various commands to the Raven during flight. Regardless of the reason, a shorter flight would manifest itself as an increase in the average current draw from the Raven.

To calculate the increased current draw, the starting capacity of the battery and average current draw are considered to determine the average capacity used at mission's end. The battery starts at 4 A-hours and drew, at the peak input current, 1.30 A. If the baseline tests lasted for an average of 126.3 minutes, or 2.11 hours, then the percentage of battery capacity used during a test, (((1.30 A)(2.11 hours))/(4 A-hours)), yields 68.4 %. The 20 seconds at 6.62 A accounts for (((6.62 A)(0.0056 hours))/(4 A-hours))100%= 0.87%, a negligible amount of drain on the battery. Translating that percentage to capacity in the case of the Raven battery, (0.684)(4 A-hours), we get 2.74 A-hours used. If those 2.74 A-hours were used in only 1.5 hours, then the average current I_{raven_avg} would be (2.74 A-hours)/(1.5 hours) = 1.82 A. That current compared to Figure 54 would appear to be closer to an average throttle position of between 65% and 70%.

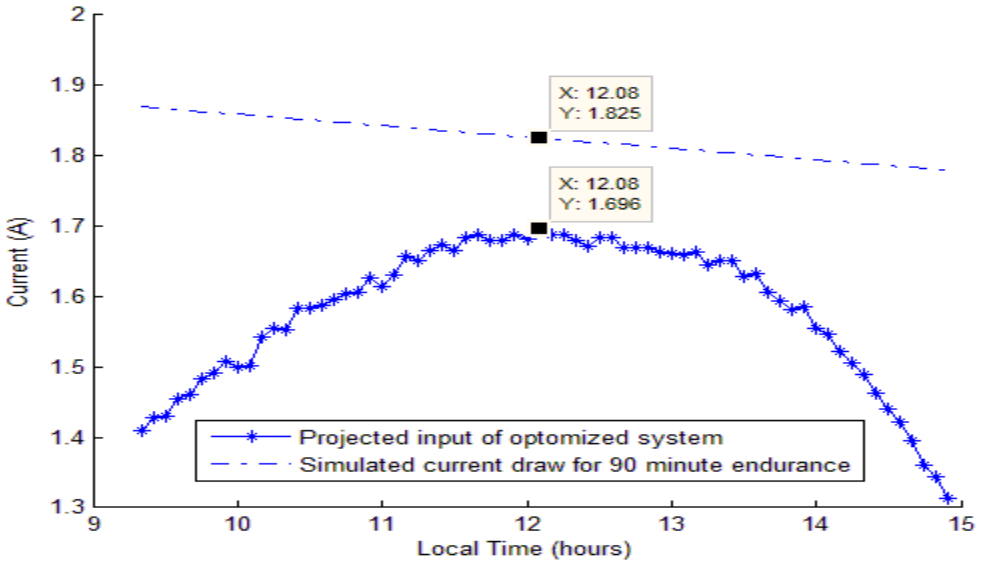

Figure 64. Simulated I_{raven_avg} with optimized system current input.

To update the Matlab program with a simulated I_{raven_avg}, the difference between the current draw at the peak load and the calculated I_{raven_avg}, 1.82 A – 1.30 A = 0.52 A, was added to the original simulated 55% load. The new average load is displayed with the optimized projection in Figure 64. The simulation represents a possible worst case scenario if the system behaves differently in flight. With that in consideration, the optimized system still provides 92.9% of the current at peak, a considerable improvement over the tested system and measured load.

F. USE WITH A STANDARD RAVEN WING

The original Raven wing and cell dimensions described in Chapter VI were not compatible. The modified wing was used to fit more cell and absorb more power. However, if the optimized system performance were applied to the standard wing dimensions, how would that system compare with the one tested?

The original wingspan was 129.8 cm, with wingtips 13.5 cm wide. Cell manufacturers can make cells of various sizes, but for purposes of comparison, the cells in this calculation use the tested cells as a basis. The tested cells could fit 12, 10 cm cells with 0.3 cm connections at either end, 12(10 cm)+13(0.3 cm)=123.9 cm, with 5.9 cm to spare. However, the 20 cm width of the cells would need to be trimmed to 13.5 cm to fit near the wingtips. Therefore, each cell would be 135 square cm. Utilizing Equation (8-1), we expect twelve, 135 square cm cells with cell and MPPT efficiencies of 0.13 and 0.95, respectively, to yield 0.816 A at peak sunlight. This current corresponds to 96.5% of the current measured during the augmented endurance test.

The array in this projection does not maximize the useable area of the original Raven wing. Use of an optimized cell size and configuration, professionally mounted, could yield even better results. However, this simple example demonstrates how closely the improvements documented during bench testing with a modified wing could translate to a virtually unchanged Raven.

G. USE WITH A PUMA

Following further research, we found the specifications of the Puma battery to be a 25.2 V lithium battery with a capacity of 13.5 A-hours and the same minimum voltage of 21 V [55]. If the behavior of the larger six cell battery parallels that of the Raven, projections can be made of its performance similar to the previous examples. If the battery reaches the 21.9 V minimum voltage after consuming 68.4% of the batteries capacity, then the average current draw to fly for two hours would be ((13.5 A-hours)(0.684 consumption))/(2 hours), 4.62 A.

The wingspan of the Puma is twice that of a Raven. The cord length of the wing also increased in comparison to the Raven. A Puma wing would easily support 25 uncut cells on the increased wing surface area. Given that increased number of optimized cells with an optimized MPPT, the peak output power would be 2.64 Amps.

The projected current would provide 57% of the calculated average current draw at peak sunlight. By comparison, the previous unchanged Raven wing would have only provided 44.8% of the calculated 1.82 A average draw for 90 minutes of flight. If the behavior of the Puma is consistent with that of the Raven under bench testing, the 55% throttle would require significantly less current to maintain altitude and further reduce the load on the battery during peak sunlight.

H. CONCLUSION

The results of testing the augmented system provided an impressive improvement over the original system in comparison to the cost and weight of the added components. However, these results were gained with degraded or poorly performing components. By systematically manipulating the data, the results of the projections demonstrated that by replacing the degraded cells only, the system could have charged the battery in flight at mid-day, while replacing the cells and MPPT could have charged the battery for the entire testing period. Those results were translated to the wingspan of an unmodified Raven wing and the larger wing and battery capacity of a Puma to demonstrate their potential benefit. Finally, the average current for 90 minute flight was derived to provide a basis for improving the model for testing. These results are further summarized in the next

chapter along with the observations from other chapters to form conclusions and make recommendations for further work.

THIS PAGE INTENTIONALLY LEFT BLANK

IX. CONCLUSIONS

A. INTRODUCTION

The completion of research provides a time to reflect on the completed work and propose a way forward. The observations and calculations detailed throughout the document are summarized in this chapter. Additionally, questions are posed that this research raised that can provide greater understanding and ingenuity to this important subject in future work.

B. SUMMARY OF FINDINGS

This research began by identifying the issues facing small tactical units regarding expeditionary energy. In order to sustain observation with SUAVs, they must choose between carrying more batteries or remaining tied to vehicles and other sources of power. As a proposed solution, previous work in solar glider planes and thesis work on solar SUAVs were referenced for a basis for improvement.

The SUAV for research was selected by comparing the currently fielded assets within the defined scope of size, compatibility with circuitry, starting endurance, and availability among other factors. The Raven was determined to be the best available asset. However, the Puma, though unavailable, was much more attractive due to a wingspan twice that of the Raven and a longer starting endurance.

After the selection of an SUAV, the theory and performance of flexible solar cells were explored. The competing technologies were compared, with efficiency and cost being the primary factors. After comparison, CIGS cells were determined to be the highest performing cells for a reasonable price.

Battery technologies were explored next, with a focus on energy density and handling procedures. The Raven's lithium polymer batteries were compared against emerging technologies and determined to be superior to lithium sulfur and lithium air batteries not yet commercially available.

After selecting the solar cells and battery, the circuitry to interface those key components was selected. A combination MPPT and boost converter was selected due to the capability to tune the circuitry independently. A battery balancer was determined to be necessary for the ability to safely and reliably charge the battery with the solar array.

During assembly, the flexibility of the MPPT became important when the original array design was determined to be incompatible with the Raven battery. The redesigned array used a minimalist approach that limited handling of the cells, reduced temperature sensitivity, and allowed the boost converter to perform its intended function. That array was mounted on a modified wing that closely resembled the airfoil of a Raven wing.

The system was bench tested before and after modification to clearly demonstrate the effectiveness of the augmenting circuitry. During testing, the current demand of the Raven was recorded at each throttle position to provide a basis for future calculations. The endurance tests were designed to reflect current tactics, techniques, and procedures to not only prevent damage to the system but also provide an easily recognizable improvement in performance.

At the conclusion of testing, it was apparent that not only were the solar cells used significantly degraded, but the MPPT did not operate at the maximum power point of the solar cells. Despite these shortcomings, the augmented system still operated 2.7 times longer than shown by the average baseline bench test of the un-augmented system. Another critical piece of data collected for the first time was the parabolic curvature of the input current to the system caused by the sun moving across a stationary solar array during the course of testing.

Simulations were created to project the performance of the system with properly functioning components by multiplying the input current to the system by factors to maintain the shape of the curve. Those projections demonstrated that the Raven battery should have charged for two hours during mid-day by replacing only the degraded cells, while replacing the MPPT and cells could have achieved day-long charging of the battery, increasing performance by at least 269%, or 3.7 times, the original endurance.

Those simulations went further to predict the performance of properly functioning cells and MPPTs on an unmodified Raven wing and the larger battery and wingspan of a Puma. Utilizing only a single string of cells on a standard Raven wing would have provided 96.5% of the current input during the actual test, while a Puma could receive a significantly increased percentage of input current to the system, which reduces demand on the battery and increases flight endurance.

Table 6. Summarized testing results compared to original system.

Specification	Original System	Augmented System	Change (%)
Endurance (minutes)	126.3	340	+169
Weight (ounces)	70.4	72.7	+3.8
Cost ($)	35,000.00	35,262.63	+0.75

The difference between the endurance of bench tests and documented endurance from actual flights were also compared. A prediction of average current draw based on battery capacity was calculated to account for the average flight and translated into the measured current draw for throttle position. A 90 minute flight, according to operator manual procedures, would require an average current draw of 1.82 Amps. That current draw was found during testing to be between 65% and 70% throttle.

The most significant finding of this research was that flight during mid-day hours provides a significant increase in the endurance of a Raven. Those results were found to be affected by the system's flight profile, the movement of the sun throughout the day, and weather conditions. However, even during cloudy and other low light conditions, the augmenting circuitry was found to provide a significant input to the original system without harming a fully charged battery or draining the battery at night. Those benefits, summarized in Table 7, were provided at a cost of 3.8% increase in weight and 0.75% increase in materials cost over the original system. In short, for minimal changes to the cost or weight of the system, a significant increase in endurance and capabilities were added using commercially available components that did no harm to the original system.

C. RECOMMENDATIONS

1. Record Current During Flight

The endurance measured during baseline bench testing was longer than anticipated. That mission profile was based on trainer advice and supported by the operator's manual. However, to deplete the battery in 90 minutes the average current draw would have to be higher than that measured at 55% throttle during bench testing.

Further research could use a device to measure and record the current draw in flight during an average mission by an actual operator. The current recorded during flight could be translated into the throttle position behavior documented in this thesis. That data could be used to create a more accurate model for bench testing while also providing greater insight into the use of these systems. Not only could the findings change the design of the system, it could also create a basis to change protocol, including flight profiles, to take advantage of the solar cells.

2. Incorporate Data into Simulink Model

The arc of the sun's movement throughout the day significantly affects the input power available to the system. When the endurance of a system stretches to several hours and, especially, near dawn and dusk, the change in available sunlight has a dramatic effect on the ability to predict the endurance of a system.

Further research should include a model of irradiance throughout the day to support predictions for flight in conditions other than mid-day. Such models could help leaders plan the best time to launch their systems to receive continuous coverage throughout the day and the best time to switch to the traditional 90 minute mission plans for night time operations.

3. Testing on Puma

Though the Puma was unavailable for this research, the specifications that were available caused significant interest in the possibility of a notable improvement over the Raven. The Puma has a starting endurance that is 30 minutes longer than the Raven and a

wingspan that could fit twice as many solar cells as a Raven. What is unknown is the current behavior of the Puma at different throttle position.

Further research should characterize the current demand at different throttle positions and translate the work already done and being pursued on the Raven for use on the Puma. While the Puma is heavier and larger than the Raven, making it less portable and preventing continuous coverage at night, the design changes could allow increased flight from dawn to dusk. Potentially, a solar augmented Puma could be launched even earlier in the morning, charge throughout the day and be retrieved even later at night than the Raven.

4. Fly an Augmented Prototype

Testing during this research was limited to bench testing due to the lack of an airworthiness certificate. As improvements are made to the existing configuration, testing should be done with a prototype in flight. The inclusion of banking, increased distances from the controller, and landings will provide greater insight and, in this writer's opinion, confidence in this technology as an important improvement in capabilities provided to our warfighters.

Testing should continue to be done in realistic conditions. For warfighters, the greatest confidence comes from knowing the technology works, not only under ideal conditions, but when it is needed in the austere conditions of combat.

THIS PAGE INTENTIONALLY LEFT BLANK

APPENDIX A. RAW DATA

A. VOLTAGE DATA FOR ENDURANCE TESTS

Time (minutes)	Battery A, Test 1 (V)	Battery B, Test 1 (V)	Battery A, Test 2 (V)	Battery B, Test 2 (V)	Average Baseline (V)	Augmented Test (V)
0	24.9	25.1	24.9	25.1	25	24.9
0.3333	23.4	23.3	23.4	23.3	23.35	23.7
5	24.3	24.4	24.4	24.5	24.4	24.6
10	24.2	24.2	24.2	24.3	24.225	24.5
15	24	24.1	24	24.1	24.05	24.5
20	23.9	23.9	23.9	24	23.925	24.3
25	23.7	23.7	23.7	23.8	23.725	24.3
30	23.5	23.6	23.6	23.6	23.575	24.2
35	23.4	23.4	23.4	23.5	23.425	24.1
40	23.2	23.3	23.3	23.4	23.3	24.1
45	23.1	23.2	23.1	23.2	23.15	24
50	23	23	23	23.1	23.025	23.9
55	22.8	22.9	22.9	23	22.9	23.8
60	22.7	22.8	22.8	22.8	22.775	23.8
65	22.6	22.7	22.7	22.7	22.675	23.7
70	22.6	22.6	22.6	22.7	22.625	23.6
75	22.5	22.5	22.5	22.6	22.525	23.6
80	22.4	22.4	22.4	22.5	22.425	23.5
85	22.4	22.4	22.4	22.4	22.4	23.5
90	22.3	22.3	22.3	22.4	22.325	23.4
95	22.2	22.3	22.3	22.3	22.275	23.3
100	22.2	22.2	22.2	22.3	22.225	23.3
105	22.2	22.2	22.2	22.2	22.2	23.2
110	22.1	22.1	22.1	22.2	22.125	23.1
115	22.1	22.1	22.1	22.2	22.125	23.1
120	22	21.9	22	22.1	22	23
125	21.9		22	22.1	22	23
130			21.9	22	21.95	22.9
135				22	22	22.9
140				21.9	21.9	22.9
145						22.9
150						22.9
155						22.8

160						22.8
165						22.8
170						22.8
175						22.7
180						22.7
185						22.7
190						22.7
195						22.6
200						22.6
205						22.6
210						22.6
215						22.6
220						22.6
225						22.5
230						22.5
235						22.5
240						22.5
245						22.5
250						22.5
255						22.4
260						22.4
265						22.4
270						22.4
275						22.4
280						22.3
285						22.3
290						22.3
295						22.2
300						22.2
305						22.2
310						22.2
315						22.1
320						22.1
325						22.1
330						22
335						22
340						21.9

B. BASELINE CURRENT DRAW

Time (minutes)	Battery A, Test 1 (A)	Battery B, Test 1 (A)	Battery A, Test 2 (A)	Battery B, Test 2 (A)	Average Base-line (A)
0	0.28	0.31	0.25	0.23	0.27
0.333	6.15	6.24	6.23	6.24	6.22
5	1.24	1.32	1.25	1.32	1.28
10	1.2	1.3	1.27	1.32	1.27
15	1.21	1.28	1.26	1.32	1.27
20	1.3	1.22	1.26	1.32	1.28
25	1.25	1.14	1.27	1.29	1.24
30	1.18	1.14	1.14	1.29	1.19
35	1.2	1.24	1.12	1.28	1.21
40	1.18	1.23	1.09	1.28	1.20
45	1.18	1.24	1.07	1.28	1.19
50	1.12	1.2	1.17	1.28	1.19
55	1.1	1.2	1.14	1.28	1.18
60	1.14	1.15	1.15	1.26	1.18
65	1.24	1.09	1.16	1.27	1.19
70	1.2	1.18	1.11	1.25	1.19
75	1.25	1.14	1.16	1.25	1.20
80	1.25	1.11	1.19	1.25	1.20
85	1.25	1.25	1.17	1.23	1.23
90	1.23	1.25	1.2	1.23	1.23
95	1.17	1.25	1.14	1.22	1.20
100	1.2	1.24	1.16	1.22	1.21
105	1.21	1.24	1.14	1.21	1.20
110	1.21	1.21	1.13	1.23	1.20
115	1.24	1.17	1.16	1.23	1.20
120	1.18	1.19	1.09	1.22	1.17
125	1.23		1.08	1.21	1.17
130				1.19	1.19
134				1.24	1.24

C. AUGMENTED ENDURANCE TEST DATA

Time (minutes)	I mppt (A)	I raven (A)	V battery (V)	I battery (A)	I array (A)	Varray (V)
0	0.054	0.299	24.9	0.245	0.17	9.4
0.3333	0.709	6.62	23.7	5.911	2.79	7
5	0.703	1.36	24.6	0.657	2.83	6.9
10	0.712	1.35	24.5	0.638	2.89	6.9
15	0.713	1.35	24.5	0.637	2.88	6.9
20	0.726	1.36	24.3	0.634	2.91	6.9
25	0.729	1.36	24.3	0.631	2.92	6.9
30	0.74	1.35	24.2	0.61	2.94	6.9
35	0.744	1.35	24.1	0.606	2.96	6.9
40	0.752	1.35	24.1	0.598	3	6.9
45	0.748	1.35	24	0.602	2.95	6.9
50	0.749	1.34	23.9	0.591	2.95	6.9
55	0.769	1.34	23.8	0.571	3.02	6.9
60	0.776	1.34	23.8	0.564	3.04	6.9
65	0.775	1.34	23.7	0.565	3.04	6.9
70	0.79	1.33	23.6	0.54	3.09	6.9
75	0.79	1.33	23.6	0.54	3.07	6.9
80	0.792	1.33	23.5	0.538	3.07	6.9
85	0.796	1.33	23.5	0.534	3.09	6.9
90	0.8	1.33	23.4	0.53	3.08	6.9
95	0.801	1.32	23.3	0.519	3.09	6.9
100	0.811	1.31	23.3	0.499	3.13	6.9
105	0.805	1.31	23.2	0.505	3.1	6.9
110	0.813	1.31	23.1	0.497	3.11	6.9
115	0.827	1.3	23.1	0.473	3.17	6.9
120	0.823	1.31	23	0.487	3.15	6.9
125	0.831	1.31	23	0.479	3.17	6.9
130	0.835	1.31	22.9	0.475	3.18	6.9
135	0.831	1.3	22.9	0.469	3.16	6.9
140	0.84	1.3	22.9	0.46	3.19	6.9
145	0.842	1.3	22.9	0.458	3.2	6.9
150	0.838	1.29	22.9	0.452	3.17	6.9
155	0.838	1.3	22.8	0.462	3.17	6.9
160	0.842	1.3	22.8	0.458	3.18	6.9
165	0.839	1.3	22.8	0.461	3.17	6.9
170	0.846	1.3	22.8	0.454	3.19	6.9

175	0.842	1.29	22.7	0.448	3.18	6.9
180	0.842	1.29	22.7	0.448	3.18	6.9
185	0.838	1.29	22.7	0.452	3.15	6.9
190	0.834	1.29	22.7	0.456	3.13	6.9
195	0.84	1.29	22.6	0.45	3.15	6.9
200	0.84	1.29	22.6	0.45	3.15	6.9
205	0.833	1.29	22.6	0.457	3.13	6.9
210	0.833	1.29	22.6	0.457	3.13	6.9
215	0.833	1.29	22.6	0.457	3.13	6.9
220	0.83	1.29	22.6	0.46	3.11	6.9
225	0.829	1.29	22.5	0.461	3.1	6.9
230	0.828	1.28	22.5	0.452	3.09	6.9
235	0.83	1.29	22.5	0.46	3.1	6.9
240	0.82	1.29	22.5	0.47	3.06	6.9
245	0.823	1.29	22.5	0.467	3.07	6.9
250	0.823	1.28	22.5	0.457	3.07	6.9
255	0.812	1.28	22.4	0.468	3.02	6.9
260	0.814	1.29	22.4	0.476	3.03	6.9
265	0.801	1.28	22.4	0.479	2.97	6.9
270	0.795	1.29	22.4	0.495	2.95	6.9
275	0.789	1.28	22.4	0.491	2.93	6.9
280	0.791	1.28	22.3	0.489	2.93	6.9
285	0.776	1.28	22.3	0.504	2.87	6.9
290	0.771	1.28	22.3	0.509	2.84	6.9
295	0.759	1.27	22.2	0.511	2.8	6.9
300	0.751	1.28	22.2	0.529	2.77	6.9
305	0.743	1.27	22.2	0.527	2.74	6.9
310	0.73	1.27	22.2	0.54	2.68	6.9
315	0.718	1.27	22.1	0.552	2.64	6.9
320	0.709	1.27	22.1	0.561	2.6	6.9
325	0.696	1.27	22.1	0.574	2.55	6.9
330	0.679	1.27	22	0.591	2.48	6.9
335	0.67	1.27	22	0.6	2.45	6.9
340	0.655	1.27	21.9	0.615	2.39	6.9

THIS PAGE INTENTIONALLY LEFT BLANK

APPENDIX B. MATLAB SOURCE CODE

```
time=[28/3:5/60:179/12];
cur-
rent=[.703,.712,.713,.726,.729,.740,.744,.752,.748,.749,.769,.776,.775,
.790,.790,.792,.796,.800,.801,.811,.805,.813,.827,.823,.831,.835,.831,.
840,.842,.838,.838,.842,.839,.846,.842,.842,.838,.834,.840,.840,.833,.8
33,.833,.830,.829,.828,.830,.820,.823,.823,.812,.814,.801,.795,.789,.79
1,.776,.771,.759,.751,.743,.730,.718,.709,.696,.679,.670,.655];
plot(time,current)
hold on
load=(-.01612*time)+1.5;% 55%Throttle Load
plot(time,load,'--')
hold on
current2=(.95/.77).*current;%only replacing MPPT
plot(time,current2,'*')
hold on
current3=(.13/.08).*current; %only replacing solar cells
plot(time,current3,'x')
hold on
current4=(.95/.77)*(.13/.08).*current;% replacing cells and MPPT
plot(time,current4,'*-')
hold on
load2=load+.52; % Theoretical load to last 90min
plot(time,load2,'-.')
```

THIS PAGE INTENTIONALLY LEFT BLANK

LIST OF REFERENCES

[1] Lexi Krock, "Time line of UAVs," NOVA. November 2002. [0nline]. Available: http://www.pbs.org/wgbh/nova/spiesfly/uavs.html. [Accessed July 2, 2012].

[2] Assistant Secretary of Defense for Operational Energy, Plans & Programs, "Energy for the warfighter: operational energy strategy," May 2011. [Online]. Available: http://energy.defense.gov/OES_report_to_congress.pdf. [Accessed July 3, 2012].

[3] Glenn W. Goodman Jr, "Three tiers: The Marine Corps takes a key step this summer to modernize its UAVs," Sea Power, July 2006. [Online] Available: http://www.navyleague.org/sea_power/jul06–18.php. [Accessed July 2, 2012].

[4] Green Rhino Energy, "Yearly sum of global irradiance," 2012. [Online] Available: http://www.greenrhinoenergy.com/solar/radiation/empiricalevidence.php#. [Accessed July 19, 2012].

[5] Daniel J. P. Riveong, "In the midst of the swarm: reconceptualizing the (mislabeled) Global War on Terrorism." [Online]. Available: http://danielriveong.com/Reconceptualizing-the-Global-War-on-Terror-(GWOT).html. [Accessed July 19, 2012].

[6] William Price, "Flexible solar panel image;" Marine Corps Expeditionary Energy. Dec. 21, 2010. [Online]. Available: http://www.marines.mil/community/Pages/ExpeditionaryEnergy.aspx. [Accessed July 3, 2012].

[7] Robert J. Boucher, "History of solar flight," presented at AIAA/SAE/ASME 20th Joint Propulsion Conference, Cincinnati OH, 1984. [Online]. Available: http://www.astroflight.com/pdfs/SolarHistory.pdf. [Accessed July 6, 2012].

[8] Zachary Shahan, "Solar-powered plane completes 1st 24-hour flight," Clean Technica, July 9, 2010. [Online]. Available: http://cleantechnica.com/2010/07/09/solar-powered-plane-completes-1st-24-hour-flight/. [Accessed July 6, 2012].

[9] Zakia Abdennebi, "Solar plane completes maiden intercontinental trip," Reuters, June 6, 2012. [Online]. Available: http://www.reuters.com/article/2012/06/06/uk-aviation-solar-idUSLNE85500720120606. [Accessed July 6, 2012].

[10] William R. Hurd, "Application of copper indium gallium diselenide Photovoltaic Cells to Extend the Endurance and Capabilities of Unmanned Aerial Vehicles," Master's thesis, Naval Postgraduate School, Monterey, CA, 2009.

[11] Javier V. Coba, "Application of copper indium gallium diselenide photovoltaic cells to extend the endurance and capabilities of the raven RQ-11B unmanned aerial vehicle," Master's thesis, Naval Postgraduate School, Monterey, CA, 2010.

[12] Chee Keen Chin, "Extending the endurance, missions, and capabilities of most UAVs using advanced flexible/ridged solar cells and new high power density Batteries Technology," Master's thesis, Naval Postgraduate School, Monterey, CA, 2011.

[13] Office of the Undersecretary of Defense (Comptroller)/ CFO, "Program Acquisition costs by weapon system," *United States Department of Defense Fiscal Year 2011 Budget Request*, February 2010, p. I-4. [Online] Available: http://comptroller.defense.gov/defbudget/fy2011/FY2011_Weapons.pdf. [Accessed July 10, 2012].

[14] Office of the Undersecretary of Defense (Comptroller)/ Chief Financial Officer, "Program Acquisition costs by weapon system," *United States Department of Defense Fiscal Year 2013 Budget Request*, February 2012, p. I-4. [Online] Available: http://comptroller.defense.gov/defbudget/fy2013/FY2013_Weapons.pdf. [Accessed July 10, 2012].

[15] IHS Jane's, "AV FQM-151A Pointer," May 31, 2010. [Online] Available: http://search.janes.com. [Accessed July 10, 2012].

[16] IHS Jane's, "Lockheed Martin Desert Hawk," September 10, 2011. [Online] Available: http://search.janes.com. [Accessed July 11, 2012].

[17] IHS Jane's, "AV RQ-11 Raven," May 26, 2011. [Online] Available: http://search.janes.com. [Accessed July 11, 2012].

[18] Department of the Navy, "Procurement, Marine Corps," *Department of Defense Fiscal Year (FY) 2013 President's Budget Submission.* February 2012, p. 205. [Online] Available: http://www.finance.hq.navy.mil/fmb/13pres/PMC_Book.pdf. [Accessed July 9, 2012].

[19] Department of the Army, "Aircraft procurement, Army," *Department of Defense Fiscal Year 2013 President's Budget Submission*. February 2012, p. 4. [Online] Available: http://asafm.army.mil/Documents/OfficeDocuments/Budget/BudgetMaterials/FY13/pforms//aircraft.pdf. [Accessed July 9, 2012].

[20] IHS Jane's, "AV Wasp III," May 26, 2011. [Online] Available: http://search.janes.com. [Accessed July 11, 2012].

[21] IHS Jane's, "AV Puma AE," May 25, 2011. [Online] Available: http://search.janes.com. [Accessed July 11, 2012].

[22] Wikipedia, "Air mass (solar power)," June 5, 2012. [Online] Available: http://en.wikipedia.org/wiki/Air_mass_(solar_energy). [Accessed July 19, 2012].

[23] Jay Jeong, "Photovoltaics: measuring the sun," Laser Focus World, May 21, 2009. [Online] Available: http://www.laserfocusworld.com/articles/2009/05/photovoltaics-measuring-the-sun.html. [Accessed July 19, 2012].

[24] Wikipedia "Electronvolt," 12 July, 2012. [Online] Available: http://en.wikipedia.org/wiki/Electronvolt. [Accessed July 26, 2012].

[25] Sherif Michael, "EC3230 space power and radiation effects," 2010. [Class Notes – Unpublished].

[26] Carston Deibel, "Intermediate: current-voltage characteristics of organic solar cells," March 5, 2008. [Online] Available: http://blog.disorderedmatter.eu/2008/03/05/intermediate-current-voltage-characeristics-of-organic-solar-cells/. [Accessed July 19, 2012].

[27] H.Y. Tada et.al, *Solar Cell Radiation Handbook,* Third Edition, Jet Propulsion Laboratory, Pasadena 1982.

[28] Miami University Solar Power Team, "What is solar power" April 22, 2007. [Online] Available: http://teams.eas.muohio.edu/solarpower/WhatIsSolarPower.html. [Accessed July 24, 2012].

[29] National Instruments, "Part II-photovoltaic cell I-V characterization theory and LabVIEW analysis code." May 10, 2012. [Online] Available: http://www.ni.com/white-paper/7230/en. [Accessed July 24, 2012].

[30] *Solar Cell Array Design Handbook,* Volume I, Jet Propulsion Laboratory, Pasadena. 1976.

[31] PVEducation.org, "Multi crystalline silicon." [Online] Available: http://www.pveducation.org/pvcdrom/manufacturing/multi-crystalline-silicon. [Accessed July 26, 2012].

[32] Mke McGehee, "An overview of solar cell technology," Stanford University. [Online] Available: http://gcep.stanford.edu/pdfs/2wh9Q1Alh3q2zMOQRKD4MQ/MikeMcGehee_SolarEnergy101.pdf. [Accessed July 27, 2012].

[33] Bob Haavind, “Industry execs hear about bright days ahead in energy,” ElectroIQ.com. [Online] Avaliable: http://www.electroiq.com/articles/sst/2009/01/industry-execs-hear-about-bright-days-ahead-in-energy.html. [Accessed July 30, 2012].

[34] Rutgers University, “Thin film amorphous silicon solar cells,” 2005. [Online] Available: http://www.rci.rutgers.edu/~dbirnie/solarclass/amorphousSi.pdf. [Accessed July 30, 2012].

[35] Richard Stevenson, “First Solar: quest for the $1 watt,” *IEEE Spectrum*, August 2008. [Online] Available: http://spectrum.ieee.org/energy/renewables/first-solar-quest-for-the-1-watt/0. [Accessed July 30, 2012].

[36] M. M. Aliyu, et al., “Recent developments of flexible CdTed solar cells on matallic Substrates: Issues and Prospects,” *International Journal of Photoenergy*, Vol. 2012. [Online] Available: http://www.hindawi.com/journals/ijp/2012/351381/. [Accessed July 30, 2012].

[37] Wikipedia, “Copper indium gallium selenide solar cells,” June 14, 2012. [Online] Available: http://en.wikipedia.org/wiki/Copper_indium_gallium_selenide_solar_cells. [Accessed July, 31, 2012].

[38] MicroLink Devices, “Epitaxial lift-off,” 2012. [Online] Available: http://www.mldevices.com/index.php/technology/epitaxial-lift-off. [Accessed August 1, 2012].

[39] Microlink Devices, “Triple-junction ELO solar cells for UAV application,” 2012. [Online] Available: http://www.mldevices.com/images/Datasheets/120213%20uav%20cell%203j.pdf. [Accessed August 1, 2012].

[40] Quest Batteries, “Lithium polymer” *Harding Battery Handbook*, January 5, 2004. [Online] http://www.hardingenergy.com/pdfs/6%20Lithium%20Polymer.pdf. [Accessed August 14, 2012].

[41] Paul Williams, “Lithium polymer cells” August 7, 2008. [Online] http://www.fastelectrics.net/lipos.php. [Accessed August 15, 2012].

[42] Department of Defense, “Raven B small unmanned aerial vehicle with digital data link (DDL) operator’s manual” Rev A1, 60707_A1, March 2011.

[43] James Robert Akridge, “Lithium sulfur rechargeable battery safety,” October 2001. [Online]

http://www.sionpower.com/pdf/articles/CellandBatterySafety0602.pdf. [Accessed: August 14, 2012].

[44] Lisa Zyga, "Rechargeable lithium-sulfur batteries get a boost from graphene," July 13, 2011. [Online] http://phys.org/news/2011–07-rechargeable-lithium-sulfur-batteries-boost-graphene.html. [Accessed: August 14, 2012].

[45] Lucas Laursen, "Lithium-air batteries get a recharge," IEEE Spectrum, July 2012. [Online] http://spectrum.ieee.org/energy/renewables/lithiumair-batteries-get-a-recharge/. [Accessed: August 14, 2012].

[46] Ucilia Wang, "Why the lithium air battery is over hyped," June 6, 2012. [Online] http://gigaom.com/cleantech/why-the-lithium-air-battery-is-over-hyped/. [Accessed: August 14, 2012].

[47] GENASUN, "Genasun GV-boost lithium overview," 2012, [Online] https://genasun.com/products-store/solar-charge-controllers/for-lithium/gvb-li/. [Accessed: October 30, 2012].

[48] STEVAL, "AN3392 application note," May 2011. [Online] http://media.digikey.com/pdf/Application%20Notes/ST%20Microelectronics%20Application%20Notes/SPV1020%20AN3392.pdf. [Accessed: October 30, 2012].

[49] Ned Mohan, Tore Undeland, ans Williams Riobbins, *Power electronics: converters applications, and design*, Third Edition,Wiley-India, Delhi, pp 172–172. 2011.

[50] Common Sense RC, " Ultra-balancer instructions," April 9, 2008.

[51] Amprobe, "Solar 600 solar analyzer," 2010. [Online] http://www.amprobe.com/amprobe/usen/Environmental-Test/Solar-Meters-and-Analyzers-/SOLAR-600.htm?PID=73346. [Accessed: November 6, 2012].

[52] Jon Stiner, private conversation at Camp Roberts August 2, 2012.

[53] Jerome Adams in private telephone conversation, August 7, 2012.

[54] U.S. Naval Observatory, "Sun or moon altitude/azimuth table," March 30, 2012. [Online] http://aa.usno.navy.mil/data/docs/AltAz.php. [Accessed: November 9, 2012].

[55] Department of Defense, "Puma AE with digital data link (DDL) operator's manual" 62869_A, June 2011.

[56] Sherif Michael, private conversation, August 15, 2012.

THIS PAGE INTENTIONALLY LEFT BLANK

INITIAL DISTRIBUTION LIST

1. Defense Technical Information Center
   Ft. Belvoir, Virginia

2. Dudley Knox Library
   Naval Postgraduate School
   Monterey, California

3. Marine Corps Representative
   Naval Postgraduate School
   Monterey, California

4. Director, Training and Education, MCCDC, Code C46
   Quantico, Virginia

5. Director, Marine Corps Research Center, MCCDC, Code C40RC
   Quantico, Virginia

6. Marine Corps Tactical Systems Support Activity (Attn: Operations Officer)
   Camp Pendleton, California

7. Dr. R. Clark Robertson, Chairman
   Department of Electrical and Computer Engineering
   Naval Postgraduate School
   Monterey, California

8. Dr. Sherif Michael
   Department of Electrical and Computer Engineering
   Naval Postgraduate School
   Monterey, California

9. Dr. Rudolf Panholzer
   Space Systems Academic Group
   Naval Postgraduate School
   Monterey, California

10. Capt Christopher R. Gromadski
    United States Marine Corps
    Monterey, California

11. Mr Christopher Sacco, Group 1 UAS Lead
Navy and Marine Corps Small Tactical UAS
PEO (U&W) PMA-263
U.S. Naval Air System Command
Pautuxent River, Maryland

12. Maj Brandon Newell
Expeditionary Energy Office
United States Marine Corps
Quantico, Virginia

13. Col James Squire, Professor
Electrical and Computer Engineering
Virginia Military Institute
Lexington, Virginia